الجمهورية الجزائرية الديمقراطية الشعبية

People's Democratic Republic of Algeria

وزارة التعليم العالي والبحث العلمي

Ministry of Higher Education and Scientific Research

جامعة زيان عاشور بالجلفة

Ziane Achour University of Djelfa

كلية العلوم و التكنولوجيا

Faculty of Science and Technology

Department: Electrical Engineering

Order N° : . …. / 2023

Defense authorization N° ……/2023

DOCTORAL THESIS

3rd Cycle Doctoral (D-LMD)

Presented by

Derradji BAKRIA

In order to obtain the degree of Doctor in 3rd Cycle Doctoral (D-LMD)

Branch: Electrical Engineering

Specialty: Power Electronics and Quality of Electrical Energy

Topic

Contribution to the Elimination of Nonlinear Phenomena of Energy Conversion Systems (realization-Simulation)

Supported, on / / 2023, before the jury composed of:

Last and first name	Grade	Institution of affiliation	Designation
Hafaifa Ahmed	Professor	University of Djelfa	President
Gozim Djamal	MCA	University of Djelfa	Supervisor
Mazouz Lakhdar	MCA	University of Djelfa	Co-Supervisor
Boudiaf Mohamed	MCA	University of Djelfa	Examiner
Bendjedia Bachir	MCA	University of Laghouat	Examiner

Djelfa University, FST – 2023

Acknowledgement

First of all, I want to thank Allah, the Almighty, for the blessings and courage he gave me, which made it possible for me to finally finish my thesis.

I would like to express my gratitude and thanks to my thesis director, ***Dr. GOZIM Djamal****, for guiding, assisting, and advising me throughout this work, and for the scientific and human support and trust he has given me.*

I extend my sincere thanks to the members of the examination committee for the honor they gave me by accepting to be part of the jury.

I also thank my friends ***KORICH Bilal****,* ***MHAMMEDI Djamel*** *and* ***TETA Ali*** *for their help and support during the preparation of this thesis.*

Finally, would like to express my love and gratitude to my beloved family, all my friends and extended family for their encouragement and support.

Bakria Derradji

Table of Contents

Chapter II: Nonlinear Phenomena in Static Converters. Application to a Buck converter

Chapter III: Metaheuristic optimization algorithms

Chapter IV: Elimination of nonlinear phenomena in buck converter using metaheuristic algorithms

List of Figures

List of abbreviation and symbols

AC/DC	*Rectifiers*
AC/AC	*Dimmers*
DC/AC	*Inverters*
DC/DC	*Choppers*
DCM	*Discontinuous conduction mode*
CCM	*Continues conduction mode*
KVL	*Kirchhoff voltage law*
KCL	*Kirchhoff current law*
PWM	*Pulse with modulation*
PID	*Proportional integral derivative*
PSO	*Particle Swarm Optimization*
GWO	*Grey Wolf Optimization*
SHO	*Spotted Hyena Optimization*
ADC	*Analog digital converter*
GND	*Ground*
$pbest$	*Vector of the best position encountered by particle*
$gbest$	*Vector of the best position encountered by the swarm*
L	*Inductor*
C	*Capacitor*
D	*Diode*
sw	*Switch*
R	*Load*
$i_L(t)$	*Inductor current*
$V_c(t)$	*Output capacitor voltage*
$V_o(t)$	*Output voltage*
$i_g(t)$	*Input current*
$\vec{s}$	*Position vector of a particle*
$\vec{v}$	*Vector of displacement of particle*
$\vec{X}$	*Position vector of a wolf*
$\vec{X}_P$	*Position vector of prey*

D	*The distance between the wolf and the prey*
$\overrightarrow{X_\alpha}$	*Vector of the α wolf position*
$\overrightarrow{X_\beta}$	*Vector of the β wolf position*
$\overrightarrow{X_\gamma}$	*Vector of the γ wolf position*
$\vec{P}$	*Position vector of a spotted hyena*
$\vec{D}_h$	*Distance between the prey and spotted hyena*
$\vec{P}_p$	*Position vector of the prey*
$\vec{C}_h$	*Group of cluster friends*

General introduction

General introduction

In recent decades, due to the growing demand for electrical systems in many application fields, electrical engineering has seen massive growth in various areas. To ensure the Efficiency of the industrial process, a modeling technique must be employed to accurately explore the system's behavior [1]. This model must incorporate both the nominal and irregular modes of operation.

Static converters are used in a wide range of industrial processes in order to manage and convert energy from one form to another. They have become increasingly complex due to the ever-changing and diversifying needs of industrial processes. The basic principle behind static converters is to use a control device to switch electrical energy from a given source into the desired energy by controlling a series of switches. This allows for efficient and reliable power conversion, making static converters very useful in a variety of industrial applications [1].

Non-linear systems, such as static converters, are known to have a range of complex behaviors, including bifurcation phenomena which can lead to chaotic behaviors. It is essential to know when bifurcation phenomena will occur in order to properly size the system and this information can be acquired through accurate modeling.

In our research, we have examined DC-to-DC converters, which allow us to get either a constant or adjustable direct voltage from any direct voltage source. These sources can include battery packs, solar panels, or even rectified and filtered AC power. The DC-DC converter is a dynamic system capable of performing voltage step-up or step-down functions, and its basic structures include the Buck, the Boost, and the Buck-Boost. Despite its simple structure, the static converter can display complex and even unpredictable behaviors [2-38].

When designing a static converter, the sizing of the parameters of the control must guarantee a stable operation regardless of the operating point. A major scientific challenge is then to create control laws that can meet the requirements of the specifications and prevent the emergence of unexpected behaviors, which can destruct the system [44-62].

Our thesis work focuses on understanding the dynamic behavior of a DC-DC converter. We will do this by first describing its behavior and exploring its various normal and abnormal behaviors. Once we have done this, we can proceed to the development of a suitable controller to meet the specifications while keeping the system's behavior simple and predictable over a wide range of operations.

In the first chapter, generalities and basic concepts about the operation of a static converter, its behavior and its operating modes are modeled. Chapter two presents the behavior of the converter as a dynamic system. We will provide in this chapter an overview of the research done to solve issues regarding analysis of abnormal behaviors of the converter and its improvement. Furthermore, we will propose a circuit of voltage PID controlled buck converter to explore the nonlinear phenomena exhibited by the converter. Finely in the same chapter, we will also discuss the effect of varying the parameters of the converter on its behavior, which can lead to undesirable nonlinear phenomena.

The optimization of the parameters of the PID controller is used as a solution to achieve the desired performance and thus provide a reliable solution. In the third chapter we will present the various metaheuristic methods that we will use in the next chapter to find the optimum solution. Finally the last chapter is devoted to the question of improving the converter's behavior in order to maintain good performance while shifting or eliminating the nonlinear phenomena that complicate it.

Chapter I

Static converters basics and modeling

1. Introduction

The complexity and variety of industrial processes has led to an increase in the sophistication of static converters. The same principle is used in all of these converters, where a given energy source must be transformed into the desired energy by controlling the switches.

Of the four main types of converters, namely rectifiers (AC/DC), dimmers (AC/AC), inverters (DC/AC) and choppers (DC/DC), the latter was selected for this study, as it allows conversion of a fixed or variable direct voltage from any direct voltage source, such as an accumulator battery, solar cell battery or rectified, filtered alternating network. DC/DC converters can be either voltage reducers or boosters, and the Buck, Boost and Buck-Boost are the primary structures of these converters.

In this chapter, we discuss various converter topologies and how they function. Transistors and diodes are the essential elements of switching regulator circuits that direct the speedy, dynamic flow of power from input to output. Pulse width modulation (PWM) is the most widely-used method for controlling the transistor to adjust the output voltage. This technique maintains the same switching frequency while altering the duty cycle. Unfortunately, the switching nature of the converter adds AC ripple to the output voltage which should be DC with limited AC ripple. To meet this requirement, an inductor and capacitor should be connected in the converter to form a low pass filter.

2. Basic operation of DC DC converters

Buck, boost, and buck-boost converters are three most known types of switching mode DC-DC converters. The buck converter converts the input voltage to a lower output voltage, whereas the boost mode increases it. The buck-boost mode combines buck and boost converters, allowing the output voltage to be kept either higher or lower than the source voltage while maintaining the opposite polarity [1]. Figure 1 illustrates the fundamental topologies of these converters.

Each of the types previously described are made up of an inductor (L), a capacitor (C), a diode (D), and a switch (sw) with two states: ON and OFF. The converters' inputs are connected to an unregulated DC power source and give a regulated voltage V_O to the load resistor R by controlling the state of the switch [1-3]. Although the load could be inductive in

some cases, such as with a DC motor, we will treat it as a resistive load for the sake of this study.

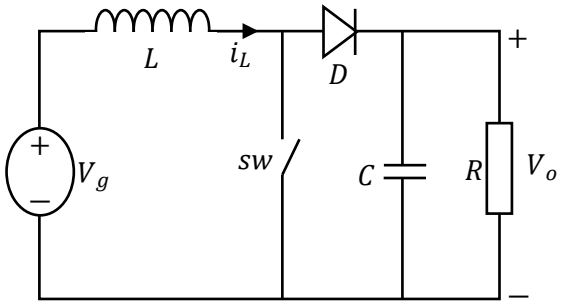

(a) Boost converter

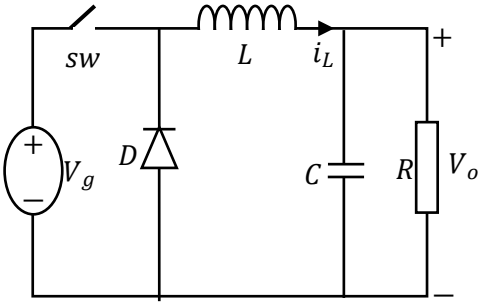

(b) Buck converter

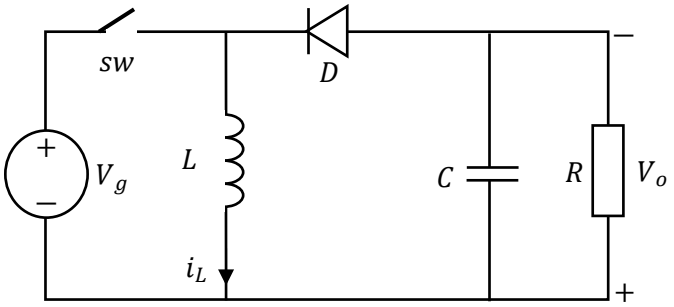

(c) Buck-Boost converter

Figure I. 1. The basic topologies of the DC-DC conveter

Static converters are known for their piecewise linearity [1]. To analyze the system, two scenarios are considered: one with ideal components and one with parasitic components (inductors, capacitors, transistors, and diodes with ON resistances). A state space description is then used to write the differential equations in a canonical form. This lets us get linear models for each configuration, of the form:

$$\begin{cases} K\dot{x}_i = A_i x_i + B_i u(t) \\ y_i(t) = C_i x_i(t) + E_i u(t) \end{cases} \quad \text{(I.1)}$$

With A_i, B_i,C_i and E_i are the state matrices for the i^{th} configuration.

For each setup, the state vector x(t) is computed as follows:

$$x(t) = [i_L(t), V_c(t)] \quad \text{(I.2)}$$

Where $i_L(t)$ and $V_c(t)$ are the inductor current and capacitor voltage, respectively

The converter is driven by the input vector $u(t)$. K is a matrix containing the values of capacitance and inductance. The output voltage $V_o(t)$ and the input current $i_g(t)$ are expressed as a victor $y(t)$ where:

$$y(t) = [\mathrm{i_g(t)}, \mathrm{V_o(t)}] \tag{I.3}$$

Examining the voltage and current of the inductor, first with the switch closed and then with the switch open, is the most crucial phase of the analysis required to estimate the voltage Vo. In order for the device to operate in a steady state, the charge of the inductor current must remain constant over the period, and the average voltage across the inductor is 0. This circuit is capable of operating in either a continuous or discontinuous conduction mode, which are the two possible operational modes.

In the continuous conduction the current passing through the coil does not drop to zero over the switching period, as shown in Figure 2(a), and the discontinuous conduction the current passing through the coil is equal to zero for part of the switching period, as shown in Figure 2(b).

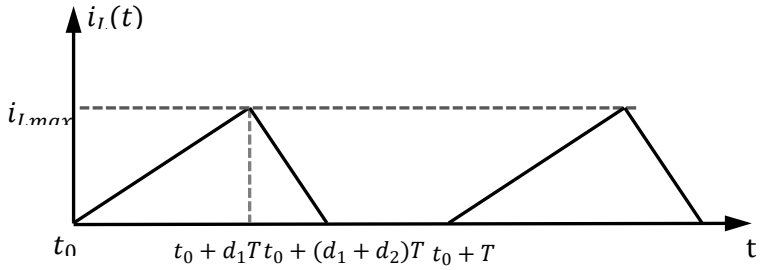

(a)

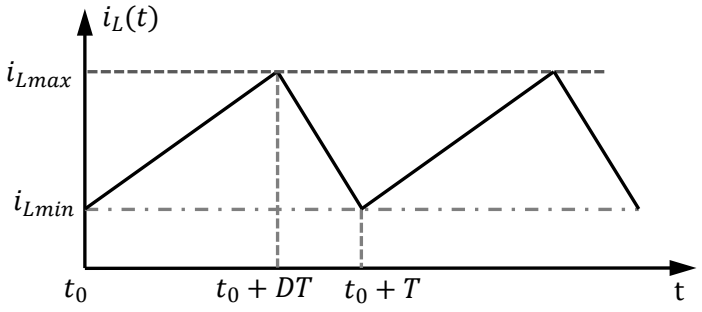

(b)

Figure I. 2. Inductor current waveforms: (a) DCM, (b) CCM

3. Buck converter

The buck converter and its output filter are shown in Figure I.1 (b). While transistor SW is ON and the diode is OFF, the input voltage appears across the inductor, and the inductor current grows linearly. During the entire cycle, the capacitor gets charged. When the diode is on and SW is off, the voltage across the inductor reverses. However, because the current in the inductor cannot change instantly, it begins to decrease linearly. During this cycle, the inductor's stored energy is used to charge the capacitor [1]. The various configurations of buck converter are shown in Figure 3.

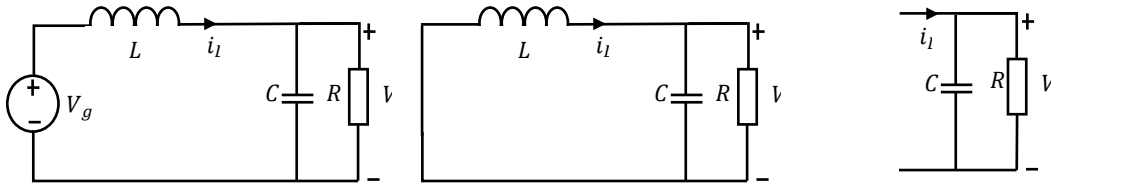

(a) sw is ON, D is OFF **(b)** sw is OFF, D is ON **(c)** sw is OFF,D is OFF

Figure I. 3. Possible configurations of Buck converter

3.1. Basic analysis

The duty cycle relationship between output and input voltage is determined by analyzing the inductor current waveform. The main goal of a well-designed converter is to have a low proportion of ripple at the output. Thus, the DC component of the output voltage can be used to approximate it.

The principle of inductor volt second balance is the observation that the net change in inductor current over one switching cycle is zero in steady state. The voltage of an inductor is defined by

$$V_L = L\frac{di_L}{dt} \tag{I.4}$$

The result of integrating over a single switching period

$$i_L(T) - i_L(0) = \frac{1}{L}\int_0^T V_L(t)dt \tag{I.5}$$

The average inductor voltage is calculated as follows

$$\langle V_L \rangle = \frac{A}{T_{SW}} = (V_G - V_o)D + (-V_o)(1-D) \tag{I.6}$$

A is the total area beneath the $V_L(t)$ waveform over one switching period, which must be zero; this leads to

$$V_o = DV_G \tag{I.7}$$

The basic equation for capacitors is the same as the inductor volt-second balance.

$$i_c = C\frac{dV_c}{dt} \tag{I.8}$$

Over the course of a single switching period, integration yields,

$$V_C(T) - V_C(0) = \frac{1}{C}\int_0^T i_C(t)dt \tag{I.9}$$

The net change in capacitor voltage over one switching period must be zero in steady state; hence the left hand side of the preceding equation must be zero.

$$\langle i_c \rangle = \frac{1}{T}\int_0^T i_C dt = O \tag{I.10}$$

3.2. State space model

3.2.1. Model with ideal components

A. Continuous conduction mode

In the continuous conduction mode, the converter is able to operate in either of the two configurations shown in Figures 5(b) and 5(c).

When the switch is closed, the system can be described as follows:

$$\begin{cases} \mathrm{L}\dfrac{\mathrm{di_L}}{\mathrm{dt}} = \mathrm{V_g} - \mathrm{V_c} \\ \mathrm{C}\dfrac{\mathrm{dV_c}}{\mathrm{dt}} = \mathrm{i_L} - \dfrac{\mathrm{V_c}}{\mathrm{R}} \end{cases} \tag{I.11}$$

Equation 12 gives the state equation matrices.

$$\begin{bmatrix} \mathrm{L} & 0 \\ 0 & \mathrm{C} \end{bmatrix}\begin{bmatrix} \dfrac{\mathrm{di_L}}{\mathrm{dt}} \\ \dfrac{\mathrm{dV_c}}{\mathrm{dt}} \end{bmatrix} = \begin{bmatrix} 0 & -1 \\ 1 & -\dfrac{1}{\mathrm{R}} \end{bmatrix}\begin{bmatrix} \mathrm{i_L} \\ \mathrm{V_c} \end{bmatrix} + \begin{bmatrix} 1 \\ 0 \end{bmatrix}\mathrm{V_g} \tag{I.12}$$

When the switch is in the closed position, the system can be represented as follows.

$$\begin{cases} L\dfrac{di_L}{dt} = -V_c \\ C\dfrac{dV_c}{dt} = i_L - \dfrac{V_c}{R} \end{cases} \quad (I.13)$$

State equation matrices are given as:

$$\begin{bmatrix} L & 0 \\ 0 & C \end{bmatrix} \begin{bmatrix} \dfrac{di_L}{dt} \\ \dfrac{dV_c}{dt} \end{bmatrix} = \begin{bmatrix} 0 & -1 \\ 1 & -\dfrac{1}{R} \end{bmatrix} \begin{bmatrix} i_L \\ V_c \end{bmatrix} + \begin{bmatrix} 0 \\ 0 \end{bmatrix} V_g \quad (I.14)$$

B. Discontinuous conduction mode (DCM)

In addition to the two configurations in CCM, the third configuration that the converter can operate in is represented in Figure 3(c).

The differential equations describe the behavior of the system when the converter is functioning in DCM are as in 15, with both the MOSFET and diode turned off.

$$\begin{cases} L\dfrac{di_L}{dt} = 0 \\ \dfrac{V_c}{R} - C\dfrac{dV_c}{dt} = 0 \end{cases} \quad (I.15)$$

From 15, the state equation matrices can be written as follow:

$$\begin{bmatrix} L & 0 \\ 0 & C \end{bmatrix} \begin{bmatrix} \dfrac{di_L}{dt} \\ \dfrac{dV_c}{dt} \end{bmatrix} = \begin{bmatrix} 0 & 0 \\ 0 & -\dfrac{1}{R} \end{bmatrix} \begin{bmatrix} i_L \\ V_c \end{bmatrix} + \begin{bmatrix} 0 \\ 0 \end{bmatrix} V_g \quad (I.16)$$

3.2.2. Model with internal resistance

In order to create an accurate buck converter model, its internal resistances must be taken into account. These internal resistances can cause losses in power, ripples in input current, and changes in the converter's output characteristics. Thus, including these resistances in the model allows for more accurate predictions and analysis of the converter's performance.

Figure 4 displays the internal resistances of the buck converter and its possible configurations.

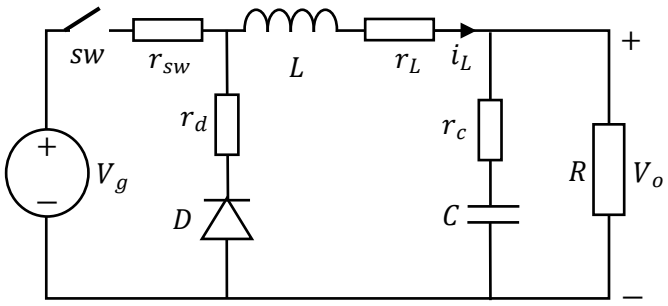

(a) Buck converter with internal resistances of the component

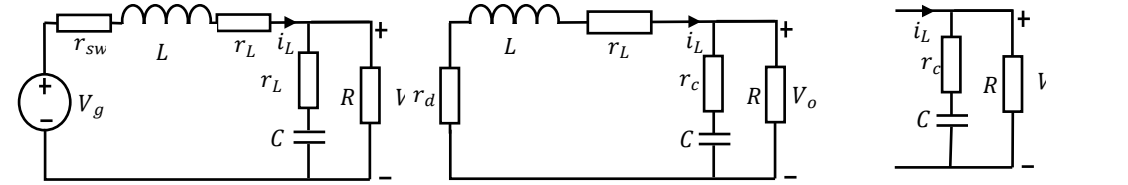

(b) sw is ON, D is OFF (c) sw is OFF, D is ON (d) sw is OFF, D is OFF

Figure I. 4. Buck converter with internal resistance and the possible configurations

A. Continuous conduction mode (CCM)

The converter in continuous conduction mode can be configured in two ways, as seen in Figure 4(b) and 4(c).

In 'ON' mode, the differential equations associated with the state variables are represented as in 17.

$$\begin{cases} V_g(t) = R_{sw} i_L(t) + L\dfrac{di_L(t)}{dt} + r_L i_L(t) + V_o(t) \\ L\dfrac{di_L(t)}{dt} = V_g(t) - R_{sw} i_L(t) - r_L i_L(t) - V_o(t) \\ C\dfrac{dV_c(t)}{dt} = \dfrac{R}{R + r_c} i_L(t) - \dfrac{1}{R + r_c} V_c(t) \end{cases} \quad \text{(I.17)}$$

This yield to:

$$\begin{cases} \dfrac{di_L(t)}{dt} = \dfrac{V_g}{L} - \dfrac{[r_{sw} + r_L + \left(\frac{Rr_c}{R + r_c}\right)]}{L} i_L(t) - \dfrac{R}{L(R + r_c)} V_c(t) \\ \dfrac{dV_c(t)}{dt} = \dfrac{R}{C(R + r_c)} i_L(t) - \dfrac{1}{C(R + r_c)} V_c(t) \\ V_o(t) = (R // r_c) i_L(t) + \dfrac{R}{R + r_c} V_c(t) \\ i_g(t) = i_L(t) \end{cases} \quad \text{(I.18)}$$

Furthermore

$$\begin{cases} \begin{bmatrix} \frac{di_L}{dt} \\ \frac{dV_c}{dt} \end{bmatrix} = \begin{bmatrix} -\frac{(r_{sw}+r_L+(R//r_c))}{L} & \frac{-R}{L(R+r_c)} \\ \frac{R}{C(R+r_c)} & \frac{-1}{C(R+r_c)} \end{bmatrix} \begin{bmatrix} i_L(t) \\ V_c(t) \end{bmatrix} + \begin{bmatrix} 1 \\ 0 \end{bmatrix} V_g(t) \\ \begin{bmatrix} V_o(t) \\ i_g(t) \end{bmatrix} = \begin{bmatrix} (R//r_c) & \frac{R}{R+r_c} \\ 1 & 0 \end{bmatrix} \begin{bmatrix} i_L(t) \\ V_c(t) \end{bmatrix} + \begin{bmatrix} 0 \\ 0 \end{bmatrix} V_g(t) \end{cases} \quad \text{(I.19)}$$

Finely

$$\begin{cases} A1 = \begin{bmatrix} -\frac{(r_{sw}+R_L+(R//R_c))}{L} & \frac{-R}{L(R+r_c)} \\ \frac{R}{C(R+r_c)} & \frac{-1}{C(R+r_c)} \end{bmatrix}, \\ B1 = \begin{bmatrix} \frac{V_g}{L} \\ 0 \end{bmatrix}, \\ C1 = \begin{bmatrix} (R//r_c) & \frac{R}{R+r_c} \\ 1 & 0 \end{bmatrix} \\ E1 = \begin{bmatrix} 0 \\ 0 \end{bmatrix} \end{cases} \quad \text{(I.20)}$$

In the 'OFF' mode, the state equation is expressed as in 21.

$$\begin{cases} L\frac{di_L(t)}{dt} = -[r_d + r_L + \left(\frac{R}{r_c}\right)]i_L(t) - \frac{R}{R+r_c}V_c(t) \\ C\frac{dV_c(t)}{dt} = \frac{R}{R+r_c}i_L(t) - \frac{1}{R+r_c}V_c(t) \\ V_o(t) = (R//r_c)i_L(t) + \frac{R}{R+r_c}V_c(t) \\ i_g(t) = 0 \end{cases} \quad \text{(I.21)}$$

State equation matrices are given as

$$\begin{cases} \begin{bmatrix} L & 0 \\ 0 & C \end{bmatrix} \begin{bmatrix} \frac{di_L}{dt} \\ \frac{dV_c}{dt} \end{bmatrix} = \begin{bmatrix} -(r_d + r_L + (R//r_c)) & \frac{-R}{R+r_c} \\ \frac{R}{R+r_c} & \frac{-1}{R+r_c} \end{bmatrix} \begin{bmatrix} i_L(t) \\ V_c(t) \end{bmatrix} + \begin{bmatrix} 0 \\ 0 \end{bmatrix} V_g(t) \\ \begin{bmatrix} V_o(t) \\ i_g(t) \end{bmatrix} = \begin{bmatrix} (R//r_c) & \frac{R}{R+r_c} \\ 0 & 0 \end{bmatrix} \begin{bmatrix} i_L(t) \\ V_c(t) \end{bmatrix} + \begin{bmatrix} 0 \\ 0 \end{bmatrix} V_g(t) \end{cases} \quad \text{(I.22)}$$

Therefore,

$$\begin{cases} A2 = \begin{bmatrix} -\dfrac{(r_d + r_L + (R//r_c))}{L} & \dfrac{-R}{L(R + r_c)} \\ \dfrac{R}{C(R + r_c)} & \dfrac{-1}{C(R + r_c)} \end{bmatrix}, \\ B2 = \begin{bmatrix} 0 \\ 0 \end{bmatrix}, \\ C2 = \begin{bmatrix} (R//r_c) & \dfrac{R}{R + r_c} \\ 0 & 0 \end{bmatrix} \\ E2 = \begin{bmatrix} 0 \\ 0 \end{bmatrix} \end{cases} \quad \text{(I.23)}$$

B. Discontinuous conduction mode (DCM)

When the converter is operating in DCM, there is an additional configuration compared to when it is operating in CCM. This configuration is shown in Figure 4(d).

When both the MOSFET and diode are 'OFF', the differential equations that represent the system can be written as:

$$\begin{cases} L\dfrac{di_L}{dt} = 0 \\ C\dfrac{dV_c}{dt} = \dfrac{1}{R + r_c}V_c \end{cases} \quad \text{(I.24)}$$

State equation matrices are given as:

$$\begin{bmatrix} \dfrac{di_L}{dt} \\ \dfrac{dV_c}{dt} \end{bmatrix} = \begin{bmatrix} 0 & 0 \\ 0 & \dfrac{1}{C(R + r_c)} \end{bmatrix} \begin{bmatrix} i_L \\ V_c \end{bmatrix} + \begin{bmatrix} 0 \\ 0 \end{bmatrix} V_g \quad \text{(I.25)}$$

4. Boost Converter

The boost converter can provide a dc output voltage that is higher than the dc input voltage. Figure I.5 (a) depicts the topology of the circuit of a boost converter.

When the transistor is turned on, the current in inductor L rises linearly, while capacitor C delivers the load current and is slightly drained at the same time. When the transistor is turned off for the second time, the diode D is turned on, and the inductor L feeds the load while also charging the capacitor C [1]. The different possible configurations of boost converter are shown in Figure 5.

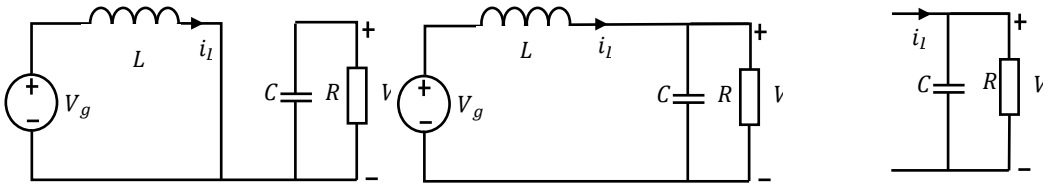

(b) sw is ON, D is OFF (c) sw is OFF, D is ON (d) sw is OFF, D is OFF

Figure I. 5. The possible configurations of boost converter

4.1. Basic analysis

In CCM and according to the state of the switch and the diode, we have the two configurations shown in figure 5(b) and (c).

Figure 6 depicts the steady-state inductor current waveform.

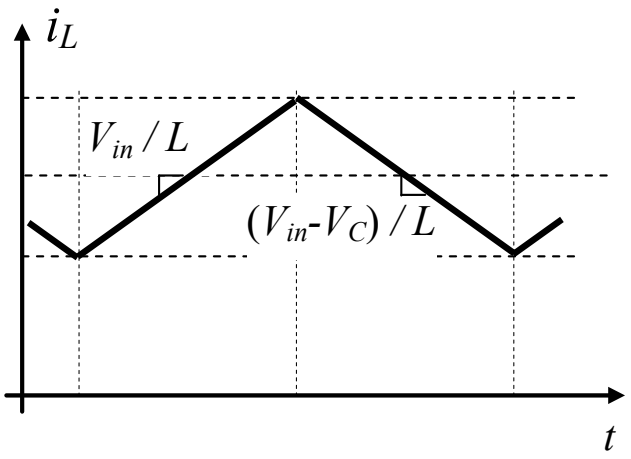

Figure I. 6. The steady-state inductor current waveform of boost converter

The steady state output voltage equation is obtained by applying the inductor volt balance principle as follow:

$$\frac{V_O}{V_G} = \frac{1}{(1-D)} \tag{I.26}$$

The input current, which is also the inductor current, is greater than the output current because the converter output voltage exceeds the input voltage. In practice, the inductor current passing through semiconductors SW and D causes the inductor winding resistance to rise significantly, resulting in significant power loss due to component non-idealities and it becomes higher as the duty cycle approaches one.

4.2. State space model

4.2.1. Model with ideal components

This subsection derives the state space model of the ideal boost converter, depicted in figure 5, where all the components of the converter are assumed to be ideal.

A. Continuous conduction mode (CCM)

As long as the converter is operating in CCM, two configurations are possible, as depicted in Figure 5(b) and 5(c).

During ON Mode the KVL and KCL of figure 5(b) give the following equations:

$$\begin{cases} V_g - L\dfrac{di_L}{dt} = 0 \\ \dfrac{V_c}{R} + C\dfrac{dV_c}{dt} = 0 \end{cases} \tag{I.27}$$

State equation matrices are given as

$$\begin{bmatrix} L & 0 \\ 0 & C \end{bmatrix}\begin{bmatrix} \dfrac{di_L}{dt} \\ \dfrac{dV_c}{dt} \end{bmatrix} = \begin{bmatrix} 0 & 0 \\ 0 & -\dfrac{1}{R} \end{bmatrix}\begin{bmatrix} i_L \\ V_c \end{bmatrix} + \begin{bmatrix} 1 \\ 0 \end{bmatrix} V_g \tag{I.28}$$

Figure 3(c) represents the system during OFF Mode, so the differential equation representing the state of the system will be as follow:

$$\begin{cases} V_g - V_c - L\dfrac{di_L}{dt} = 0 \\ i_L - \dfrac{V_c}{R} - C\dfrac{dV_c}{dt} = 0 \end{cases} \tag{I.29}$$

State equation matrices are given as:

$$\begin{bmatrix} L & 0 \\ 0 & C \end{bmatrix}\begin{bmatrix} \dfrac{di_L}{dt} \\ \dfrac{dV_c}{dt} \end{bmatrix} = \begin{bmatrix} 0 & -1 \\ 1 & -\dfrac{1}{R} \end{bmatrix}\begin{bmatrix} i_L \\ V_c \end{bmatrix} + \begin{bmatrix} 1 \\ 0 \end{bmatrix} V_g \tag{I.30}$$

B. Discontinuous conduction mode (DCM)

When the converter is in DCM, there is an additional configuration compared to the two configurations in CCM, as shown in Figure 3(d).

When both the MOSFET and diode are off, the differential equations representing the system are given in 31.

$$\begin{cases} L\dfrac{di_L}{dt} = 0 \\ \dfrac{V_c}{R} - C\dfrac{dV_c}{dt} = 0 \end{cases} \tag{I.31}$$

State equation matrices are given as:

$$\begin{bmatrix} L & 0 \\ 0 & C \end{bmatrix} \begin{bmatrix} \dfrac{di_L}{dt} \\ \dfrac{dV_c}{dt} \end{bmatrix} = \begin{bmatrix} 0 & 0 \\ 0 & -\dfrac{1}{R} \end{bmatrix} \begin{bmatrix} i_L \\ V_c \end{bmatrix} + \begin{bmatrix} 0 \\ 0 \end{bmatrix} V_g \tag{I.32}$$

4.2.2. Model with internal resistance

Unlike the previous subsection, the internal resistances are taken into consideration to have more accurate converter model. Figure (4) shows the boost converter with internal resistances and its possible configurations.

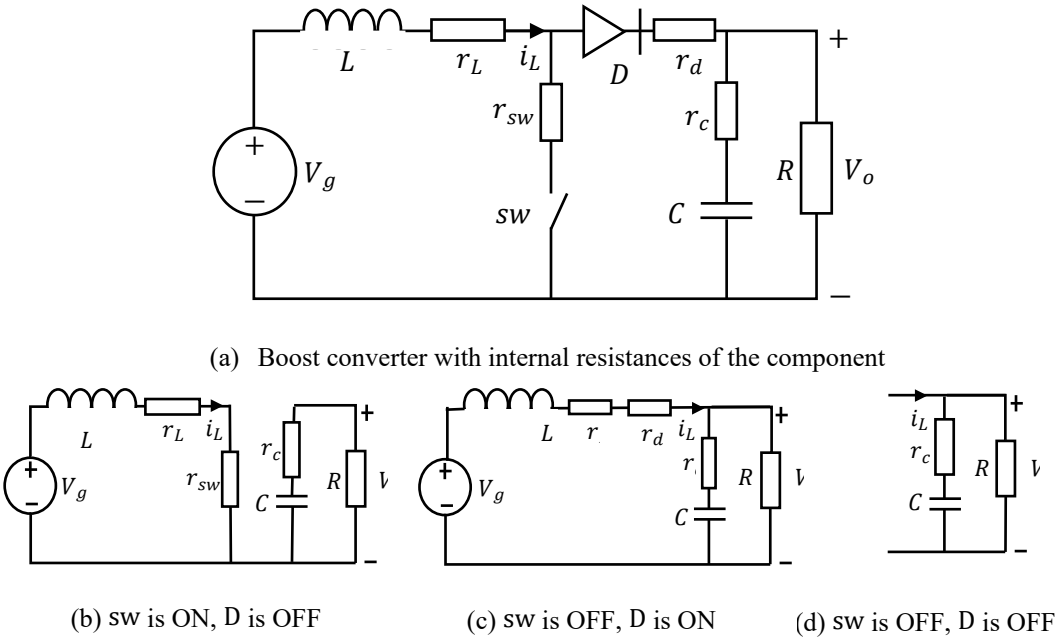

(a) Boost converter with internal resistances of the component

(b) sw is ON, D is OFF (c) sw is OFF, D is ON (d) sw is OFF, D is OFF

Figure I. 7. Boost converter with internal resistance and the possible configurations

A. Continuous conduction mode (CCM)

When the converter is working in continuous-conduction mode (CCM), there are two possible configurations, as shown in Figure 7(b) and 7(c).

When in "ON" mode, the system can be represented by the differential equation in 1.

$$\begin{cases} \mathrm{L}\dfrac{\mathrm{di_L}}{\mathrm{dt}} = \mathrm{V_g} - (\mathrm{r_L} + \mathrm{r_{sw}})\mathrm{i_L} \\ \mathrm{C}\dfrac{\mathrm{dV_c}}{\mathrm{dt}} = -\dfrac{1}{\mathrm{R} + \mathrm{r_c}}\mathrm{V_c} \\ V_o = \dfrac{R}{R + r_c}V_c \\ I_g = I_L \end{cases} \tag{I.33}$$

State equation matrices are given as:

$$\begin{cases} \begin{bmatrix} \mathrm{L} & 0 \\ 0 & \mathrm{C} \end{bmatrix}\begin{bmatrix} \dfrac{\mathrm{di_L}}{\mathrm{dt}} \\ \dfrac{\mathrm{dV_c}}{\mathrm{dt}} \end{bmatrix} = \begin{bmatrix} -(\mathrm{r_L} + \mathrm{r_{sw}}) & 0 \\ 0 & -\dfrac{1}{(\mathrm{R} + \mathrm{r_c})} \end{bmatrix}\begin{bmatrix} \mathrm{i_L} \\ \mathrm{V_c} \end{bmatrix} + \begin{bmatrix} 1 \\ 0 \end{bmatrix}\mathrm{V_g} \\ \begin{bmatrix} \mathrm{V_o(t)} \\ \mathrm{i_g(t)} \end{bmatrix} = \begin{bmatrix} 0 & \dfrac{R}{R + r_c} \\ 1 & 0 \end{bmatrix}\begin{bmatrix} \mathrm{i_L(t)} \\ \mathrm{V_c(t)} \end{bmatrix} + \begin{bmatrix} 0 \\ 0 \end{bmatrix}V_g(\mathrm{t}) \end{cases} \tag{I.34}$$

Therefore,

$$\begin{cases} \mathrm{A1} = \begin{bmatrix} -\dfrac{(\mathrm{r_L} + \mathrm{r_{sw}})}{L} & 0 \\ 0 & -\dfrac{1}{C(\mathrm{R} + \mathrm{r_c})} \end{bmatrix} \\ \mathrm{B1} = \begin{bmatrix} \dfrac{\mathrm{V_g}}{L} \\ 0 \end{bmatrix}, \\ \mathrm{C1} = \begin{bmatrix} 0 & \dfrac{\mathrm{R}}{\mathrm{R} + \mathrm{r_c}} \\ 1 & 0 \end{bmatrix} \\ \mathrm{E1} = \begin{bmatrix} 0 \\ 0 \end{bmatrix} \end{cases} \tag{I.35}$$

During 'OFF' Mode:

$$\begin{cases} \mathrm{L}\dfrac{\mathrm{di_L}}{\mathrm{dt}} = \left(-\mathrm{r_d} - \mathrm{r_L} - \dfrac{\mathrm{Rr_c}}{\mathrm{R} + \mathrm{r_c}}\right)\mathrm{i_L} - \dfrac{\mathrm{R}}{\mathrm{R} + \mathrm{r_c}}\mathrm{V_c} + \mathrm{V_g} \\ \mathrm{C}\dfrac{\mathrm{dV_c}}{\mathrm{dt}} = \dfrac{\mathrm{R}}{\mathrm{R} + \mathrm{r_c}}\mathrm{i_L} - \dfrac{1}{\mathrm{R} + \mathrm{r_c}}\mathrm{V_c} \\ \mathrm{V_o(t)} = (\mathrm{R}//\mathrm{r_c})\mathrm{i_L(t)} + \dfrac{\mathrm{R}}{\mathrm{R} + \mathrm{r_c}}\mathrm{V_c(t)} \\ I_g = I_L \end{cases} \tag{I.36}$$

State equation matrices are given as:

$$\begin{cases} \begin{bmatrix} L & 0 \\ 0 & C \end{bmatrix} \begin{bmatrix} \frac{di_L}{dt} \\ \frac{dV_c}{dt} \end{bmatrix} = \begin{bmatrix} r_d - r_L - \frac{Rr_c}{R+r_c} & -\frac{R}{(R+r_c)} \\ \frac{R}{(R+r_c)} & -\frac{1}{(R+r_c)} \end{bmatrix} \begin{bmatrix} i_L \\ V_c \end{bmatrix} + \begin{bmatrix} 1 \\ 0 \end{bmatrix} V_g \\ \begin{bmatrix} V_o(t) \\ i_g(t) \end{bmatrix} = \begin{bmatrix} (R//r_c) & \frac{R}{R+r_c} \\ 1 & 0 \end{bmatrix} \begin{bmatrix} i_L(t) \\ V_c(t) \end{bmatrix} + \begin{bmatrix} 0 \\ 0 \end{bmatrix} V_g(t) \end{cases} \quad \text{(I.37)}$$

Therefore,

$$\begin{cases} A2 = \begin{bmatrix} \frac{r_d - r_L - \frac{Rr_c}{R+r_c}}{L} & -\frac{R}{L(R+r_c)} \\ \frac{R}{C(R+r_c)} & \frac{-1}{C(R+r_c)} \end{bmatrix} \\ B2 = \begin{bmatrix} \frac{V_g}{L} \\ 0 \end{bmatrix}, \\ C2 = \begin{bmatrix} (R//r_c) & \frac{R}{R+r_c} \\ 1 & 0 \end{bmatrix} \\ E2 = \begin{bmatrix} 0 \\ 0 \end{bmatrix}, \end{cases} \quad \text{(I.38)}$$

B. Discontinuous conduction mode (DCM)

In DCM, there is an additional configuration in addition to the two configurations in CCM, which is represented in Figure 7(d).

When both the MOSFET and diode are 'OFF', the differential equations that represent the system are given in Equation 1.

$$\begin{cases} L\frac{di_L}{dt} = 0 \\ C\frac{dV_c}{dt} = \frac{1}{R+r_c}V_c \end{cases} \quad \text{(I.39)}$$

State equation matrices are given as:

$$\begin{bmatrix} \frac{di_L}{dt} \\ \frac{dV_c}{dt} \end{bmatrix} = \begin{bmatrix} 0 & 0 \\ 0 & \frac{1}{C(R+r_c)} \end{bmatrix} \begin{bmatrix} i_L \\ V_c \end{bmatrix} + \begin{bmatrix} 0 \\ 0 \end{bmatrix} V_g \quad \text{(I.40)}$$

5. Buck-Boost Converter

The buck-boost converter is a useful tool for applications that require a constant dc voltage but the input voltage may vary. For example, it can be used to power microprocessor-based systems that need a regulated voltage, as the input voltage may vary when the system is

supplied by a battery. It is also useful for applications where the output voltage needs to be both higher and lower than the input voltage, like when powering a variable speed motor or lighting system. The buck-boost converter can also be used to step up or step down the voltage for applications such as power supplies, motor drives, and solar power conversion [1].

Figure 8 illustrates the topology of a buck-boost converter.

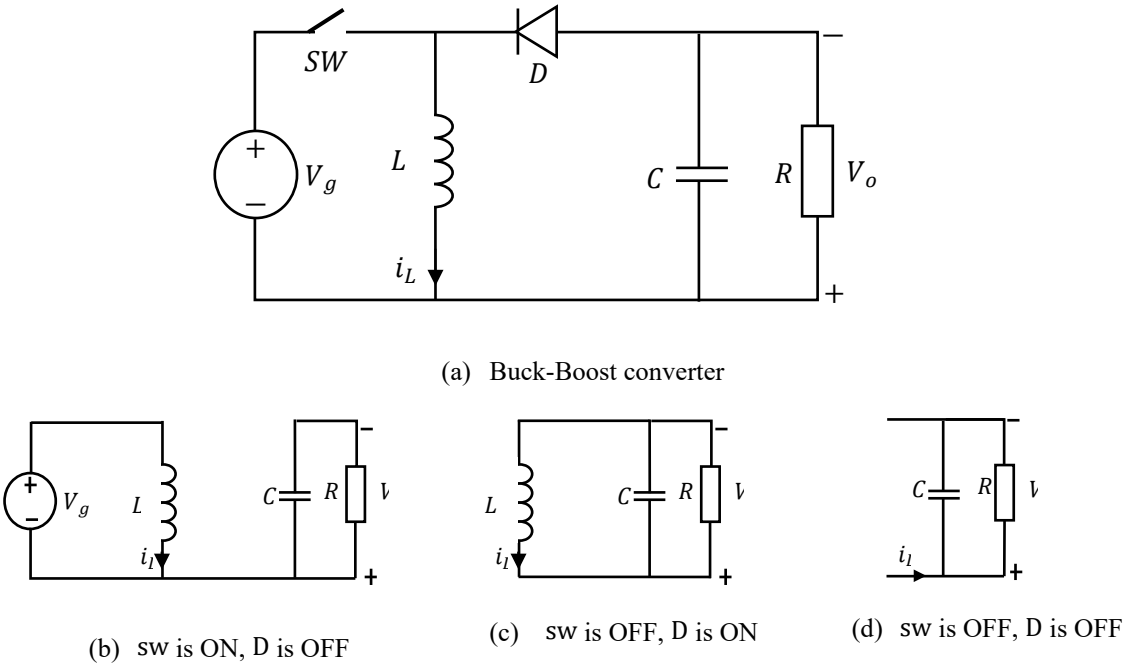

(a) Buck-Boost converter

(b) sw is ON, D is OFF (c) sw is OFF, D is ON (d) sw is OFF, D is OFF

Figure I. 8. Buck-boost converter without internal resistance and the possible configurations

5.1. Basic analysis

When the switch is turned on, the input voltage is applied across the inductor L, causing the current to rise linearly. During this time, the capacitor C supplies the load current and is partially discharged. When the switch is off, the voltage across the inductor reverses in polarity and the diode conducts. At this point, the energy stored in the inductor is used to both supply the load and recharge the capacitor. Figure 9 depicts the steady-state inductor current and voltage waveform.

The steady state output voltage equation can be found using the inductor volt balance concept as follow:

$$V_G.T_{on} + V_O.T_{off} = 0 \tag{I.41}$$

$$\frac{V_O}{V_G} = -\frac{D}{1-D} \tag{I.42}$$

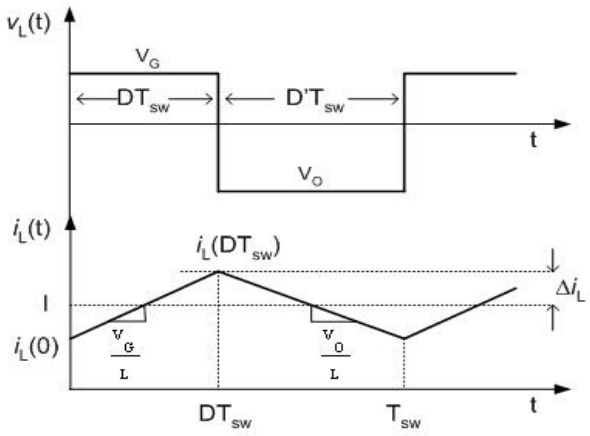

Figure I. 9. Steady-state inductor current and voltage waveform

5.2. State space model

5.2.1. Model without internal resistance

In this subsection, the state space model of the Buck-boost converter is derived, with the assumption that the components of the converter are ideal. The various configurations of the converter are shown in Figure 8.

A. Continuous conduction mode (CCM)

When the converter is operating in CCM, two possible configurations can be seen in Figures 8(b) and 8(c).

The system can be represented by the differential equation in 1 when it is in "ON" mode.

$$\begin{cases} L\dfrac{di_L}{dt} = V_g \\ C\dfrac{dV_c}{dt} = \dfrac{V_c}{R} \end{cases} \tag{I.43}$$

State equation matrices are given as:

$$\begin{bmatrix} \dfrac{di_L}{dt} \\ \dfrac{dV_c}{dt} \end{bmatrix} = \begin{bmatrix} 0 & 0 \\ 0 & -\dfrac{1}{RC} \end{bmatrix} \begin{bmatrix} i_L \\ V_c \end{bmatrix} + \begin{bmatrix} \dfrac{1}{L} \\ 0 \end{bmatrix} V_g \tag{I.44}$$

When the switch is open the differential equation can be written as in in 45.

$$\begin{cases} L\dfrac{di_L}{dt} = -V_g \\ C\dfrac{dV_c}{dt} = i_L - \dfrac{V_c}{R} \end{cases} \tag{I.45}$$

State equation matrices are given as:

$$\begin{bmatrix} L & 0 \\ 0 & C \end{bmatrix}\begin{bmatrix} \dfrac{di_L}{dt} \\ \dfrac{dV_c}{dt} \end{bmatrix} = \begin{bmatrix} 0 & -\dfrac{1}{L} \\ \dfrac{1}{L} & -\dfrac{1}{R} \end{bmatrix}\begin{bmatrix} i_L \\ V_c \end{bmatrix} + \begin{bmatrix} 0 \\ 0 \end{bmatrix}V_g \tag{I.46}$$

B. Discontinuous conduction mode (DCM)

In DCM, there is an additional configuration in addition to the two in CCM, which is shown in Figure 7(d).

When both the MOSFET and the diode are off, the differential equations representing the system are as represented in 46.

$$\begin{cases} L\dfrac{di_L}{dt} = 0 \\ \dfrac{V_c}{R} - C\dfrac{dV_c}{dt} = 0 \end{cases} \tag{I.47}$$

State equation matrices are given as:

$$\begin{bmatrix} L & 0 \\ 0 & C \end{bmatrix}\begin{bmatrix} \dfrac{di_L}{dt} \\ \dfrac{dV_c}{dt} \end{bmatrix} = \begin{bmatrix} 0 & 0 \\ 0 & -\dfrac{1}{R} \end{bmatrix}\begin{bmatrix} i_L \\ V_c \end{bmatrix} + \begin{bmatrix} 0 \\ 0 \end{bmatrix}V_g \tag{I.48}$$

5.2.2. Model with internal resistance

In this section, the internal resistances of the Buck-Boost converter are included to create a more precise model. This can be seen in Figure (6), which displays the internal resistances and configurations of the Buck-boost converter.

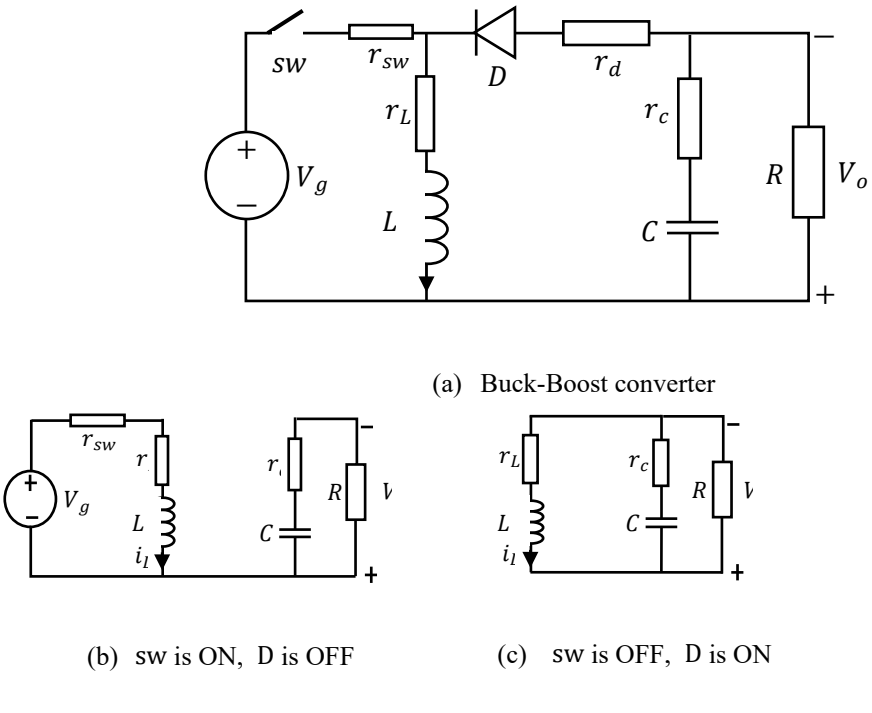

(a) Buck-Boost converter

(b) sw is ON, D is OFF (c) sw is OFF, D is ON (d) sw is OFF, D is OFF

Figure I. 10. Buck-boost converter with internal resistance and the possible configurations

A. Continuous conduction mode (CCM)

When operating in CCM, the converter has two possible configurations, as illustrated in Figure 8(b) and 8(c).

The relevant differential equations for the state variables are given in Equation 1.

$$\begin{cases} L\dfrac{dI_L}{dt} = V_g - (r_L + r_{sw})i_L \\ C\dfrac{dV_c}{dt} = -\dfrac{V_c}{R + r_c} \\ V_o = \dfrac{R}{R + r_c}V_c \\ i_g = i_L \end{cases} \tag{I.49}$$

State equation matrices are given as :

$$\begin{cases} \begin{bmatrix} L & 0 \\ 0 & C \end{bmatrix} \begin{bmatrix} \dfrac{di_L}{dt} \\ \dfrac{dV_C}{dt} \end{bmatrix} = \begin{bmatrix} -(r_L + r_{sw}) & 0 \\ 0 & -\dfrac{1}{R + r_c} \end{bmatrix} \begin{bmatrix} i_L(t) \\ V_c(t) \end{bmatrix} + \begin{bmatrix} 1 \\ 0 \end{bmatrix} V_g(t) \\ \begin{bmatrix} V_o(t) \\ i_g(t) \end{bmatrix} = \begin{bmatrix} 0 & \dfrac{R}{R + r_c} \\ 1 & 0 \end{bmatrix} \begin{bmatrix} i_L(t) \\ V_c(t) \end{bmatrix} + \begin{bmatrix} 0 \\ 0 \end{bmatrix} V_g(t) \end{cases} \tag{I.50}$$

Therefore,

$$\begin{cases} \mathrm{A1} = \begin{bmatrix} \dfrac{-(r_L + R_{sw})}{\mathrm{L}} & 0 \\ 0 & \dfrac{-1}{\mathrm{C(R + r_c)}} \end{bmatrix}, \\ \mathrm{B1} = \begin{bmatrix} \dfrac{\mathrm{V_g}}{\mathrm{L}} \\ 0 \end{bmatrix}, \\ \mathrm{C1} = \begin{bmatrix} 0 & \dfrac{\mathrm{R}}{\mathrm{R + r_c}} \\ 1 & 0 \end{bmatrix} \\ \mathrm{E1} = \begin{bmatrix} 0 \\ 0 \end{bmatrix} \end{cases} \quad \text{(I.51)}$$

Similarly the equivalent circuit when switch SW is off and D is ON

State equation for above circuit is given by:

$$\begin{cases} L\dfrac{dI_L}{dt} = -\dfrac{R}{(R + r_C)}V_C + (r_c \,//\, R - r_L - r_d)i_L \\ C\dfrac{dV_c}{dt} = -\dfrac{V_C}{(R + r_c)} + \dfrac{R}{(R + r_c)}i_L \\ \mathrm{V_o(t) = (R//r_C)i_L(t) + \dfrac{R}{R + r_c}V_c(t)} \\ \mathrm{i_g(t) = 0} \end{cases} \quad \text{(I.52)}$$

State equation matrices are given as

$$\begin{cases} \begin{bmatrix} \mathrm{L} & 0 \\ 0 & \mathrm{C} \end{bmatrix} \begin{bmatrix} \dfrac{\mathrm{di_L}}{\mathrm{dt}} \\ \dfrac{\mathrm{dV_c}}{\mathrm{dt}} \end{bmatrix} = \begin{bmatrix} (r_c \,//\, R - r_L - r_d) & \dfrac{-\mathrm{R}}{\mathrm{R + r_c}} \\ \dfrac{\mathrm{R}}{\mathrm{R + r_c}} & \dfrac{-1}{\mathrm{R + r_c}} \end{bmatrix} \begin{bmatrix} \mathrm{i_L(t)} \\ \mathrm{V_c(t)} \end{bmatrix} + \begin{bmatrix} 0 \\ 0 \end{bmatrix} \mathrm{V_g(t)} \\ \begin{bmatrix} \mathrm{V_o(t)} \\ \mathrm{i_g(t)} \end{bmatrix} = \begin{bmatrix} \mathrm{(R//r_c)} & \dfrac{\mathrm{R}}{\mathrm{R + r_c}} \\ 0 & 0 \end{bmatrix} \begin{bmatrix} \mathrm{i_L(t)} \\ \mathrm{V_c(t)} \end{bmatrix} + \begin{bmatrix} 0 \\ 0 \end{bmatrix} \mathrm{V_g(t)} \end{cases} \quad \text{(I.53)}$$

Therefore,

$$\begin{cases} A2 = \begin{bmatrix} \frac{(r_c // R - r_L - r_D)}{L} & \frac{-R}{L(R + r_c)} \\ \frac{R}{C(R + r_c)} & \frac{-1}{C(R + r_c)} \end{bmatrix}, \\ B2 = \begin{bmatrix} 0 \\ 0 \end{bmatrix}, \\ C2 = \begin{bmatrix} (R//r_c) & \frac{R}{R + r_c} \\ 0 & 0 \end{bmatrix} \\ E2 = \begin{bmatrix} 0 \\ 0 \end{bmatrix}, \end{cases} \quad \text{(I.54)}$$

B. Discontinuous conduction mode (DCM)

When the converter is functioning in DCM there is one more configuration in addition to those two in CCM, these configuration is represented in figure 8(d).

When both Mosfet and diode are 'OFF', the differential equations that represent the system will be as follow:

$$\begin{cases} L\frac{di_L}{dt} = 0 \\ C\frac{dV_c}{dt} = \frac{1}{R + r_c}V_c \end{cases} \quad \text{(I.55)}$$

State equation matrices are given as :

$$\begin{bmatrix} \frac{di_L}{dt} \\ \frac{dV_c}{dt} \end{bmatrix} = \begin{bmatrix} 0 & 0 \\ 0 & \frac{1}{C(R + r_C)} \end{bmatrix} \begin{bmatrix} i_L \\ V_c \end{bmatrix} + \begin{bmatrix} 0 \\ 0 \end{bmatrix} V_g \quad \text{(I.56)}$$

6. Conclusion

Static converters ensure energy conversion in two conduction modes CCM and DCM depending on the context of use. The efficiency and performance of these systems is affected by the imperfection of the elements constituting the converter and a modeling and control technique must not overlook this concept.

The development of a model for the converter represents a key element for understanding its behavior and for achieving, then, the objectives of the control, each modeling technique has advantages as it has disadvantages and the choice is determined by the context of use and the objectives.

The average model gives a description of non-linearity, at the low frequency scale, of the converter and allows the synthesis of nonlinear controllers. However, this model is unable to describe abnormal behaviors at the high frequency scale of the system. In the other hand, the detailed model allows the restitution or reproduction of the state of the system for verification and/or validation purposes. Nevertheless, the calculation time and the memory space allocated to this model are the major disadvantage of this technique.

Chapter II

Nonlinear phenomena in static converters. Application to a buck converter

1. Introduction

Static converters are often designed to operate in a stable and periodic manner, with the waveforms of the converter state variables being repeated at a rate equal to the switching frequency defined by the PWM block in steady state. This behavior is described as typical or in period 1 and it has the benefit of being basic and predictable, making the converter's analysis and control much easier. Despite this, a vast number of characteristics can affect the periodic regime and the stability of static converters, which can switch from one regime to another in a complex and unpredictable manner.

The study of energy conversion systems has become increasingly important due to the growing demand for efficient and reliable power supplies. Advanced modeling approaches can be used to simulate the behavior of these systems, which enables researchers to gain a better understanding of their behavior. Furthermore, advanced analysis techniques can be used to identify potential problems in the system, which can then be addressed with appropriate solutions. These analysis techniques can also help identify areas where further research is needed in order to improve the performance of the system. Additionally, these methods can be used to develop better control strategies for energy conversion systems, which can help reduce energy losses and improve overall efficiency. With the help of these tools, researchers can gain a better understanding of how energy conversion systems work, and develop better solutions to make them more efficient.

Furthermore, advancements in computer technology have made it possible to develop specialized software that can be used to model and simulate nonlinear systems. This software can be used to predict and investigate the responses of nonlinear systems in scenarios that would be too difficult or impossible to analyze with analytical methods. Additionally, this software can be used to compare the performance of different nonlinear systems, providing valuable insights into how these systems behave under a variety of conditions.

In this chapter, we will explore nonlinear behaviors of static converters when their parameters are varied. To do so, we will first review the key definitions for the different behaviors of dynamic systems, including chaos and bifurcation, the most complex and unpredictable behaviors, followed by simulation results that illustrate the various nonlinear phenomena that emerge as the parameters of the buck converter are varied.

2. Nonlinear phenomena in the literature

Numerous research papers from around the world have investigated nonlinear phenomena. In 1988, D. C. Hamil published an article regarding the dynamic analysis of bifurcation and chaos in a voltage-mode controlled converter [2]. To our knowledge, this was the first analysis of bifurcation and chaotic dynamics in static converters, using differential equations to describe the behavior of the converter, and a feedback-type control in conjunction with the PWM technique to identify the stable and unstable regions of the closed-loop system.

In 1992, a team headed by D. C. Hamil identified a wide selection of power electronic circuits with chaotic behavior [3]. In [4], researchers further examined the first and second order PWM controls in the voltage mode of the Buck converter. By using the input voltage as the bifurcation parameter, the converter moved from a stable operation to sub-harmonic oscillations, and eventually to chaos as the value of the parameter was changed. This chaos was illustrated by determining the boundary conditions of the circuit's differential equations through simulation and experimentation. Bifurcation diagrams, phase plane, and time responses were used to represent the results.

In 1990, Krein and Bass [5] highlighted the importance of studying nonlinear phenomena in the domain of power electronics. Through the results of their experiments, they identified the zones of instability, the borders of these zones, and the area of chaotic behavior.

The work of D.C. Hamill has been widely accepted in the area of power electronics, as his paper on a control attempt for a Buck converter operating in continuous conduction mode has allowed for the exploration of period doubling and chaos in simulations and laboratory measurements. Utilizing SPICE software, his 1992 paper provided a platform for the application of chaos theory to power electronic circuits, which has since been studied in detail. Various numerical techniques have been developed in order to further explore the chaotic behavior of this type of converter, with many researchers attempting to develop a better understanding of the effects of chaos on the system. The implications of chaos theory on a power electronic system have been studied in depth, and the work of D.C. Hamill has provided a foundation for further exploration.

C.K. Tse conducted a comprehensive analysis in 1994 [6] on the period doubling bifurcation phenomenon for the Boost converter operating in discontinuous conduction mode. He employed both analytical and numerical techniques, such as linearization of the circuit

equations and a shooting method to solve the boundary value problem, to develop a successful model. Subsequent simulations and laboratory measurements validated the model's accuracy, demonstrating close agreement with the physical system.

Tse also conducted a similar study on a Buck converter operating in discontinuous mode in the same year [7]. Finally, the publication of [8] in 1997 provided a formal theoretical study of period doubling in the discontinuous mode of static converters.

In the same context, Cha in 1995 published supplementary material on bifurcation and abnormal behaviors of the Buck converter [9]. This study investigated in depth the nonlinear behavior of a converter when any of its circuit parameters, including inductance, load resistance, and output capacitance, were altered.

K. Tse studied the occurrences of bifurcation and chaos in a current-controlled Cuk-type static converter in 1995 [10]; the experimental verification was published in 1996 [11].

In 1996, the authors of [12] presented a mathematical analysis of the in-period and in-period behaviors of a Buck converter, as well as the limits of its chaotic attractor. Based on the concept of state density, the authors of [13] performed an analysis of nonlinear phenomena in static converters.

The study of the nonlinear phenomena of the Buck converter in voltage mode occupies a significant portion of the literature. While the current mode compels the Boost and Buck-Boost converters to exhibit a wide range of nonlinear phenomena, the Boost and Buck-Boost converters are subject to a number of nonlinear effects. In fact, Dean et al. [14], [15] reported for the first time the chaotic behavior of the current-mode controlled Boost converter. In this context, it is also important to mention the works [16] and [17] devoted to the investigation of the various routes and routes to chaos and their dependence on the selection of bifurcation parameters.

Banerjee et al. [18] performed a similar analysis of bifurcation in a current-mode controlled boost converter. In their works [19] and [20], the two bifurcation and chaos phenomena were theoretically examined. Marrero et al. in 1999 investigated nonlinear phenomena in a current-controlled boost converter by using the average model to describe the dynamic behavior of the converter [21], with frequency and input voltage as analysis parameters.

In addition to the period doubling phenomenon, the behavior of static converters has also revealed bifurcation, quasi-periodicity, and chaos. El-Aroudi examined the nonlinear behaviors of Boost and Buck-Boost converters controlled in voltage mode to investigate their quasi-periodic and chaotic responses [22, 23].

Due to the fact that static converters are non-autonomous systems operating at a fixed frequency, the discrete time model is an effective method for studying and analyzing their dynamics, allowing for an accurate description of the converter's slow and fast dynamics. Di Bernardo [24,25] examined various sampling schemes and their applications in the identification of bifurcation and chaos within this framework. An autonomous system is deemed autonomous when external clock signals are absent. This condition occurs, for instance, if the converter is controlled by current hysteresis and the terminals of the hysteresis band control the opening and closing of the switch.

K. Tse [26,27] investigated the behavior of a current-controlled Cuk converter using a fourth-order model to characterize the Hopf-type bifurcation and the chaotic behaviors displayed by this type of converter. Using the average model of a static Boost type converter, the same group investigated the nonlinear phenomena observed at low frequencies in 2003 [28]. The author in [29] provides a summary of the state on the topic of nonlinear phenomena in static converters.

Another experimental study [30] focused on the appearance mechanism of Hopf-type bifurcation in a Buck-type converter. The same group of researchers [31] looked at nonlinear events in the Luo converter.

In addition, Hong's [32] research focuses on exploiting the spectrum of the converter's chaotic signal in order to minimize component interference. In this case, the Prony method was used to figure out the spectrum of the chaotic signals coming from the converter.

In 2009, El Guezar [33] took a hybrid approach to the problem and proposed a semi-analytical approach that uses the analytical expression of the solutions to analyze the nonlinear behavior of the converters and find the instants of the status events and the periodic type of temporal events.

Due to the saturation of the field in terms of obtained results, work on the analysis of nonlinear behavior of converters has become increasingly uncommon since 2009. Much greater emphasis has been placed on control, stabilization, and elimination those behaviors.

3. Definition

The study of dynamics focuses primarily on how state variables deviate from their current values over time. The dynamics can be represented geometrically by constructing a space with the state variables as coordinates. This is referred to as the state or phase space. A point in this space represents the system's state at any given time [34], [35], [36];

Starting from a given initial condition, the orbit or trajectory described by the state variables is known as the system trajectory or orbit. The evolution of the system is then translated by a displacement of the representative point in phase space, thereby tracing a phase trajectory.

When a discretized representation of the system is utilized, these trajectories are specified by an iterative application rather than by the differential equations, which are used when a continuous-time model of the system is used. We are therefore able to define the system as follows:

$$\frac{dx}{dt} = f(x,t,\mu) \; ou \; x_{n+1} = f(x_n,\mu) \tag{II.1}$$

where μ is one of the system's parameters.

Multiple equilibrium solutions exist for a dynamical system. The system converges to one of the equilibrium solutions for a given set of parameters and initial condition. This equilibrium is referred to as the attractor. An attractor is a geometric object toward which all trajectories in phase space gravitate, i.e. a state (or group of states) toward which a system evolves regardless of its original conditions. There can be multiple attractors in nonlinear systems, and depending on the initial condition, the system will converge towards one of them. Consequently, in order to determine the steady-state behavior of a system, it is necessary to identify the potential attractors and their related basins of attraction.

4. Different types of attractors

In general, we can classify attractor types as follows [36]:

A. Regular attractors

Which characterize the evolution of non-chaotic systems, can be of three types:

- ***Fixed point*:** The steady state solution is a point in the state space.

- ***Limit cycle:*** In a limit cycle or periodic orbit in state space, the trajectory follows a closed contour. In addition, this motion is associated with a finite number of frequencies that are related through rational ratios. Periodic motion occurs. Figures 1 and 2 display examples. Sometimes the phase trajectory will close in on itself. The temporal evolution is then cyclical, with the system exhibiting permanent oscillations. Limit cycles are only found in nonlinear systems, and no matter what the initial conditions were, they always lead to the same periodic regime.
- ***Quasi-periodic orbit:*** This is a type of the preceding case. The phase trajectory does not close on itself but rather rolls up on a two-dimensional manifold (for example, the trajectory moves on the surface of a torus). Motion is associated with a finite number of frequencies that are linked by irrational ratios. The motion appears to be "almost periodic," but it isn't.

B. Strange attractors

- ***Chaotic attractor:*** In state space, the trajectory appears to move randomly. Furthermore, the trajectory is bounded and the displacement is non-periodic.

5. Bifurcation

The bifurcation diagram is the most commonly used tool to highlight a typical phenomenon in nonlinear dynamical systems. If the parameters are allowed to vary, the system may abandon its equilibrium solution and seek another equilibrium solution. For example, when the parameters vary, the present equilibrium solution becomes unstable and the system is attracted to another stable equilibrium solution. This phenomenon is called bifurcation [36].

The bifurcation diagram is used to represent the value of a sampled quantity as a function of a parameter called the bifurcation parameter. Different sampling methods are presented in the literature and can be used to draw the bifurcation diagram. Among the main sampling methods are the Poincaré plan, the stroboscopic card, and different types of iterated cards. In our work, the method mainly used for sampling is the stroboscopic card.

To define the bifurcation diagram, different methods can be used. One can either use a discrete model or use the results of a numerical simulation. When approximations are used to build the model, a slight shift can be observed on the bifurcation diagram [28].

The bifurcation parameters studied in static converters are numerous. Work has been carried out considering bifurcation parameters [36]:

- The input voltage's amplitude.
- The load resistance value.
- The current reference's amplitude.
- The capacity value.
- The inductance's value.
- The switching frequency of semiconductors.
- The value of an inductor's and/or a capacitor's series resistance.
- The feedback channel's gains.

Static converters primarily used for their simplicity of structure are:

- Buck type.
- Boost type in continuous or discontinuous conduction mode
- Buck-boost.
- Reversible boost.
- H-bridge inverters with a single phase.
- Cuk and Luo types.

In the literature, many different types of non-linear controllers have been thought of as ways to control the current or voltage of a converter when used with the structures of a converter mentioned above.

There are numerous types of bifurcations, the so-called local bifurcations being one of the most commonly explored in the study of dynamical systems. During the bifurcation, they are distinguished by the cancellation of the eigenvalues (continuous) or the intersection of the eigenvalues with the unit circle (discrete) [38].

In this category, we differentiate the following types:

- **Node-pass bifurcation:** characterized by the disappearance of the solution (solution of the differential equations of the system). This bifurcation is therefore dangerous.
- **Trans critical bifurcation:** characterized by the passage from one set of solutions to another and for which a stable solution always exists, which means that this bifurcation is not dangerous.
- **Supercritical fork bifurcation:** this is the transition from a stable solution to a set of solutions among which there are stable solutions, and this bifurcation is qualified as non-dangerous.
- **Forked subcritical bifurcation:** refers to the transition from a set of solutions to an unstable solution, and therefore, this bifurcation is dangerous.
- **Supercritical Hopf bifurcation:** characterized by the passage from a stable solution to a set of solutions among which we find stable behavior in the limit cycle (oscillation), and therefore, this bifurcation is not dangerous.
- **Subcritical Hopf bifurcation:** characterized by the transition from a set of solutions containing an unstable limit cycle to an unstable solution. This bifurcation is qualified as dangerous.

In our work, we are interested in examining the nonlinear phenomena in static converters, but we are not going to pay a lot of attention to determining the type of bifurcation that is occurring. The elimination of these undesirable phenomena, which make both the analysis and the control of the behavior of the system more difficult, will be our ultimate goal. Because of this, we are primarily interested in the elimination of these behaviors through the use of a command that does not depend on the type or family of bifurcations observed in the various operating scenarios of the converter.

6. Exploration of nonlinear phenomena in voltage-controlled buck converter with an analogic PID controller

As we discussed earlier, nonlinear phenomena generally appear in static converters when there is a variation in one of the following parameters: clock frequency, inductance, load, input voltage, and set point (current voltage or reference voltage depending on the control mode). Generally, the clock frequency and the inductance are not subject to significant fluctuations, and from this observation, it is only the load, the input voltage, and the set point that can vary excessively and affect the system response. In our study, we will consider one

example of converters. This converter we looked at is a typical buck converter as an example from literature that has a lot of nonlinear phenomena and shows them clearly [38].

Figure 1 shows the circuit diagram of a PID voltage-controlled buck converter, with the controller supposed in this example as an analogic PID (continues time model). The buck converter is used to regulate the output voltage of the converter, while the PID controller adjusts the duty cycle of the converter's switch accordingly to achieve the desired output voltage.

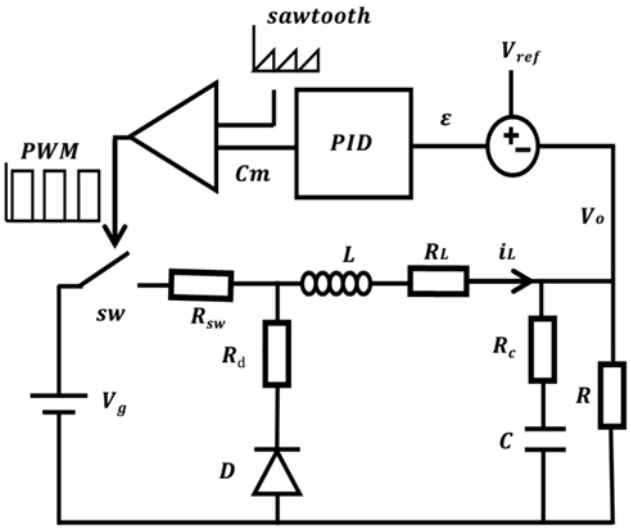

Figure II. 1 PID voltage-controlled buck converter

With:

The parameters of the converter are: $V_g = 24V, L = 20mH, C = 47\mu F, R = 22\Omega$ *and* $f_{SW} = 2500Hz$ [38].

The parameters of the controller are: $K_p = 8.4$ [38],$K_i = 100$,$K_d = 10^{-4}$.

To see how parameters variations affect the behavior of the converter, we will present the bifurcation diagram, phase planes as well as the voltage and inductor waveforms for different values of converter parameters.

6.1. Reference voltage variation

As seen in Figure 3, when the reference voltage V_{ref} was increased gradually from 1V to 23V the dynamics of the converter changed from Period1 to Period2 then Period4, eventually leading to a chaotic behavior.

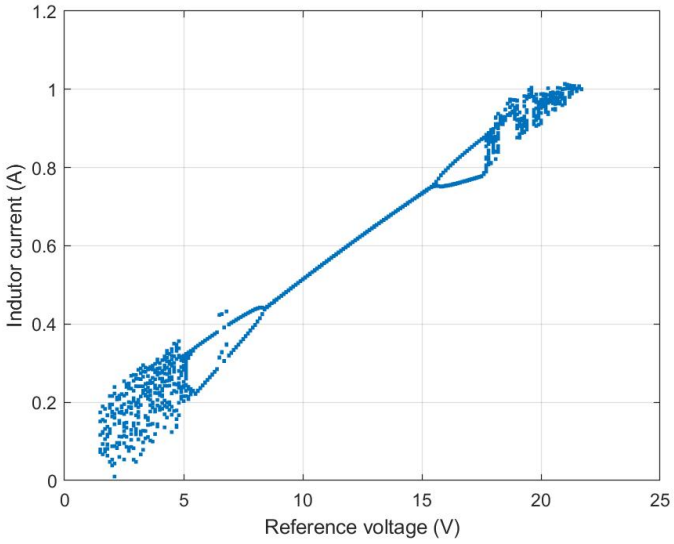

Figure II. 2. Reference voltage variation

The bifurcation diagram clearly shows that when $8.6V < V_{ref} < 15.4V$ the converter exhibits stable period 1 behavior. Furthermore, Figures 3 confirms also that the system operates in period 1, where period 1 is defined by a single closed curve and a single maximum inductor current value is reached.

When $5.5V < V_{ref} < 8.6V$ and $15.4V < V_{ref} < 17.6$, the converter behaves in Period 2, The phase plane depicted in figure 4 also confirms this information, showing two closed curves with two maxima for the inductance current. This result was obtained using V_{ref}=5V.

The analysis and prediction of the system's behavior become increasingly difficult as the reference voltage varies across the test range, eventually leading to a chaotic state. The phase plan in Figures 5 for a reference voltage of 3.3V confirms this conclusion.

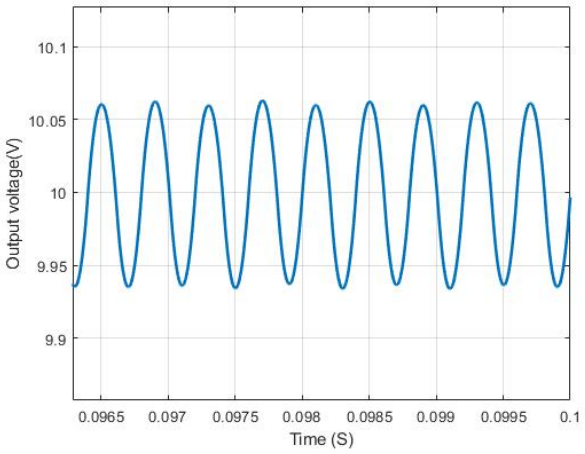

(a)

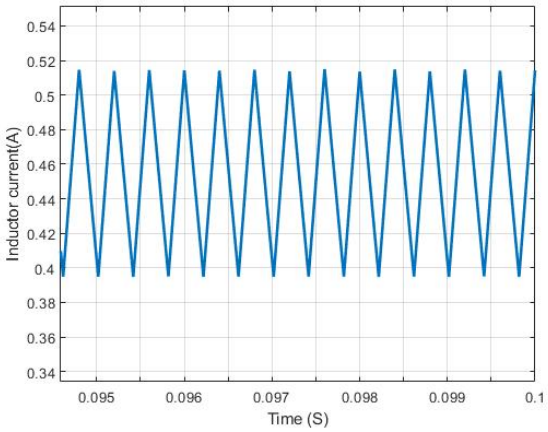

(b)

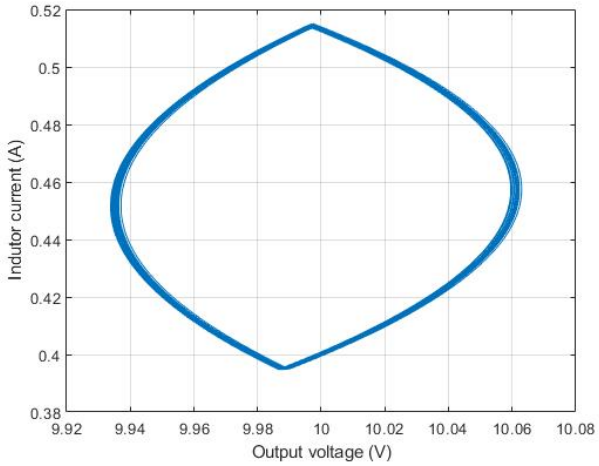

(c)

Figure II. 3. The behavior of the system when $\boldsymbol{V_{ref} = 10V}$, **(a)** Output voltage, **(b)** Inductor current, **(d)** Phase plan

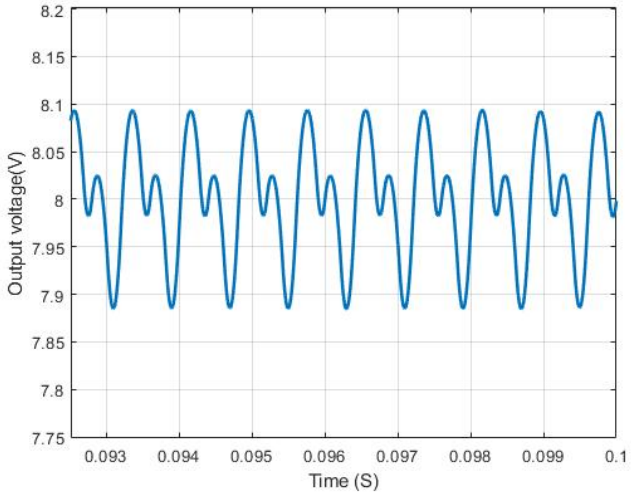

(a)

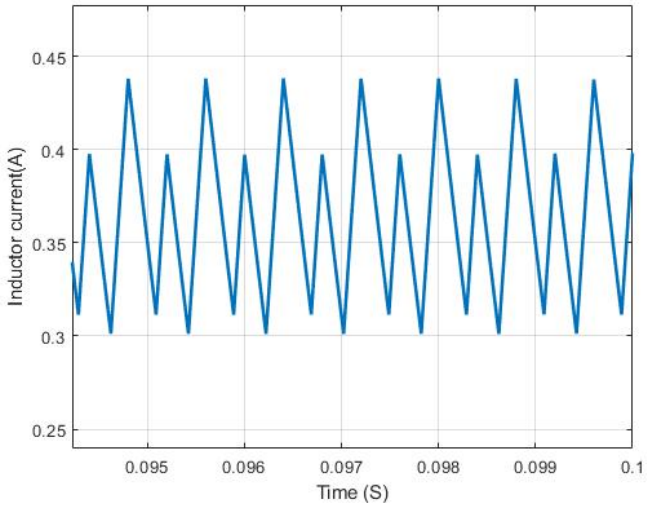

(b)

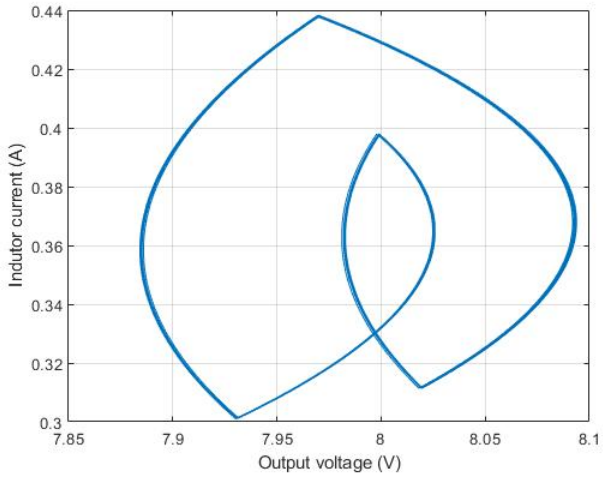

(c)

Figure II. 4. The behavior of the system when $\boldsymbol{V_{ref} = 8V}$, (a) Output voltage, (b) Inductor current, (d) Phase plan

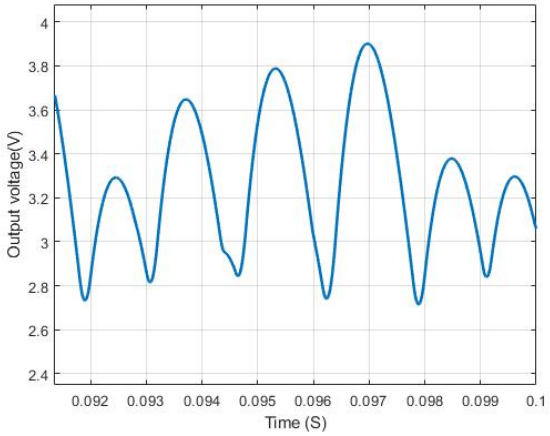

(a)

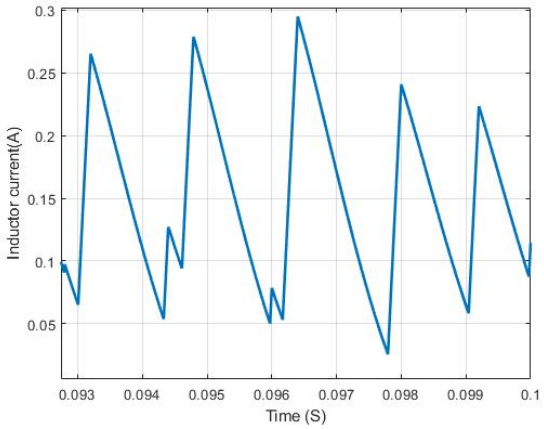

(b)

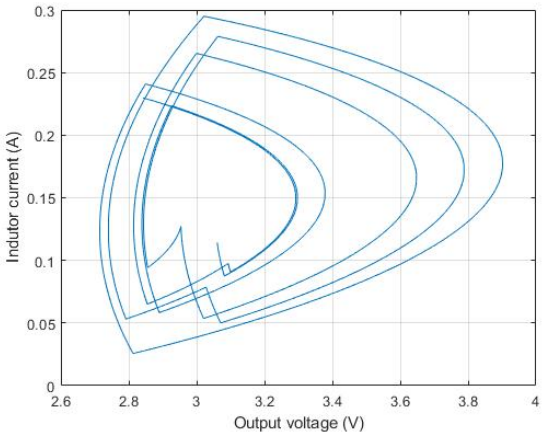

(c)

Figure II. 5. The behavior of the system when $\boldsymbol{V_{ref} = 3.3V}$, (a) Output voltage, (b) Inductor current, (d) Phase plan

6.2. Load variation

In this subsection we will explore the effect of charge variation on the behavior of the system, figure 6 exhibits the bifurcation diagram using load as bifurcation parameter; in this test the load was set to start from 5 to 30 Ω. As it is obvious in the diagram, there are three different behaviors of the converter depending on the value of the load; the first is the period 1 behavior, which appears when the load is higher than 7Ω. This last is followed by the period 2 behavior when the load is between 7 and 16Ω, as the load goes lower during the rest of the test, the behavior of the converter becomes more complicated until it reach the chaotic region.

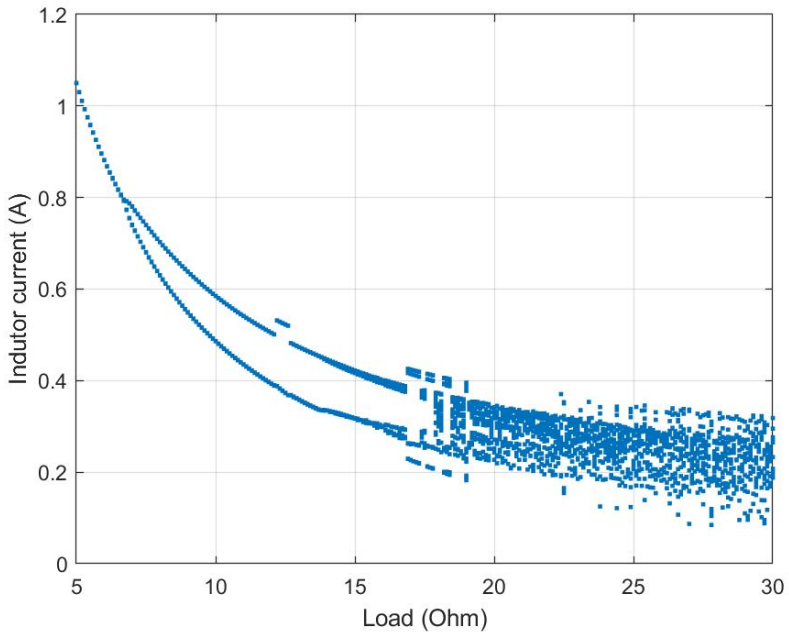

Figure II. 6. Load variation

The phase plane representation, the voltage and current waveforms of the converter are shown in figure 7, this figure show how the converter behaves when the resistance R is set to 5Ω. It provides a clear visual representation of the converter's behavior which helps to gain a better understanding of the system's dynamics. As it is clear the converter is in the stable period 1 behavior.

Figure 8 shows the second behavior of the converter for $R = 22\Omega$, The result shows that the converter has two closed curves with two maximum values for the inductance current, which proves that it works in period two mode.

Figure 9 depicts the third behavior of the converter when $R = 30\Omega$. The result demonstrates that the converter has many different maximum values for the inductance current with unpredictable behavior, indicating that the system's behaviors have become chaotic.

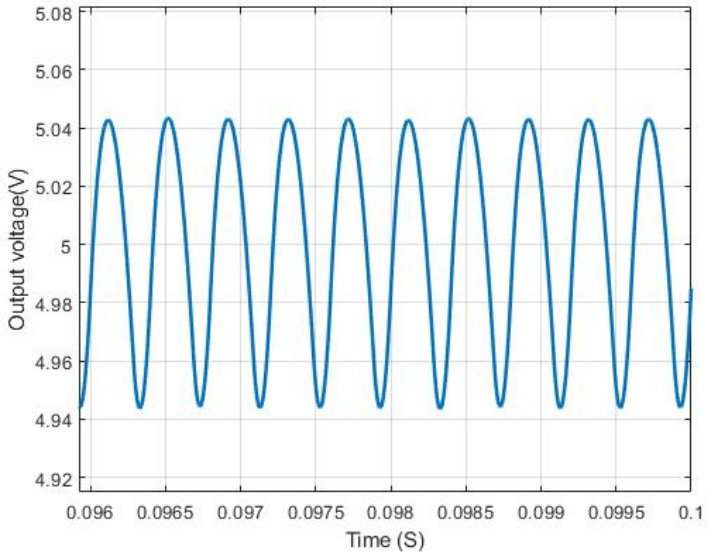

(a)

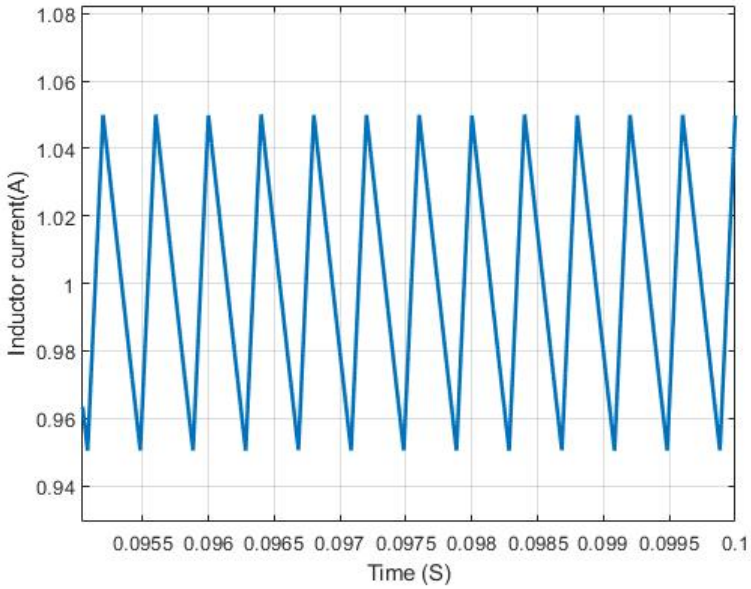

(b)

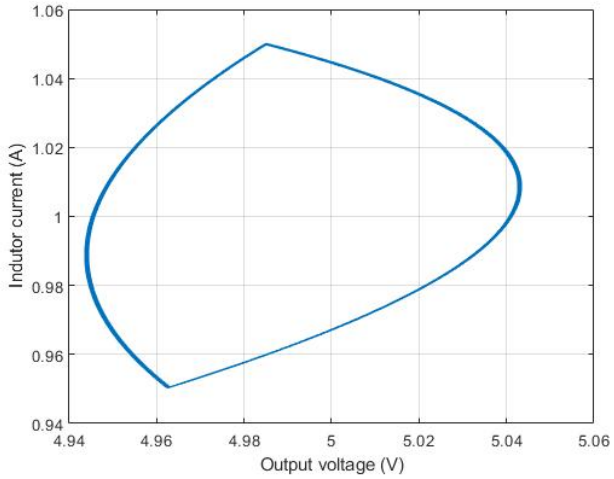

(c)

Figure II. 7. The behavior of the system when R=5Ω, (a) Output voltage, (b) Inductor current, (d) Phase plan

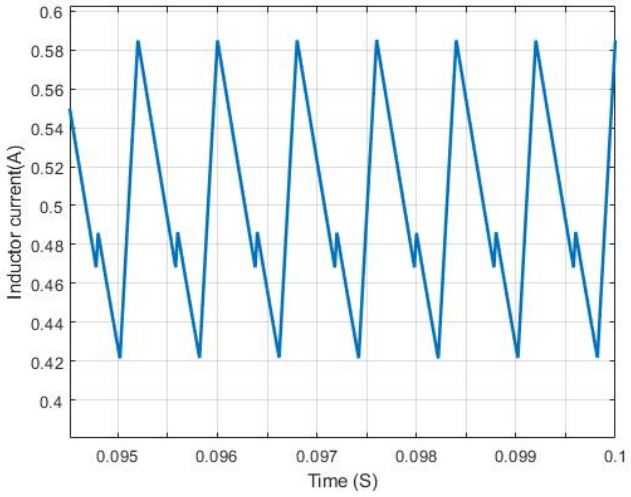

(a)

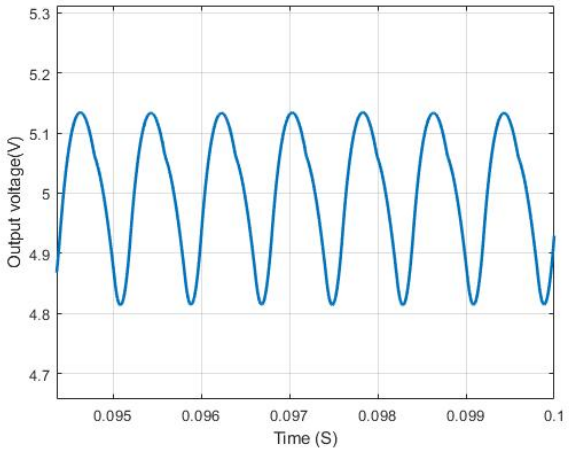

(b)

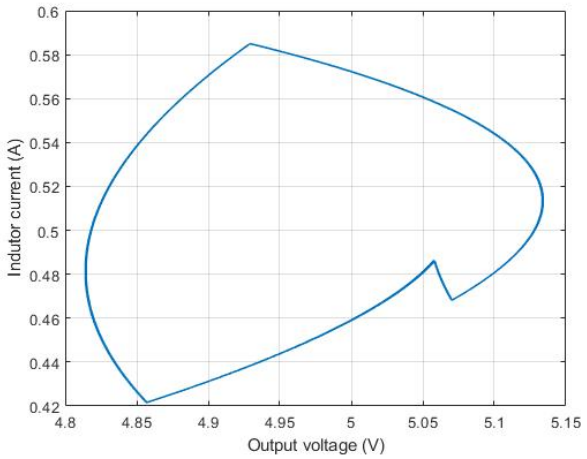

(c)

Figure II. 8. The behavior of the system when R=22Ω, (a) Output voltage, (b) Inductor current, (d) Phase plan

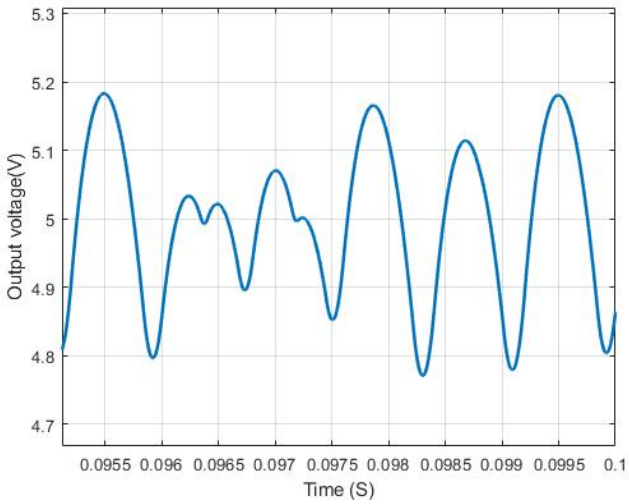

(a)

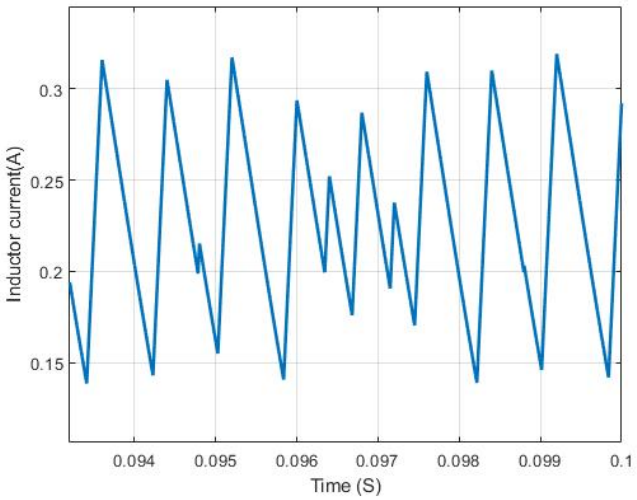

(b)

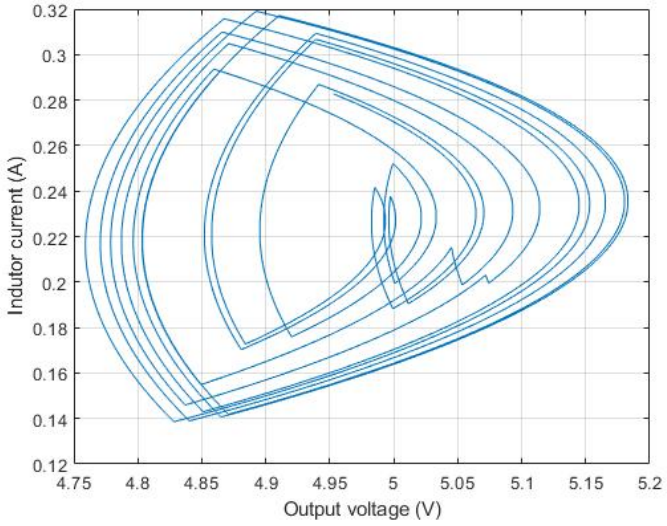

(c)

Figure II. 9. The behavior of the system when R=30Ω, (a) Output voltage, (b) Inductor current, (d) Phase plan

6.3. Input voltage variation

In this part, we will investigate how variations in input voltage affect the system's behavior. As depicted in Figure 10, the dynamics of the converter varied from Period 1, to Period 2, to Period 4, and then to chaotic behavior, when the input voltage Vg increased from 20V to 80V. Initially, the converter showed stable Period 1 behavior when Vg was less than or equal to 26V; then, the converter exhibited unstable period 2 behavior when $26 < V_g \leq 33.25V$; following this, the converter displayed unstable Period 4 behavior when $33.25 < V_g \leq 34.75V$; and finally, the converter demonstrated irregular chaotic behavior when Vg was greater than 34.75V.

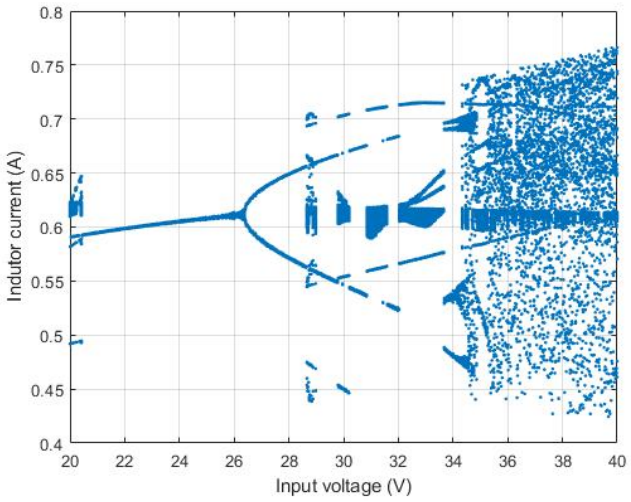

Figure II. 10. Input voltage variation

The phase-plane diagrams of Figures 11, 12 and 13 show the periodic, period 2 and chaotic behaviors of the converter when the input voltage is set to 12 V, 28 V and 48 V respectively. The first diagram displays a periodic closed curve, while the second one exhibits two peak values for the inductance current, indicating that the converter is operating in period 2. The third diagram demonstrates that the converter is in a chaotic state, as it has numerous maximum values for the inductance current with an unpredictable pattern.

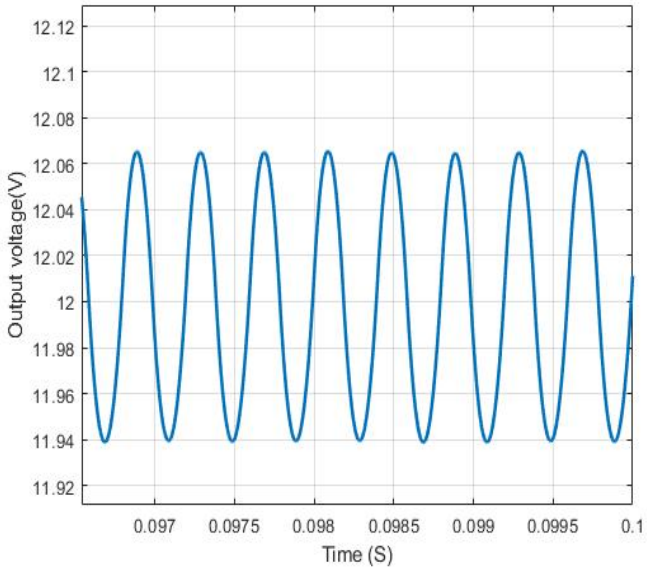

(a)

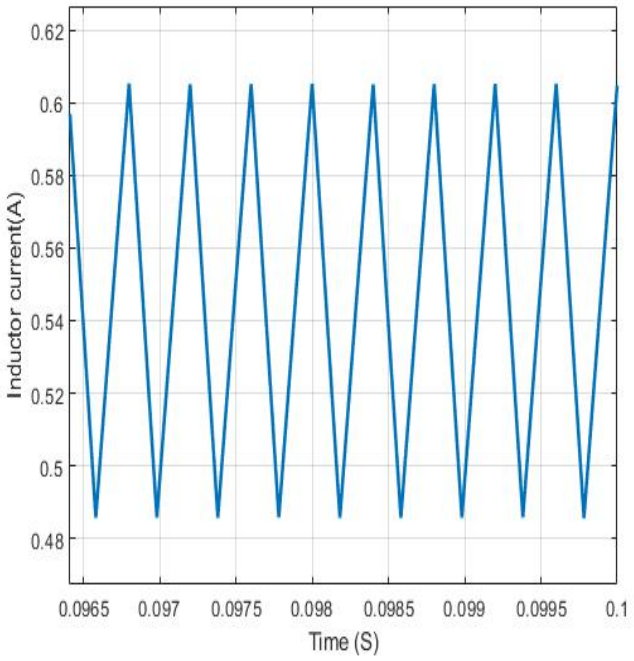

(b)

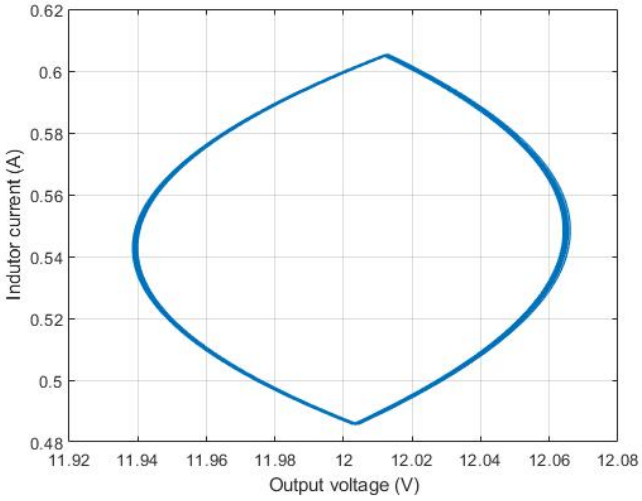

(c)

Figure II. 11. The behavior of the system when Vg=24V, (a) Output voltage, (b) Inductor current, (d) Phase plan

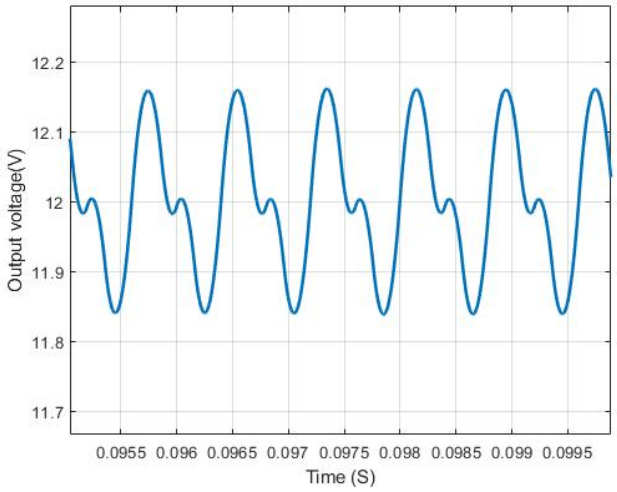

(a)

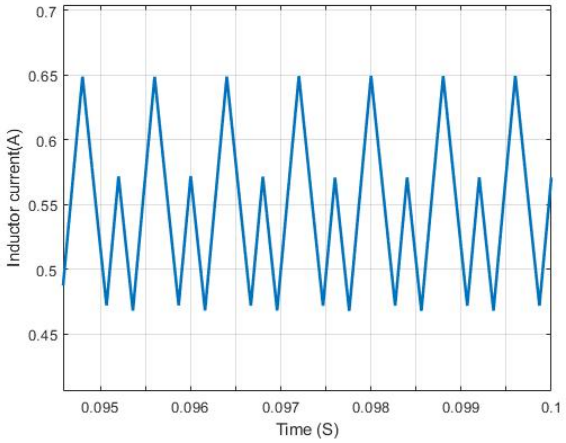

(b)

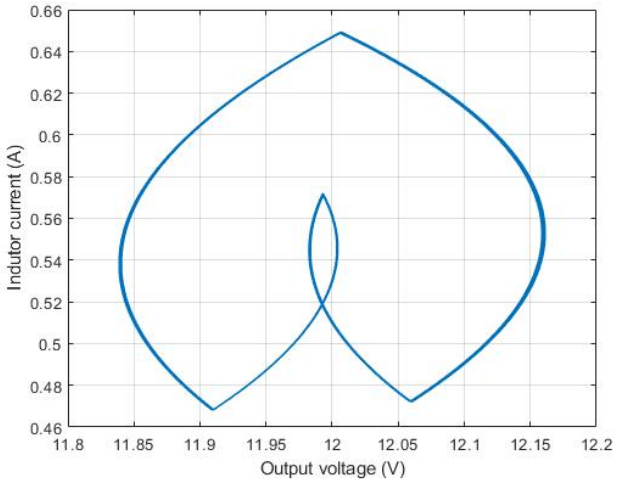

(c)

Figure II. 12. The behavior of the system when Vg=28V, (a) Output voltage, (b) Inductor current, (d) Phase plan

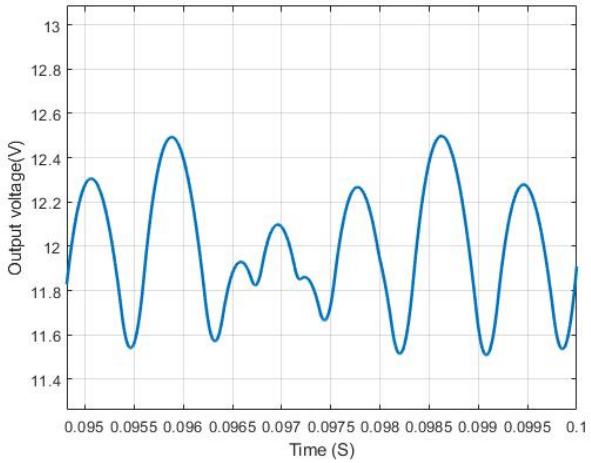

(a)

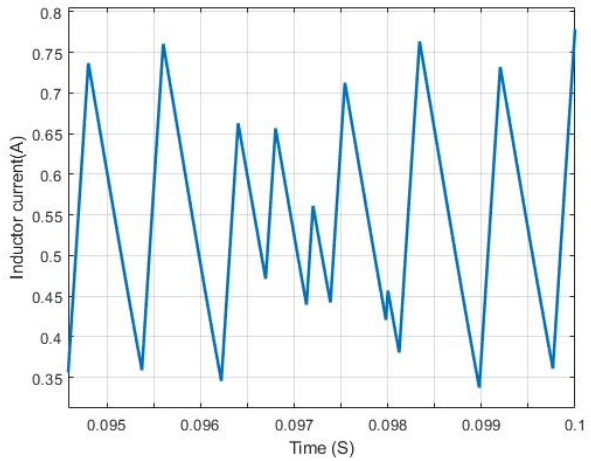

(b)

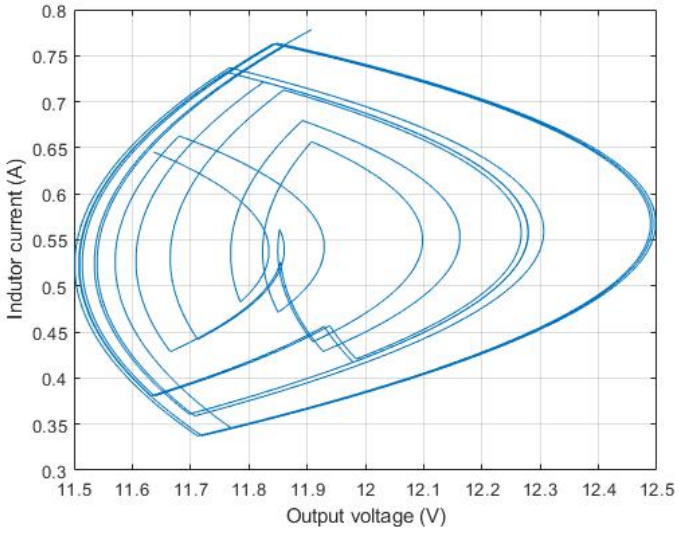

(c)

Figure II. 13. The behavior of the system when Vg=48V, (a) Output voltage, (b) Inductor current, (d) Phase plan

7. Conclusion

This chapter explores the various nonlinear behaviors and phenomena exhibited by static converters. After providing an overview of the research conducted in this field, we used a proposed circuit to study the different nonlinear and undesired behaviors of the static converter.

The results demonstrated that the converter can show abnormal behaviors that are difficult to predict or totally unpredictable, thus making it challenging to analyze the system's behavior and control it.

In the next chapters, we will address the problem of controlling the static converter while maintaining the stability of the system and eliminating the nonlinear phenomena caused by parameter variations.

Chapter III

Metaheuristic optimization algorithms

1. Introduction

In the last few decades, the complexity of real-world problems has necessitated the development of improved optimization techniques to obtain the optimal solution for engineering design problems. The metaheuristic techniques are more popular than classical methods due to their efficiency and simplicity. The two key components of metaheuristics are exploration and exploitation. Exploration allows the algorithm to reach different promising regions of the search space, while exploitation enables the search for optimal solutions within the given region [38-40]. However, the difficulty of balancing these components due to the stochastic nature of optimization problems necessitates a thorough knowledge of the system.

Recently, numerous nature-inspired metaheuristic algorithms have been proposed. These algorithms differ in their source of inspiration and the techniques used for their search, yet they all strive to achieve a balance between exploration and exploitation. At the start of a generation, metaheuristic algorithms use the exploration process to create new solutions. This process then gradually transitions to exploitation, which is focused on refining the solutions obtained in the exploration phase. Exploitation produces new solutions based on the best solution currently available to the population.

The objective of this chapter is to provide a comprehensive overview of the various optimizers we will use to solve our optimization problem. By gaining a thorough comprehension of these optimizers, we will be able to effectively address our optimization challenges and arrive at an optimal solution.

2. Overview to the used algorithms

Optimization is the process of finding the best possible or desirable solution(s) to a problem encountered in many fields. Stochastic or randomized algorithms, such as heuristic and metaheuristic algorithms, offer a practical and efficient solution to challenging optimization problems. These algorithms search “wise regions” of a search space and require less complicated calculations than deterministic algorithms. Consequently, they can yield an optimal solution with reasonable time and computational resources. Nature-inspired stochastic algorithms have been suggested as an effective approach to tackle complex optimization problems.

Metaheuristics can be applied to a wide range of due to their relative simplicity and ease of implementation, as well as their capacity to outperform local search algorithms. These

metaheuristic optimization algorithms are typically divided into four main categories: nature-based methods, physics-based methods, swarm-based methods, human-based methods. All of these algorithms offer almost the same advantages while still having distinct differences between them. Indeed, there is no single algorithm that is sufficient for all optimization problems; different algorithms offer better solutions for different problems.

In this section, we will discuss the four well-known metaheuristic algorithms, which are: the Particle Swarm Optimization (PSO), the Grey Wolf Optimization (GWO), and the Spotted Hyena Optimization (SHO).

3. Particle Swarm Optimization

In 1995, Kennedy and Eberhart introduced Particle Swarm Optimization algorithms, which mimic the group movements of living beings such as swarms of insects, shoals of fish, or flocks of birds. These algorithms are designed to search for solutions to an optimization problem. A particle swarm consists of individuals, or particles, that decide their next movements based on their own experience, with the goal of reaching a better position. Each particle has three tendencies: to continue on its own path, to return to its best previously-reached position, or to move towards its best neighbor.

Figure III. 1. Swarm behavior

A particle's movement can be represented by 1.

$$\overrightarrow{v_i^{k+1}} = w\,\overrightarrow{v_i^k} + \delta_1\left[C_1\left(\overrightarrow{pbest_i} - \overrightarrow{s_i^k}\right)\right] + \delta_2\left[C_2\left(\overrightarrow{gbest_i} - \overrightarrow{s_i^k}\right)\right] \quad \text{(III.1)}$$

With:

$\overrightarrow{v_i^k}$: Vector of displacement of particle i at iteration k.

w: Inertia Weight Constant

$\overrightarrow{pbest_i}$: Vector of the best position encountered by particle i up to iteration k,

$\overrightarrow{gbest_i}$: Vector of the best position encountered by the swarm up to iteration k.

C_1: Acceleration factor related to *pbest*

C_2: Acceleration factor related to *gbest*

$\delta_{1,2}$: Random number between 0 and 1,

$\overrightarrow{s_i^k}$: Vector of current position of particle i at iteration k,

Based on Equation 4.1, the position of the particle can be updated using the following equation:

$$\vec{s}_i^{k+1} = \vec{s}_i^k + \vec{v}_i^{k+1} \quad \text{(III.2)}$$

The concept of updating the position of a particle is illustrated in Figure 3, [40-41]

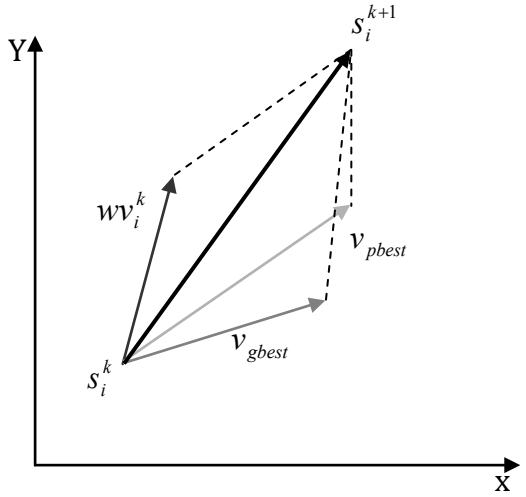

Figure III. 2. Concept of updating the position of a particle

The PSO process involves seven steps:

- **Step 1** reads the parameters of the system.
- **Step 2** initializes the particle positions randomly in the search space.
- **Step 3** randomly initializes the particle movements.
- **Step 4** evaluates each particle's position and updates pbest and gbest if necessary.
- **Step 5** calculates the movements of each particle using equation (III.1).
- **Step 6** updates the positions of each particle based on equation (III.2).
- **Step 7** checks the stopping criterion. If the maximum number of iterations has been reached, the process restarts at Step 4.

Figure 3 represent the flowchart of the PSO algorithm that summarizes the entire algorithm.

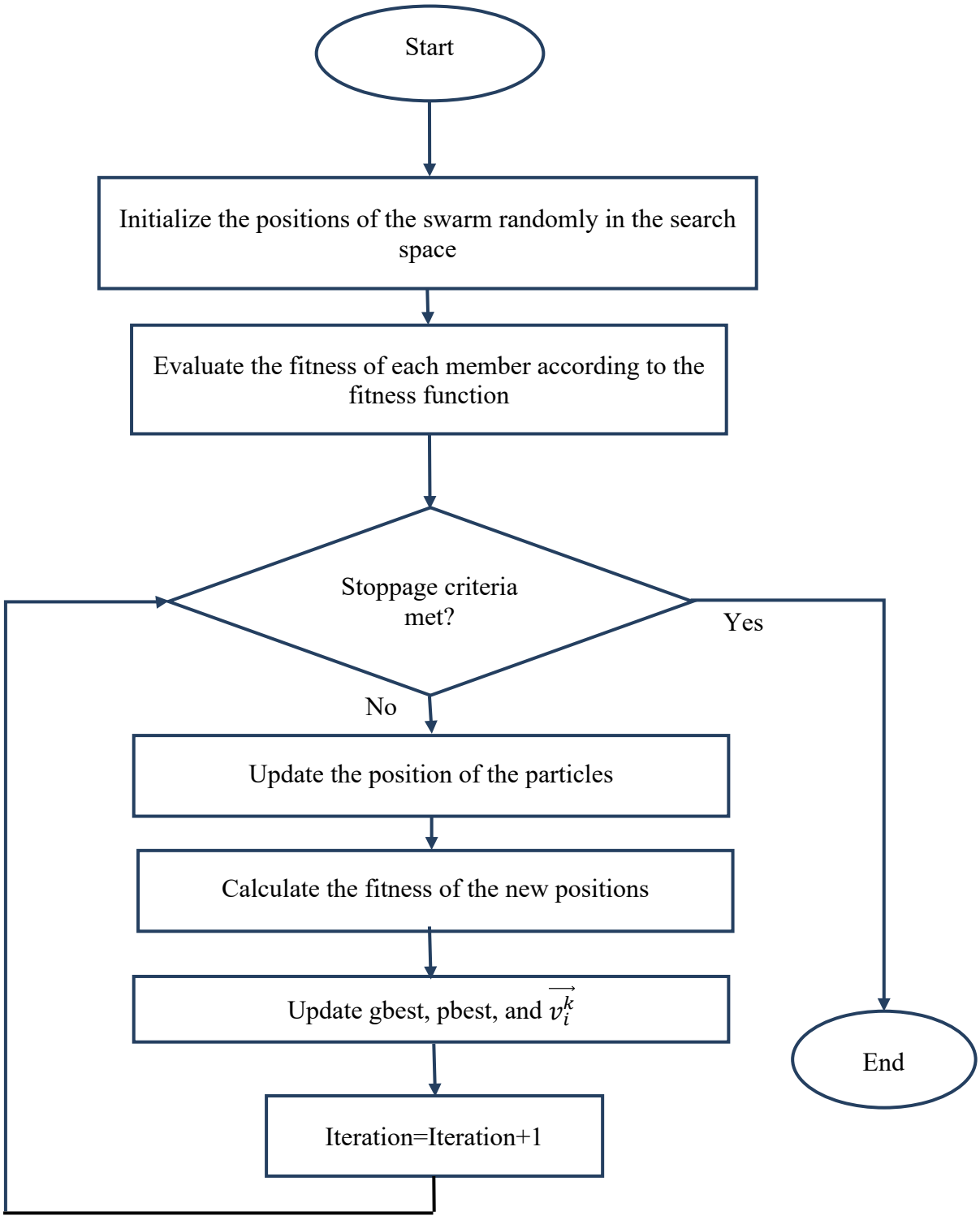

Figure III. 3. PSO Algorithm Flowchart

4. Grey wolf optimizer

4.1. Inspiration

The Grey Wolf (Canis lupus) is a member of the Canidae family and is an apex predator, sitting atop the food chain. Grey Wolves typically live in packs, with the average group size being between 5-12. These packs have a very strict social hierarchy, with a male and female, known as alphas, taking on the roles of leadership. The alpha is responsible for making decisions such as when to hunt and sleep, as well as where to rest, which are then communicated to the rest of the pack. Fig. 1 provides an example of this hierarchy [42,43].

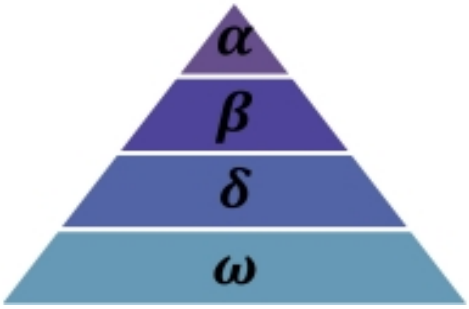

Figure III. 4. Grey wolf social structure [42]

The alpha wolves are the dominant members of a wolf pack, responsible for making decisions regarding hunting, sleeping, and waking times. The alpha's orders are to be followed by the pack and they are acknowledged during gatherings by all members holding their tails down. While the alpha is not necessarily the strongest member of the pack, they are usually the best at managing it, demonstrating that organization and discipline are more important than strength. Only the alphas are allowed to mate in the pack [42,43].

The betas are subordinate wolves helping the alpha. They may be male or female and are likely to be the next alpha if the current one dies or is too old. The beta respects the alpha, but also commands and disciplines the other wolves. It gives feedback to the alpha and reinforces commands [42].

The lowest-ranking grey wolf is the omega, which plays the role of scapegoat. It submits to all other dominant wolves and is the last to eat. Even though it may seem unimportant, the pack may suffer if it loses its omega, as it is a way to vent violence and frustration. The omega may also be the pack's babysitter [42].

Subordinate wolves, also known as deltas, are not part of the alpha, beta, or omega hierarchy. They must submit to alphas and betas, while dominating the omega wolves. Deltas

can act in various roles within the pack, such as scouts, sentinels, elders, hunters, and caretakers. Scouts are responsible for keeping watch of the pack's boundaries and warning the pack of any danger. Sentinels protect and guard the pack's safety. Elders are experienced wolves who have previously held alpha or beta positions. Hunters help alphas and betas hunt for prey and provide food for the pack. Caretakers look after the weaker, ill, and injured wolves in the pack [42].

Grey wolves exhibit an impressive social behavior in the form of group hunting. Muro et al. [43] identify three main phases that comprise a typical wolf hunt: tracking and approaching the prey; encircling, and harassing it until it stops moving; and finally, attacking the prey (see figure 3).

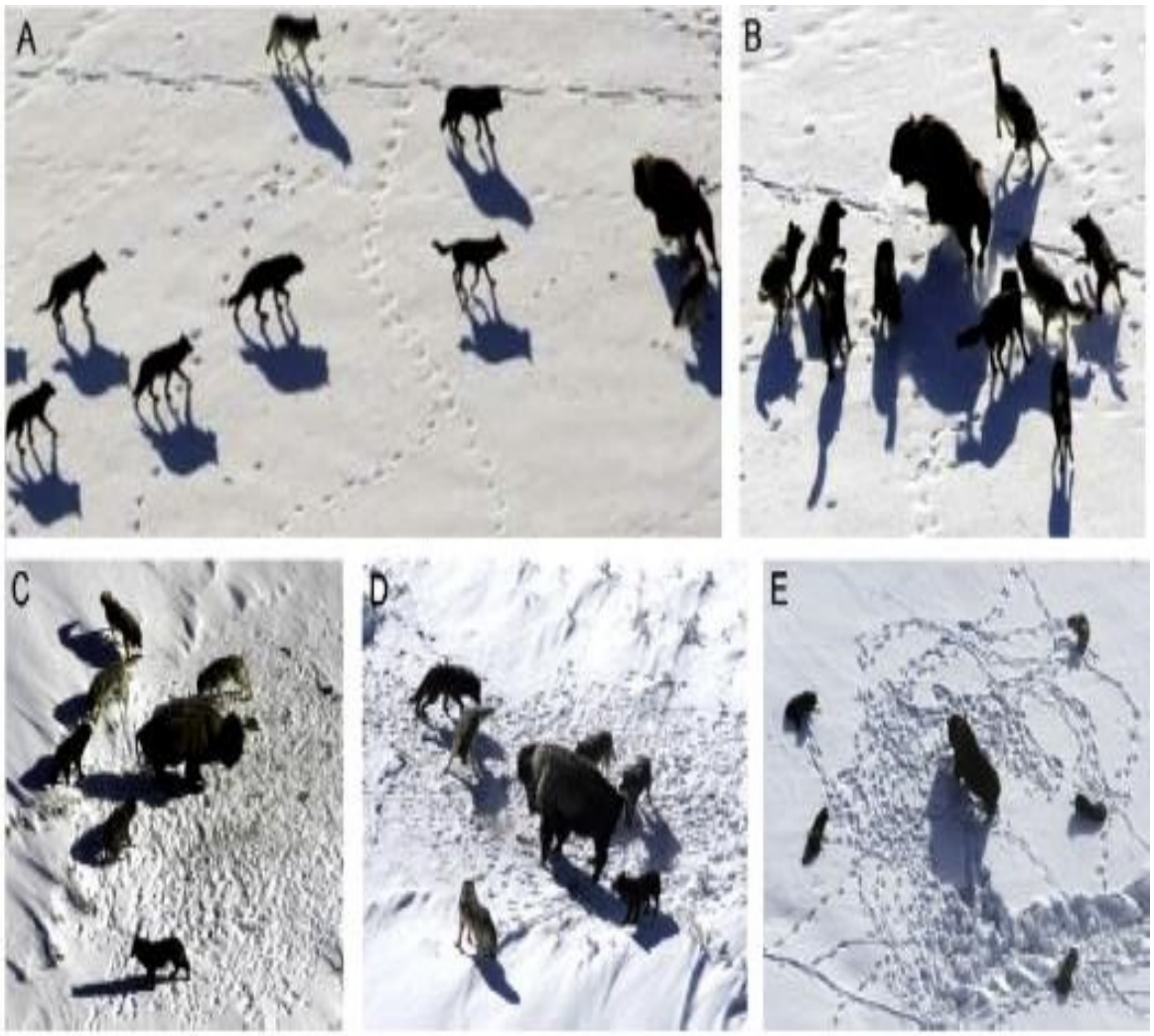

Figure III. 5. Hunting behavior of grey wolves [42]

4.2. Mathematical model and algorithm

The Grey Wolves Optimization (GWO) algorithm was developed to imitate the social hierarchy of grey wolves and their behaviors while hunting [42-44]. A pack of grey wolves can be divided into four populations of wolves: Alpha wolves, Beta wolves, Delta wolves and Omega wolves. Alpha wolves are considered the best solutions and lead the hunt, while Beta and Delta wolves help Alpha wolves in decision making, and Omega wolves are followers.

The four main phases of GWO are recognizing the position of the prey, encircling it, harassing it until it stops moving, and finally attacking it (see Figure 3) [44]. Figure 4 shows the updating of the wolf's positions during the hunt.

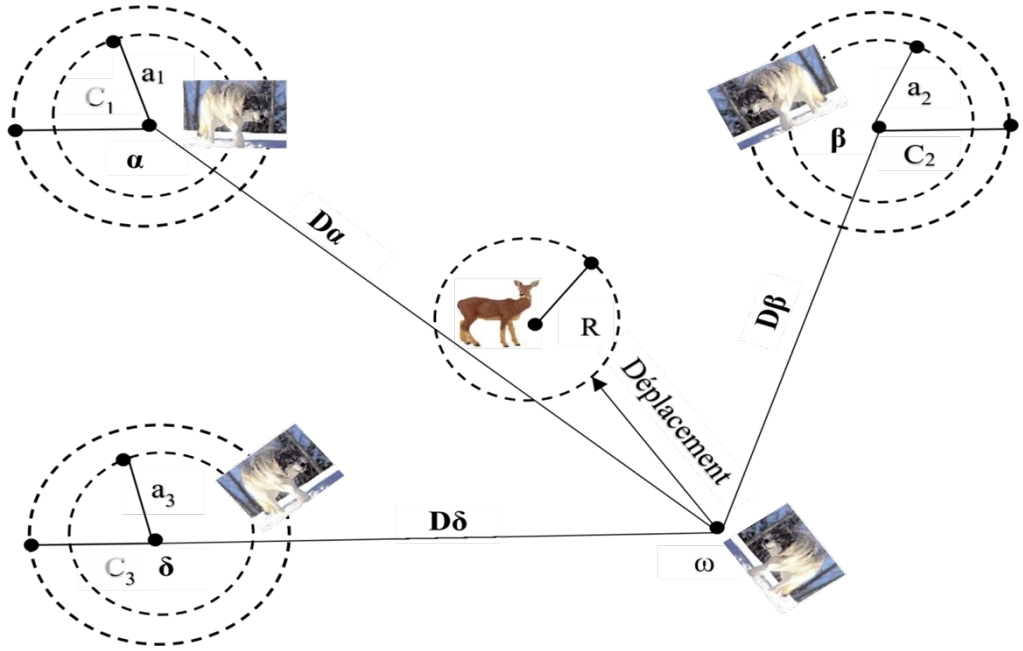

Figure III. 6. Updating the positions of the wolves

The GWO algorithm starts with random initialization of alpha, beta, and delta wolves' positions in the search space bounded by the minimum and maximum values of the search space. The fitness of the current wolf is compared to the fitness of alpha, beta, and delta. If the current wolf's fitness is better than the alpha's, it will become the new alpha. If it is better than beta's but worse than alpha's, it will become the new beta. Finally, if the current wolf's fitness is worse than both alpha and beta's and better than delta's, it will become the new delta.

The update of the wolves' positions is done in every iteration according to Equations 3-8. Parameters A and C are also updated, reducing the search space and the distance between the

wolves and the prey. In GWO, the fitness and position of the wolves are recalculated and updated in all iteration until the final iteration is reached, which serves as the stopping criterion. [46], [47].

$$D = |CX_p - AX(t)| \tag{III.3}$$

$$X(t+1) = X_p(t) - AD \tag{III.4}$$

$$\overrightarrow{X_1} = \overrightarrow{X_\alpha} - \overrightarrow{A_1} * \left(\overrightarrow{D_\alpha}\right) \tag{III.5}$$

$$\overrightarrow{X_2} = \overrightarrow{X_\beta} - \overrightarrow{A_2} * \left(\overrightarrow{D_\beta}\right) \tag{III.6}$$

$$\overrightarrow{X_3} = \overrightarrow{X_\delta} - \overrightarrow{A_3} * \left(\overrightarrow{D_\delta}\right) \tag{III.7}$$

$$\vec{X}(t+1) = \frac{X_1 + X_2 + X_3}{3} \tag{III.8}$$

With: A and C are vectors of coefficients whose elements are randomly determined. X is a vector that represents the wolf's position, while X_p is a vector that represents the prey's position. The distance between the wolf and the prey is represented by the value of D.

Figure 7 represent the flowchart of the GWO algorithm that summarizes the entire algorithm.

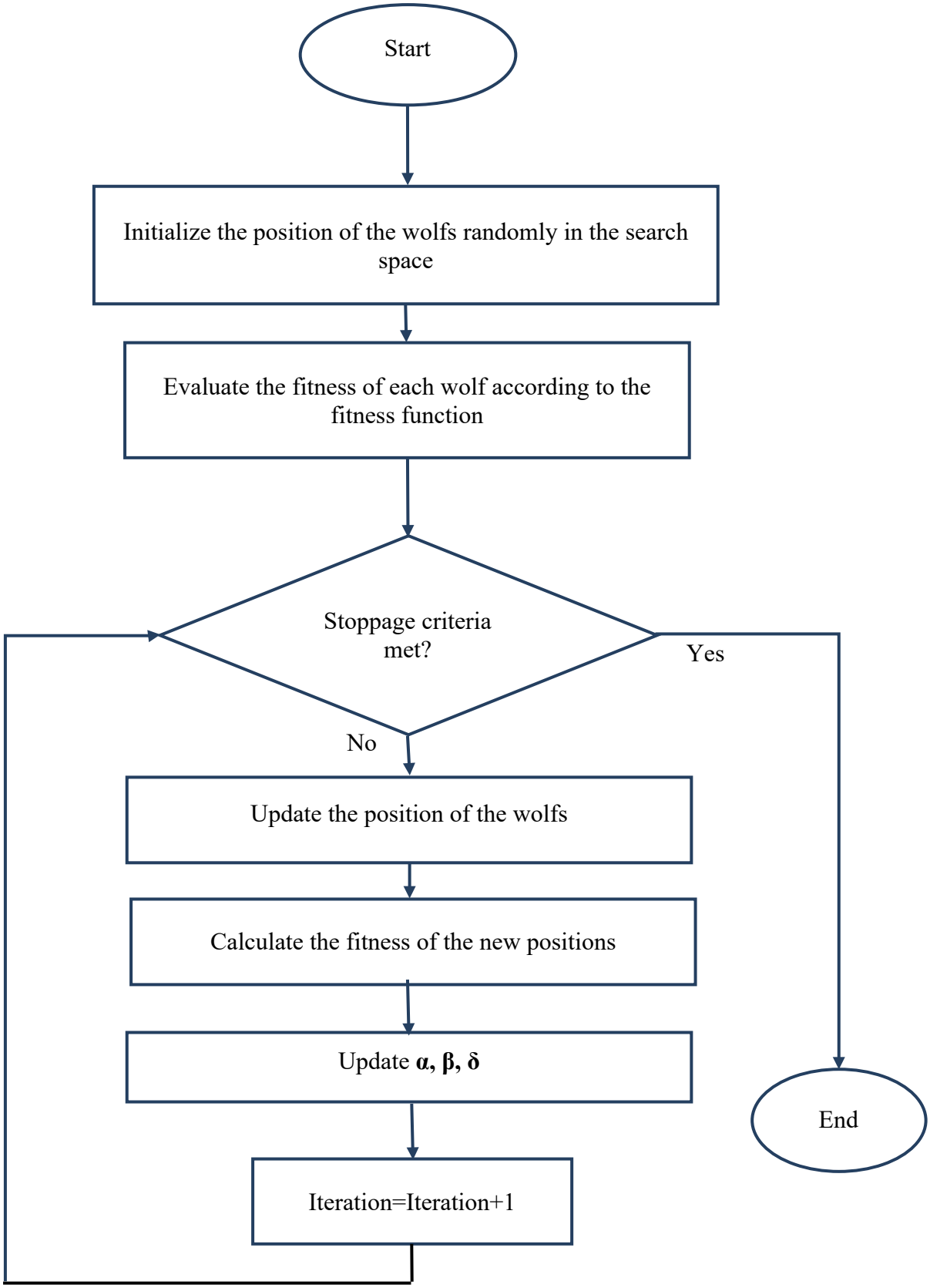

Figure III. 7. GWO Algorithm Flowchart

5. Spotted hyenas optimizer

In 2017, Gaurav Human and Vijay Kumar presented for the first time the Spotted Hyena Optimizer [48]. This bio-inspired optimization method takes inspiration from the social hierarchy and group hunting behaviors of the spotted hyenas to solve various optimization problems.

5.1. Inspiration

The nature of social relationships is dynamic, affected by changes in the relationships among comprising the network and individuals joining or leaving the population. Social Network Analysis of animal behavior has been divided into three categories [39,44]:

- Environmental factors, such as resource availability and competition with other species;
- Social preferences based on individual behavior or quality;
- Social relations of species itself, which has received less attention from scientists.

In [39] the work was inspired by the social interactions between animals, particularly the spotted hyena, scientifically known as Crocuta. Hyenas are large, dog-like carnivores, which inhabit savannas, grasslands, sub-deserts and forests across Africa and Asia.

Spotted Hyenas, also known as Laughing Hyenas due to their sounds resembling a human laugh, are the largest of the four hyena species (Striped, Brown, Aardwolf, and Spotted). Their fur is reddish-brown with black spots, giving them their name. These animals are highly social and intelligent, and they are very skilled hunters and are known to be surprisingly persistent in their fights over territory and food.

Spotted hyenas live in clans with female members as the dominant ones. When males reach adulthood, they leave their original clan and join a new one, where they become the lowest ranking members. Unlike females, who always have a stable place within the clan, males must form relationships with their new clan-mates in order to secure their share of the meal. When a new food source is discovered, these hyenas communicate with each other using a sound that is surprisingly similar to human laughter.

Spotted hyenas are highly social animals, living and hunting in groups of up to 100 members that are connected through a network of trusted friends, family, and kin [39,44]. They can communicate with each other through specialized calls, postures, and signals, and can recognize third party kin and rank the relationships between their clan mates. In addition,

they use multiple sensory procedures to track prey by sight, hearing, and smell. By forming cohesive clusters, they maximize their efficiency in hunting and co-operation. The author in [44] modeled the hunting technique and social relation of spotted hyenas mathematically in order to design SHO and perform optimization. Figure 8 illustrates the tracking, chasing, encircling, and attacking mechanism of spotted hyenas.

Figure III. 8. Hunting behavior of the spotted hyenas, (A) tracking prey (B) chasing (C) encircling (D) attack prey [39]

5.2. Mathematical model and algorithm

Spotted hyenas are social animals that use specialized calls, postures, signals, and sensory procedures to recognize their kin and other individuals, as well as third-degree relatives. They often live and hunt in groups of over 100 members, and bond with other hyenas who are related to or friends with their friends, rather than with unknown hyenas. When tracking their prey, spotted hyenas use vision, hearing, and smell, and form cohesive clusters in order to efficiently cooperate and maximize physical form.

As in [39] we can mathematically model the social hierarchy of spotted hyenas by considering the target prey or objective as a close approximation to the optimum due to the unknown search space a priori. The other search agents then attempt to update their positions in relation to the best search candidate solution. This behavior can be represented by the following equations:

$$\vec{D}_h = \left|\vec{B} \cdot \vec{P}_p(x) - \vec{P}(x)\right| \quad \text{III.9}$$

$$\vec{P}(x+1) = \vec{P}_p(x) + \vec{E} \cdot \vec{D}_h \quad \text{III.10}$$

$\vec{D}_h$ is defined as the distance between the prey and spotted hyena, where x is the current iteration, $\vec{B}$ and $\vec{E}$ are co-efficient vectors, $\vec{P}_p$ is the position vector of the prey, and $\vec{P}$ is the position vector of the spotted hyena.

$\vec{B}$ and $\vec{E}$ can be calculated using the following equation:

$$\vec{B} = 2 \cdot \vec{r}_1 \quad \text{(III.11)}$$

$$\vec{E} = 2\vec{h} \cdot \vec{r}_2 - \vec{h} \quad \text{(III.12)}$$

$$\vec{h} = 5 - \left(current_{iteration} * \frac{5}{Maximum_{iteration}}\right) \quad \text{(III.13)}$$

Figure 9 illustrates the position updating of a spotted hyena (A, B) in a two-dimensional environment. By adjusting the value of vectors B and E, the hyena can move from its current position towards the position of its prey (A∗, B∗). This adjustment allows for a wide range of possible destinations the hyena can reach.

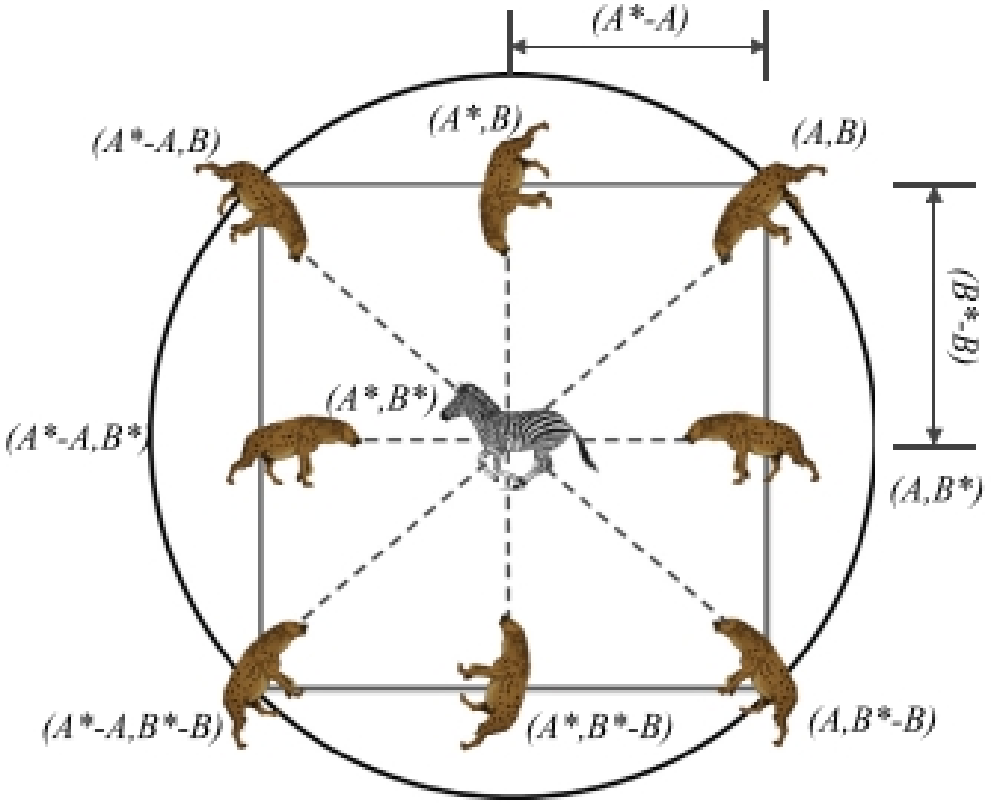

Figure III. 9. Positions updating during the hunt [39]

As the iteration value increases, $\vec{h}$ is linearly decreased from 5 to 0, which allows for a proper balance between exploration and exploitation. Additionally, $\vec{r}_1$ and $\vec{r}_2$ are random vectors that range from 0 to 1.

It is proposed that a mathematical model of spotted hyena behavior can be formulated by assuming that the best search agent (the one that is optimal) has knowledge of the location of the prey [39]. The other search agents form a cluster, or 'trusted friends group," around the best search agent, and save the best solutions they have obtained so far to update their own positions. The following equations are used in this mechanism:

$$\vec{D}_h = \left|\vec{B} \cdot \vec{P}_h - \vec{P}_k\right| \tag{III.14}$$

$$\vec{P}_k = \vec{P}_h - \vec{E} \cdot \vec{D}_h \tag{III.15}$$

$$\vec{C}_h = \vec{P}_k + \vec{P}_{k+1} + \ldots + \vec{P}_{k+N} \tag{III.16}$$

$$N = count_{nos}(\vec{P}_h, \vec{P}_{h+1}, \ldots, (\vec{P}_h + \vec{M})) \tag{III.17}$$

The position of the first best-spotted hyena is denoted by $\vec{P}_h$, while the position of other spotted hyenas is indicated by $\vec{P}_k$. Let $\vec{M}$ be a random vector in the range [0.5, 1], and let $\vec{C}_h$

be a group or cluster of N optimal solutions. After adding $\vec{M}$ to all candidate solutions and counting them, we can determine how many solutions are very similar to the best optimal solution in a given search space (denoted by nos).

The flowchart of the SHO algorithm is shown in Figure 10.

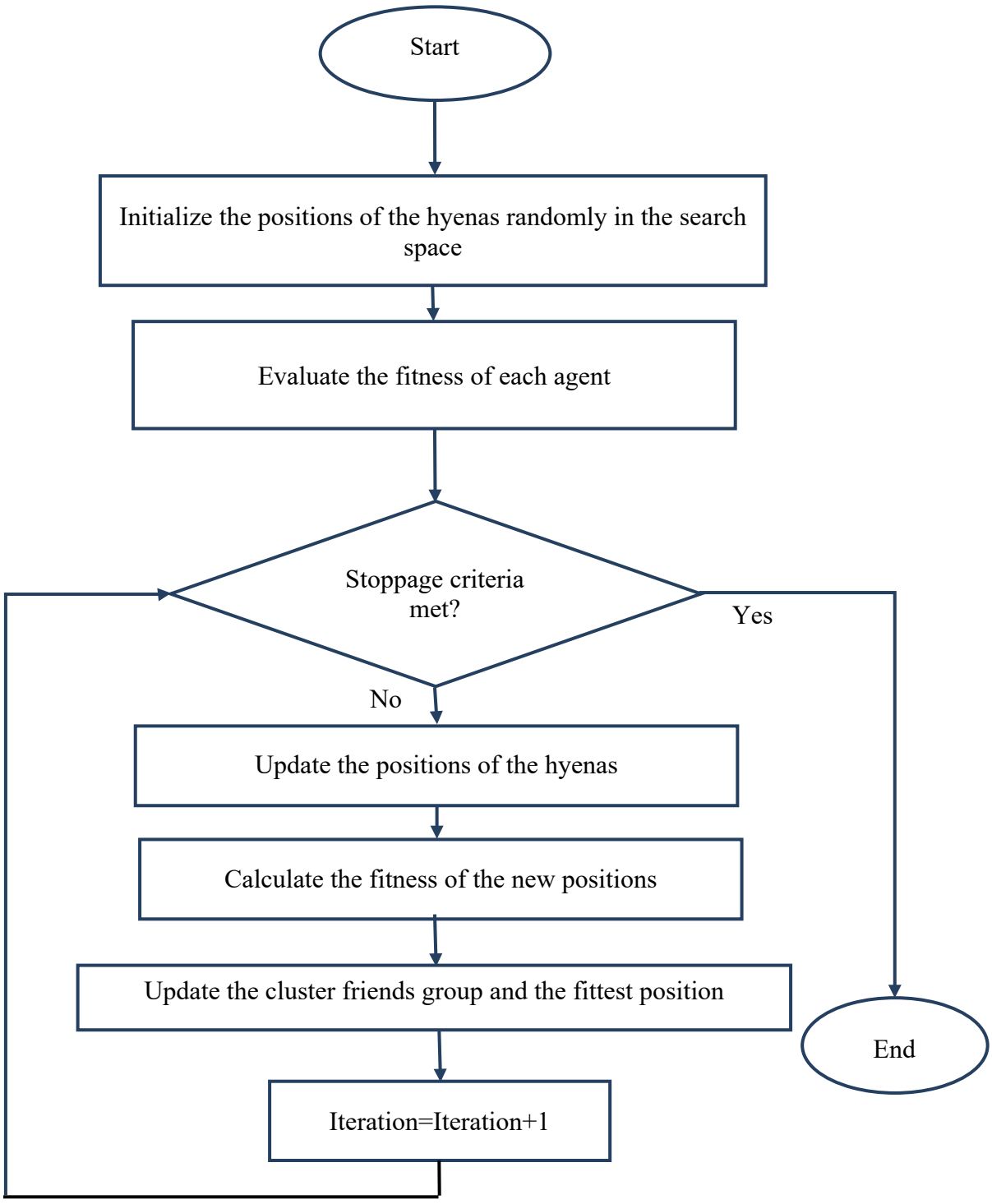

Figure III. 10. SHO Algorithm Flowchart

When $1 > |\vec{h}|$, the attack starts and each search agent must modify its position in the existing space between its current location and the location of the prey. This behavior is mathematically modeled by the following equation:

$$\vec{P}(x+1) = \frac{\vec{C}_h}{N} \tag{III.18}$$

6. Conclusion

Metaheuristic algorithms use both exploration and exploitation processes to prevent getting stuck in local optimum and converges to the optimal solution. They are employed in various fields of engineering. Researchers have devoted significant attention to the implementation of various optimization techniques to enhance the performance of classical control approaches such as optimized PI and PID controllers for DC-DC power supplies.

In this chapter, we have discussed two of the most popular meta-heuristic methods for optimization in the literature: PSO and GWO. Additionally, we have introduced the new SHO method which is applicable in various optimization problems. In the next chapter, we will present a comparison of the results of the SHO method with those of the PSO and GWO algorithms in terms of improving the behavior of the buck converter.

Chapter IV

Elimination of nonlinear phenomena in buck converter using metaheuristic algorithms

1. Introduction

Linear system theory-based controllers provide low-frequency scale results with the advantages of easy implementation and a low cost of implementation. However, due to their inability to handle non-linear phenomena at high-frequency scales and the lack of guarantees for system stability, they are not suitable for use in such cases [44, 45].

Many solutions for stabilizing the system's orbit have been proposed in the literature. However, these approaches only guarantee control performance in a small neighborhood of the considered equilibrium point [46-49]. Disturbances can then take the system away from the equilibrium point and affect the system's performance, or even destroy its stability. In addition, these approaches focus only on stabilizing the system's orbit and neglect other performance.

Recent research has proposed numerous solutions to address the above-mentioned problems, most of this works are based on analytical solutions and are a bit complex, and hard to implement in real plant. Fuzzy logic-based controllers have been used to control chaos in many studies. However, the use of fuzzy logic complicates the control system and requires considerable computation time and a large memory space, while the use of the controllers based on metaheuristic algorithms ensure, at least, the same performance as fuzzy controller with less complexity and implementation cost [50-62]. Nonetheless, most of previous works that use this type of controllers are using the integral absolute error (IAE) as an adaptation coefficient which is insufficient to estimate the fitness of each solution during the search.

In this chapter, we have proposed a method to shift the nonlinear phenomena and expand the stability range of the converters without the need for complicated analysis methods or additional circuits. Using the powerful tools of MATLAB and the state-space model of the buck converter as an example, we designed a PID regulator that guarantees both the global stability of the system and parameter disturbance rejection (load, input voltage, reference voltage); this design is based on metaheuristic optimizers to determine the optimum gains of the controller using appropriate adaptation coefficients. The experimental and simulation results of two application examples are presented in this chapter. The DSPACE 1104 is used to implement the digital PID controller; meanwhile, simulation results using MATLAB will be presented for the analogic PID controller.

2. Application examples

In this chapter, the optimization algorithms will be used to optimize the gains of both a digital and an analogic PID controller. The circuit of the PID voltage controlled buck converter in the optimization is the same as described in II.6.

For the digital PID controller (discrete time model of the controller) the sampling time will be considered $10^{-5}S$.

For both examples the parameters of the controller are considered as in [38], table IV.1 shows the values of the parameters of the proposed study circuit.

Table 1. The parameters of the buck converter

	Parameter	Value
Buck Converter	V_g	24 Ω
	F	2500 Hz
	$R_{sw} = R_D$	0.0177 V
	L	0.02 H
	R_L	2 Ω
	C	47 μF
	R_C	0.2 Ω
	R	22 Ω

3. Application of the optimization algorithm

The optimization methods were used in this work to find the ideal PID controller parameters to enhance the converter dynamics. The search is based on minimizing the steady-state error between the reference voltage and the measured voltage, as well as the error between the peaks of the inductor current. The proposed fitness function is given by Equation 1.

$$F(t) = w_1 F_1 + w_2 F_2 \tag{IV.1}$$

$$F_1 = \sqrt{\frac{\sum_i^N (P_i - \mu)^2}{N}} \tag{IV.2}$$

$$F_2 = \int_{t_0}^{t_f} |\varepsilon(t)|\, dt \tag{IV.3}$$

Where F_1 is the inductor current peak standard deviation and F_2 is the integral absolute error (IAE) between the reference voltage and the measured one.

The control block diagram is shown in figure 1, where the optimized gains are indicated as K_p, K_i, and K_d, which stand for proportional, integral, and derivative gains, respectively.

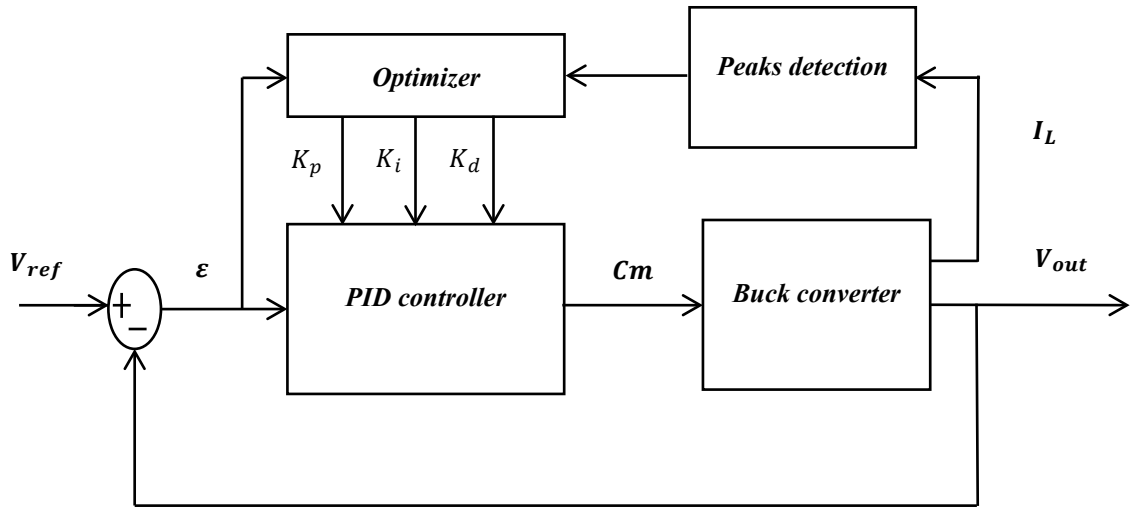

Figure IV. 1. Closed loop system with the optimizer

4. Optimization Results

Optimization has been evaluated and implemented on a Matlab 19a (R2019R) laptop running Windows 10 PRO 64-bit with an Intel Core i5-5300U 2.3GHz processor and 8.00GB RAM, with 10 populations and 100 iterations for all performance tests.

In this study, the SHO optimization algorithm was chosen as powerful and innovative optimization algorithms, while the GWO and PSO are chosen because they are widely used in the literature for many optimization problems.

Figure 8 presents the convergence curves of the optimization algorithms, the purpose of the convergence analysis is to gain insight into the exploration and exploitation strategies employed by the algorithms. It is observed that the SHO search agents are capable of both exploring promising regions of the search space and exploiting the best one which is justified the rapid trend of convergence and the superior performance of the SHO algorithm. As seen in the chart, the SHO algorithm achieves significantly better fitness values than other optimization techniques. This reflects its strong ability to balance the exploration and exploitation phases, as getting good results in many tests requires strong abilities in both.

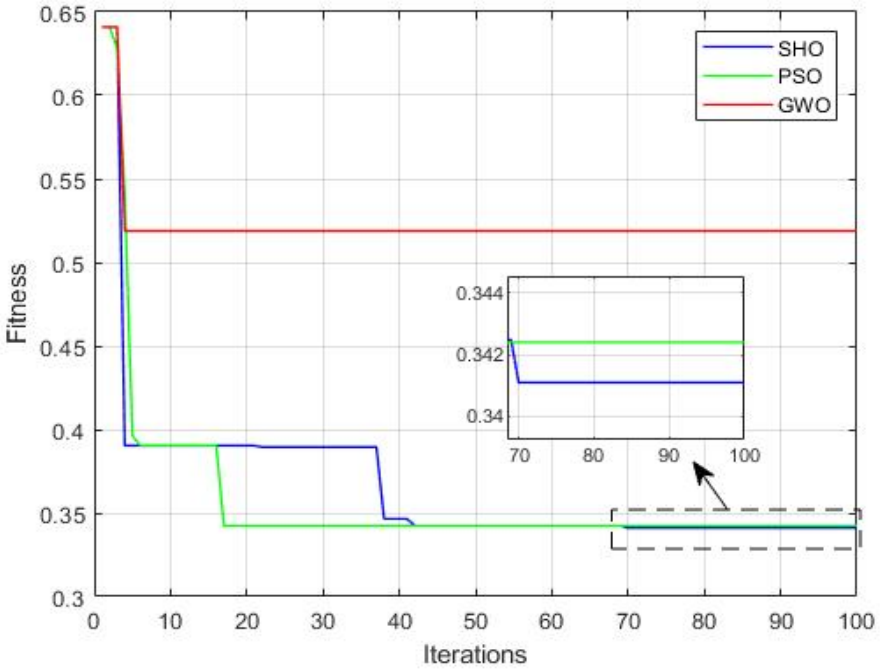

(a)

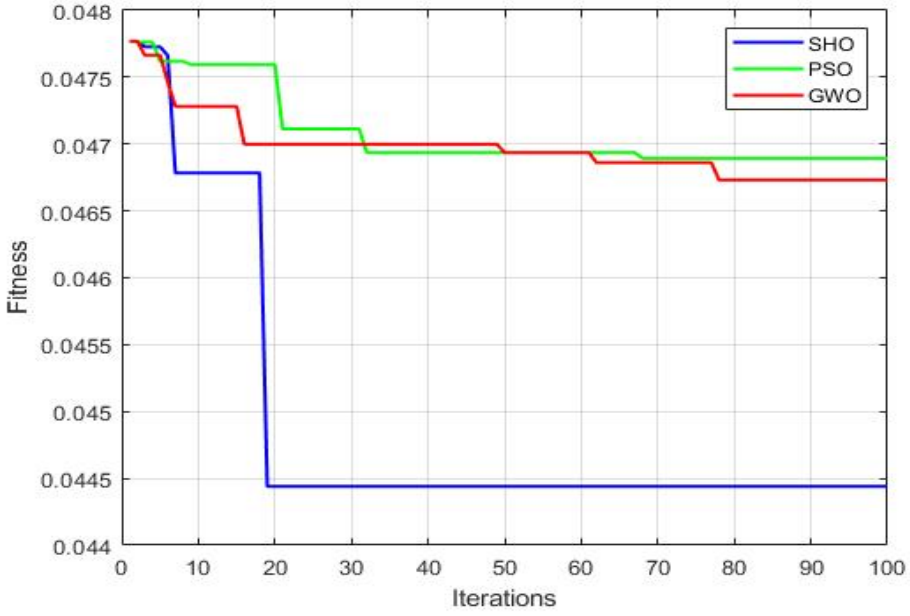

(b)

Figure IV. 2. Convergence curve for (a) Digital controller, (b) Analogic controller

In the next sections, different tests will be done to show how well the proposed solution improves the different behaviors of a voltage-controlled buck converter.

5. Digital PID controller

The results of the real-time communication between the buck converter prototype, the DSPACE 1104R&D board, and the microcomputer are presented in this section. The different tests were conducted on a test bench composed of a buck converter, a DSPACE 1104R&D module and a computer. Figures 3, 4 and 5 show the block diagram, a picture of the experimental setup and the Simulink model that will be compiled and transferred to DSAPCE respectively.

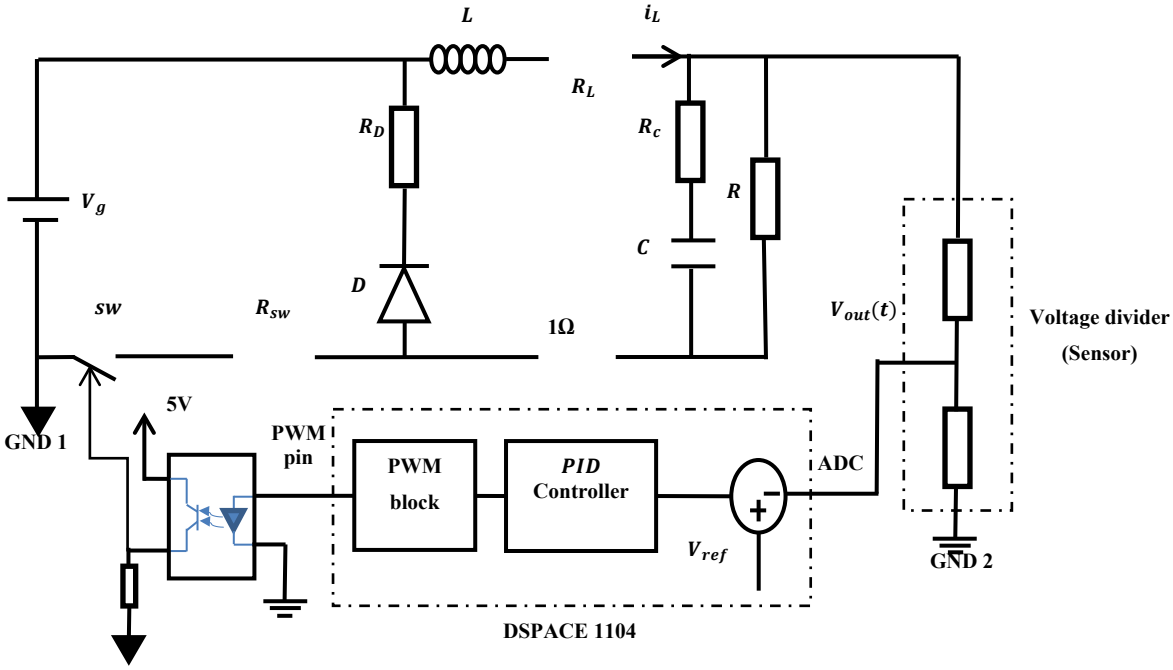

Figure IV. 3. Block diagram of the PID voltage controlled buck converter using DSPACE 1104

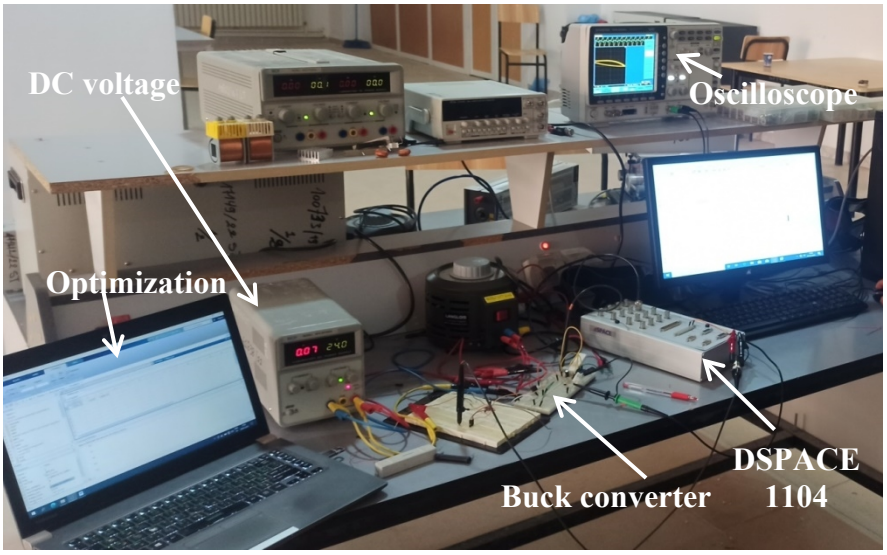

Figure IV. 4. Experimental setup

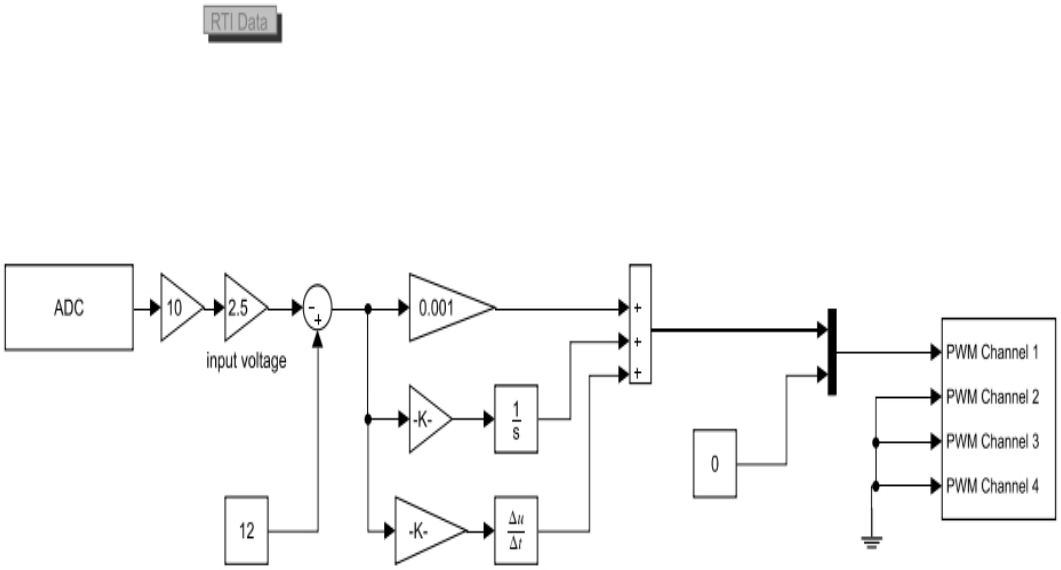

Figure IV. 5. Simulink model that will be transferred to DSPACE

A voltage divider is used to convert the output voltage of the converter into a suitable voltage for the ADC of the DSPACE. The DSPACE then calculates the difference between the measured voltage and the reference voltage, and the digital PID controller within the DSPACE uses this difference to generate a control signal. This signal is sent to a PWM modulator to create a PWM signal, which is then passed through an optocoupler to change the 5V of the PWM signal into a suitable voltage for the switch. The optocoupler is also used to protect the control circuit and to insulate the GND of the power stage from the GND of the control circuit.

5.1. Periodic behavior of the converter

Figures 6 show the response of the system when Vref=12V. The waveform of the inductor current and output voltage as well as the phase plan demonstrate the periodicity of the system, with the inductor charge during a portion of the period and its discharge during the rest of the period. The inductor current does not reach zero during the period, indicating that the converter is in CCM.

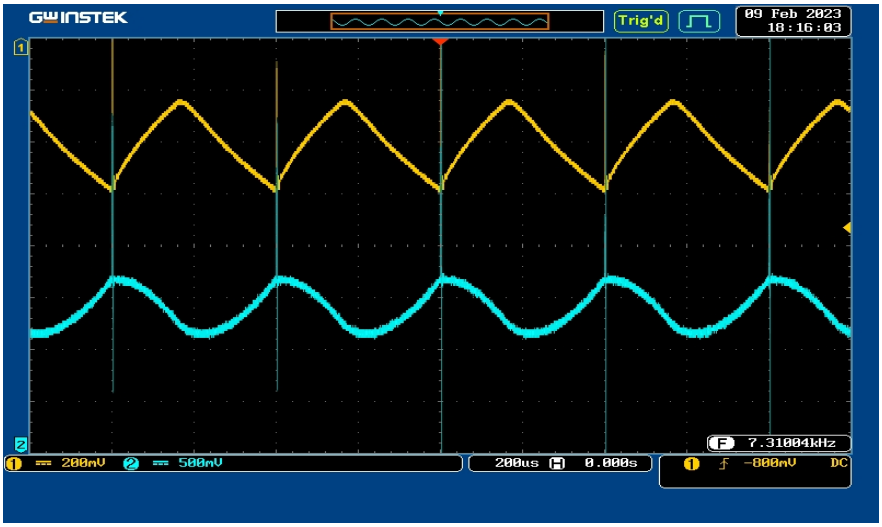

(a)

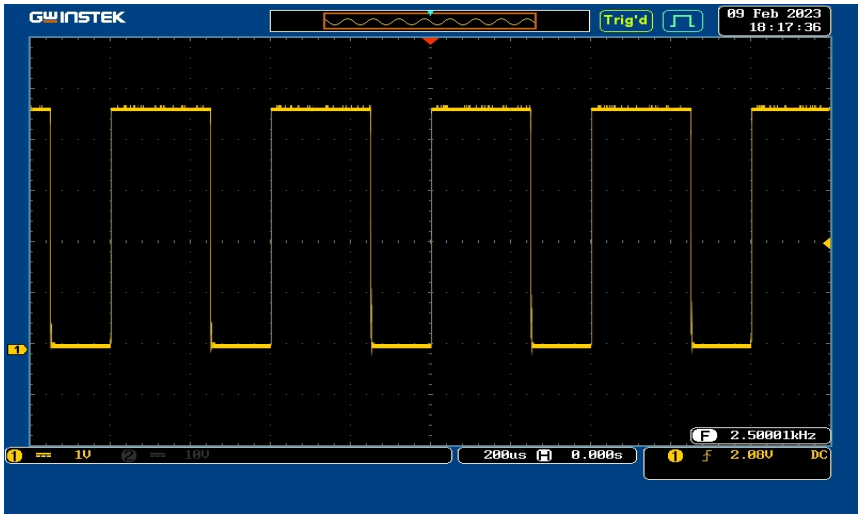

(b)

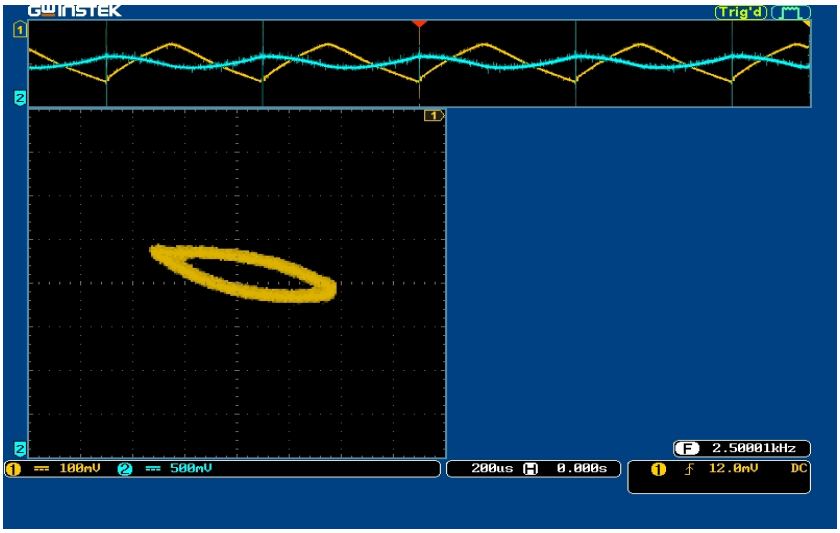

(c)

Figure IV. 6. Periodic behavior of the converter

5.2. Parameters variation

5.2.1. Reference voltage variation

By analyzing Figures 5 and 6, we gain further insights into the impact of the proposed SHO method on the system responses under different reference voltage values. In Figure 5a, the system exhibits quasi-periodic behavior when the reference voltage is set to 5V, indicating undesired performance. Similarly, Figure 6a shows a similar quasi-periodic response for a reference voltage of 18V. These undesirable behaviors can lead to instability and degraded system performance.

However, upon applying the optimized controller gains obtained through the SHO method, we observe significant improvements in the system's response. Figures 5b and 6b demonstrate the effect of the optimized controller on the system behavior for the same reference voltage values. Notably, the undesired quasi-periodic phenomena are effectively eliminated, giving way to a more desirable response. The system now operates within an extended range of desirable behavior, indicating the success of the proposed approach in mitigating the abnormal behaviors exhibited by the converter.

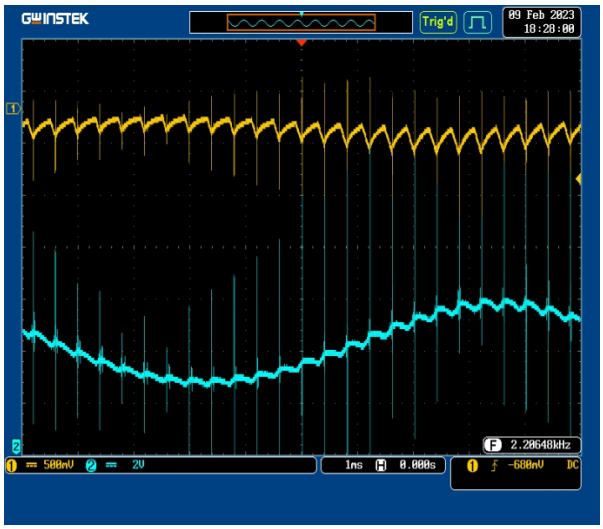

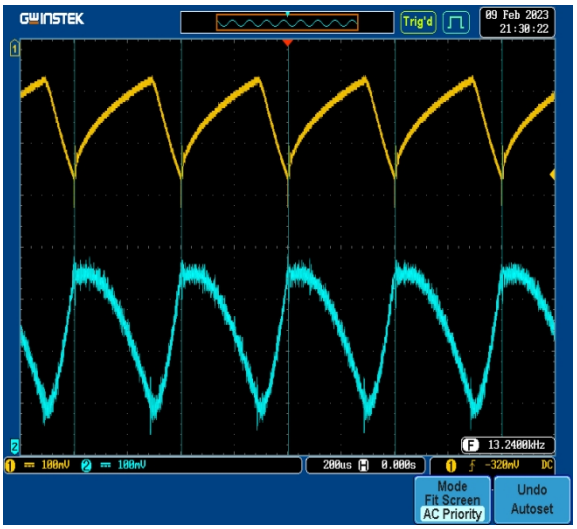

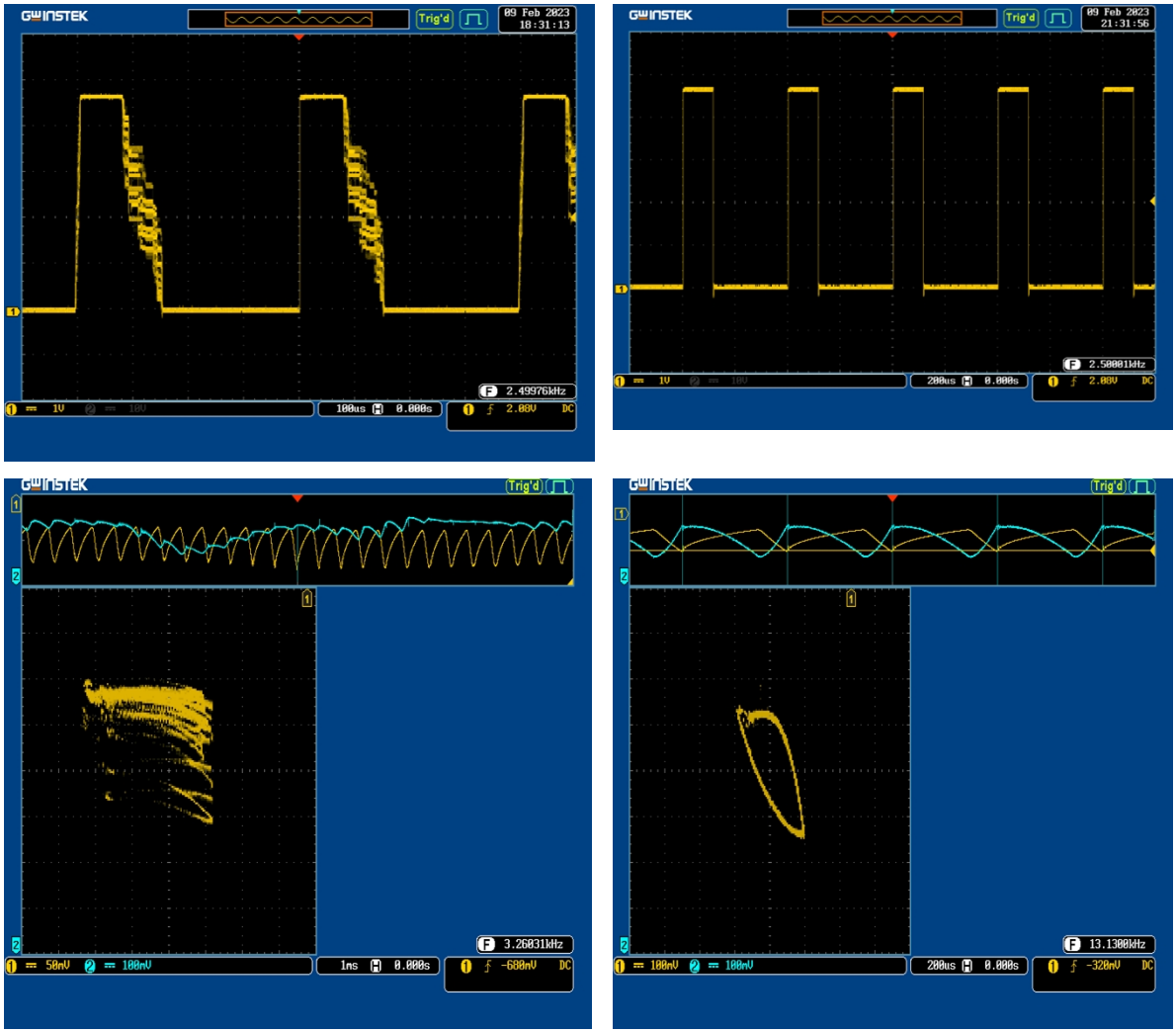

(a) Original behavior **(b)** Optimized behavior

Figure IV. 7. System response with $V_{ref} = 5V$

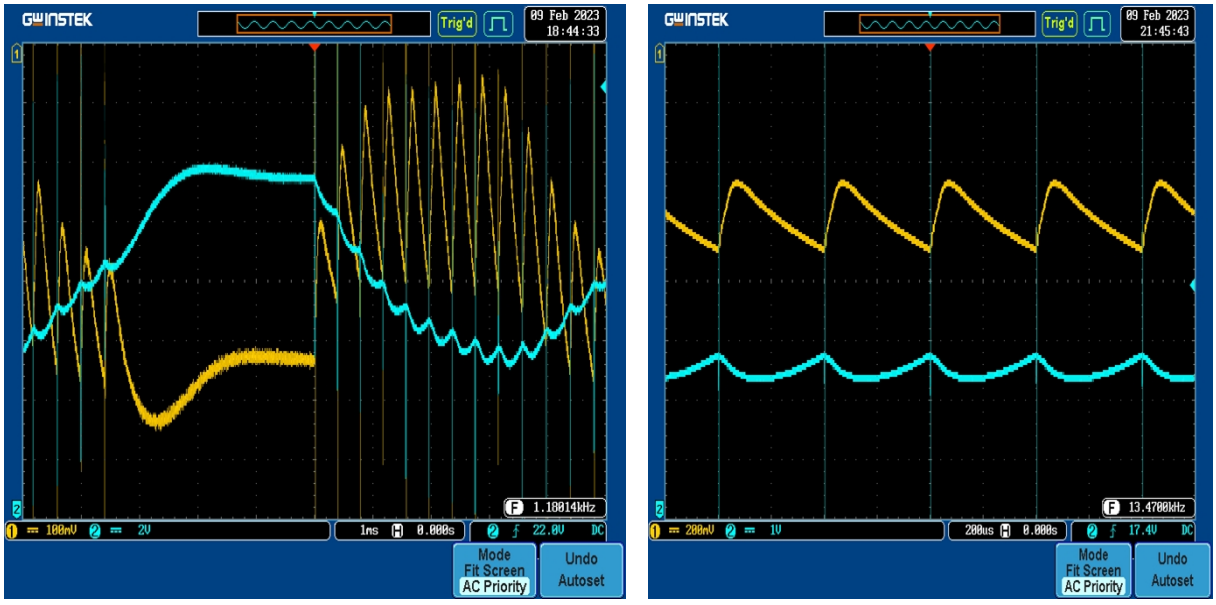

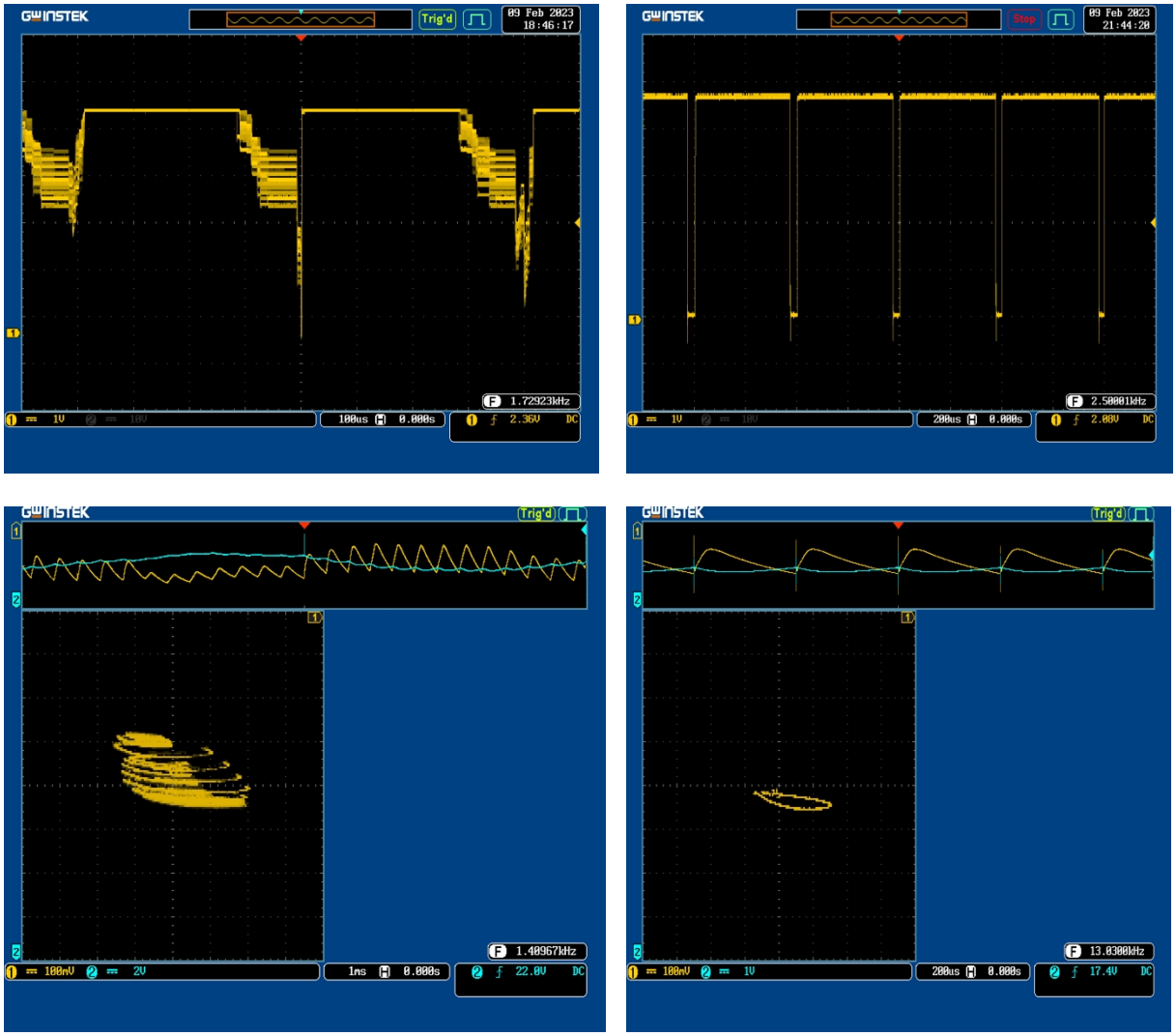

(a) Original behavior **(b)** Optimized behavior

Figure IV. 8. System response with $V_{ref} = 18V$

5.2.2. Load Variation

Figure 9 shows the phase plans when the load varies. In Figure 9a, we notice that the converter operates in an unstable manner and exhibits a quasi-periodicity. With the use of the optimized controller, Figure 9b shows a significant improvement, as the desired behavior is achieved over a wider range of operation and nonlinear phenomena are completely eliminated.

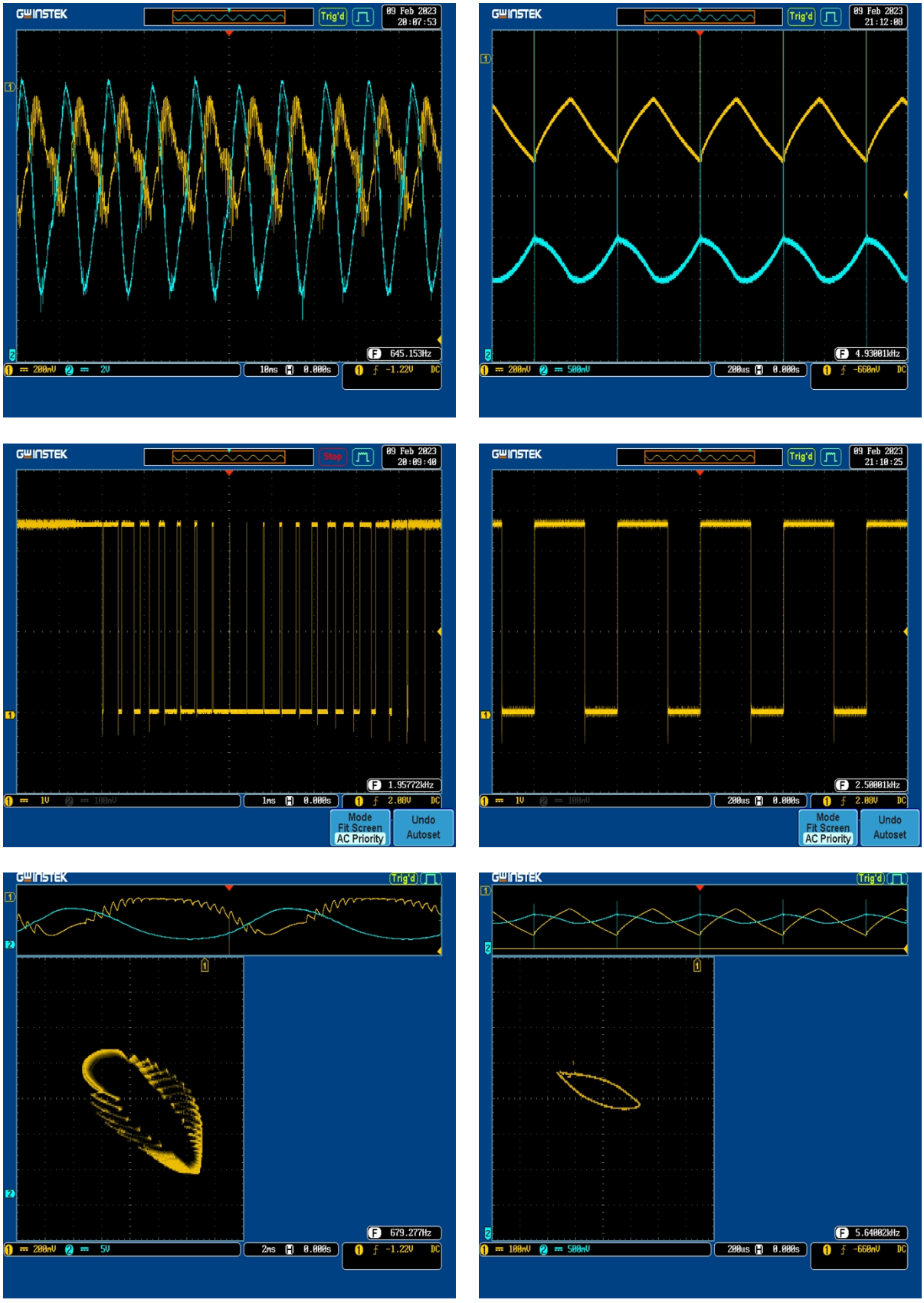

(a) Original behavior **(b)** Optimized behavior

Figure IV. 9. System response with $R = 30\Omega$

5.2.3. Input voltage variations

Figures 10 and 11 show the phase plane with input voltage variation. When the input voltage was set to 25 or 30, the converter exhibited quasi-periodic and chaotic behavior (Figure 10a and 11a). However, the use of an optimized regulator (Figure 10b and 11b) successfully eliminates the nonlinear phenomena and ensures the desired periodic behavior.

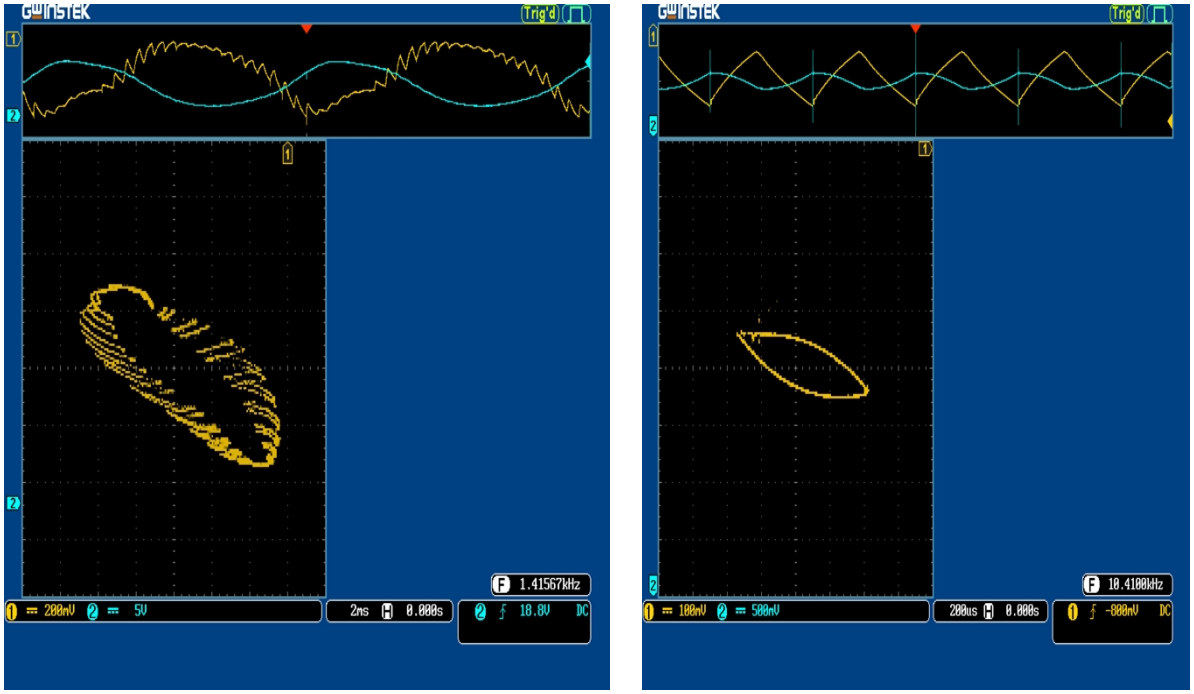

(a) Original behavior **(b)** Optimized behavior

Figure IV. 10. System response with $V_g = 25V$

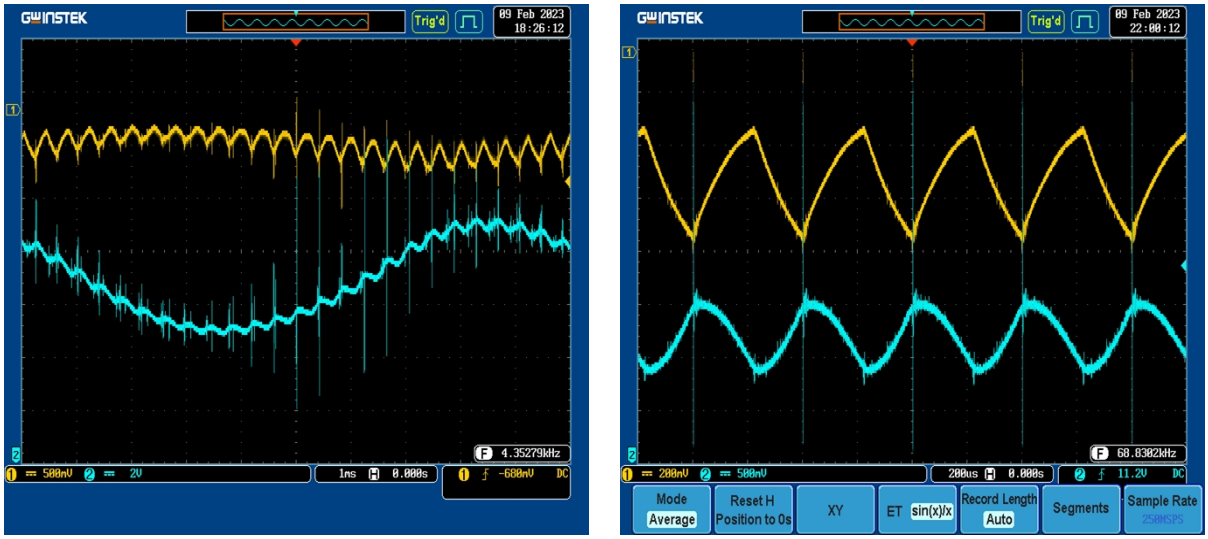

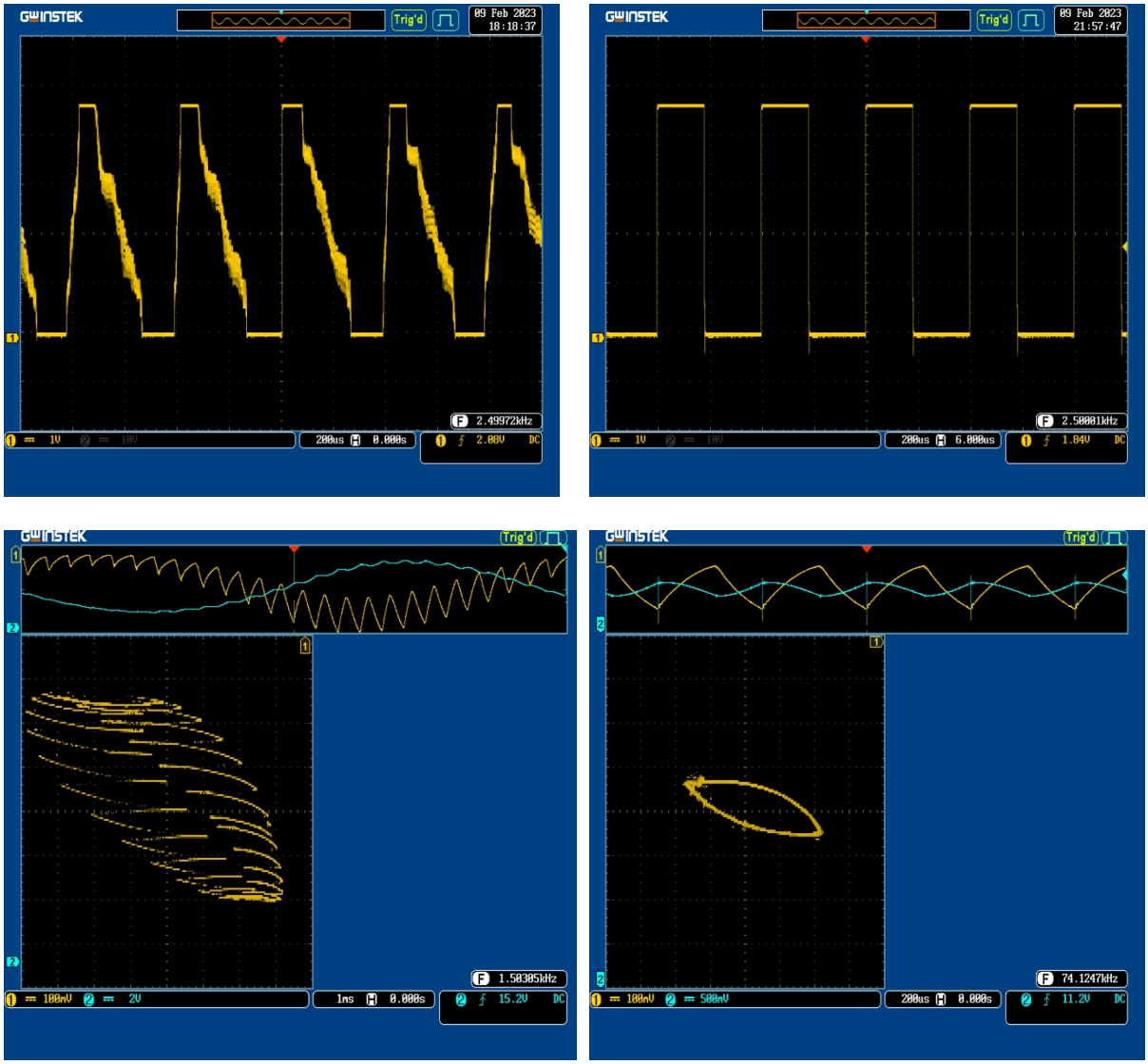

(a) Original behavior (b) Optimized behavior

Figure IV. 11. System response with $V_g = 30V$

6. Optimized Analogic PID controller

Figure 12 is the voltage wave diagram obtained before and after the optimized PID controller was implemented, where the latter begins after 0.06 seconds. It is clear from the wave form of the output voltage and the phase plan diagram $V_o - i_L$ that the converter returns to the stable Period 1 behavior at 0.067s.

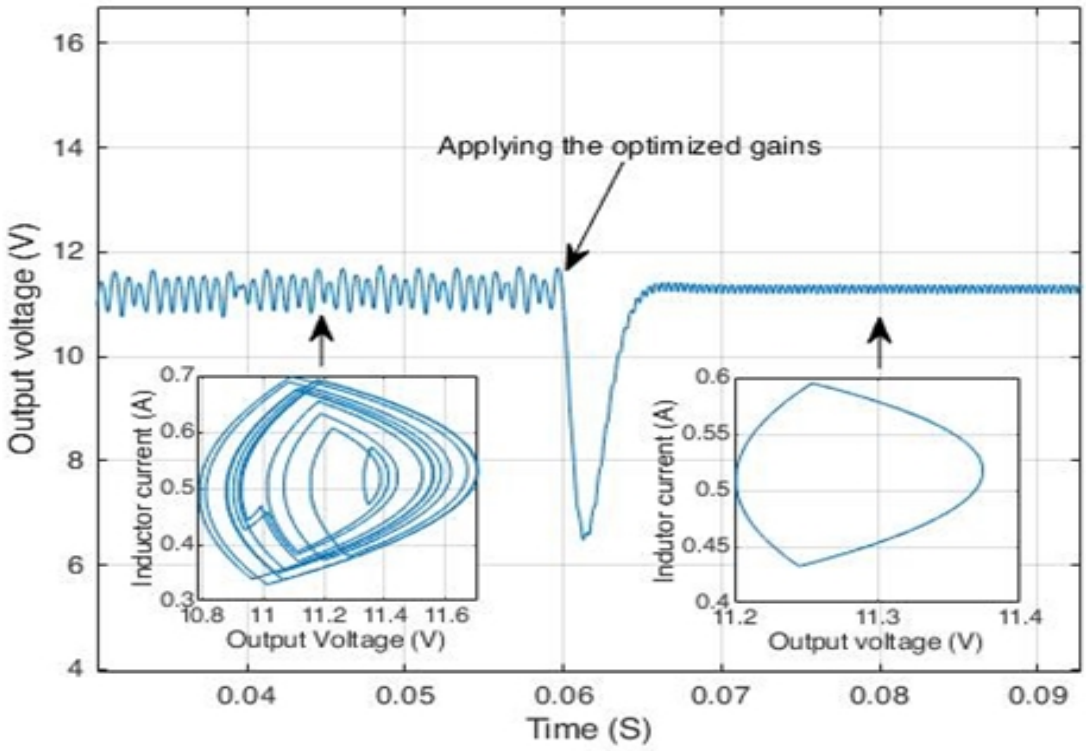

Figure IV. 12. Vo after applying the optimized parameters

The bifurcation diagrams in figure 13 proves that the optimized controller is able to extend the stability rang of the converter for the different converter parameters, where the converter exhibits the period 1 behavior for a values up to of $V_g = 70V$, $V_{ref} = 3.3V$ and $R = 70\Omega$

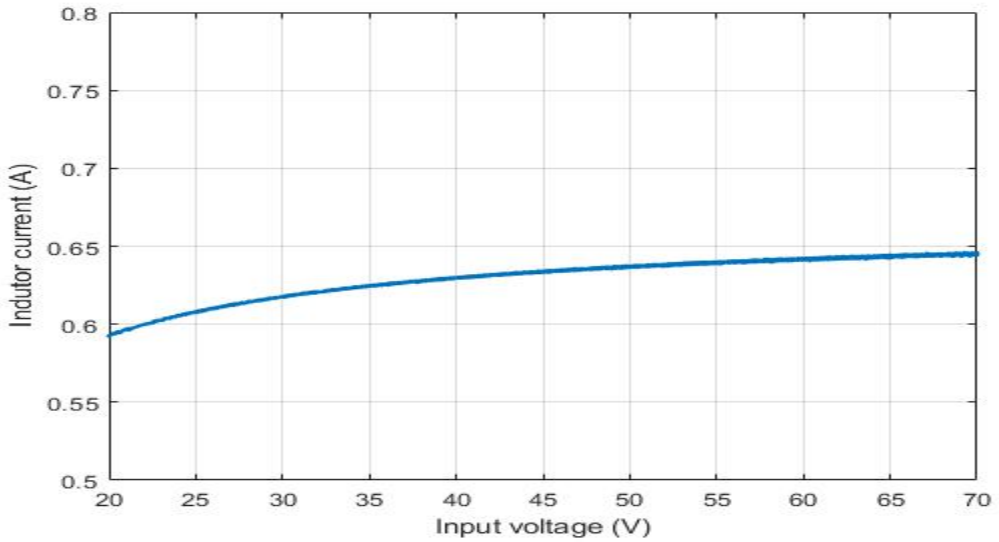

(a)

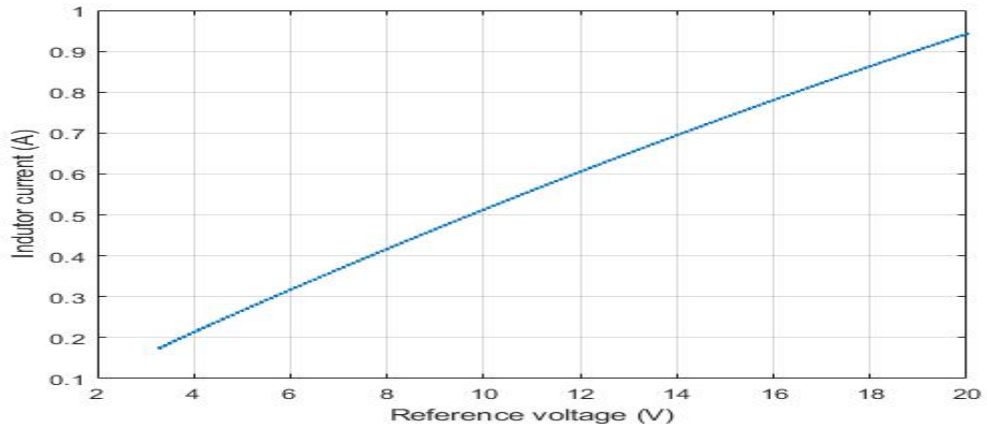

(b)

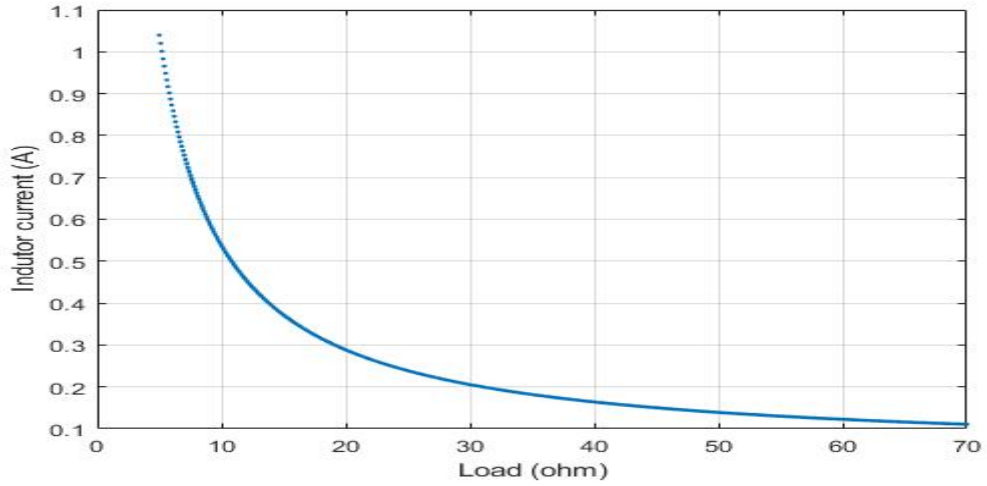

(c)

Figure IV. 13. Bifurcation diagram varying: (a) The input voltage Vg, (b) The reference voltage, (c) the load

For more efficiency evaluation, the robustness of the control to the sudden changes in the parameters of the converter has been tested. The response of output voltage V_o to a sudden change in the input voltage, the reference voltage and load is presented in figure 14. In the first 40 ms, the system is subject to the parameters given in table 1, as shown in figure 14(a). The steady state is reached in 6 ms with no overshoot. At t=40ms, the input voltage is increased to 30V, as it is remarked, the controller was able to stabilize the system. At the same instant as before, we repeated the same scenario by inducing a sudden change in the reference voltage; at t=40ms, the reference voltage is changed to 5V, and the controller adapts with the change and stabilizes the system to the new operating point; results are shown in figure 14(b). The same scenario is repeated again to test the response of the system to the change in load, at t=40ms we changed the load to 35Ω; from figure 14(c), it can be seen that the system remains stable and tracks the reference voltage.

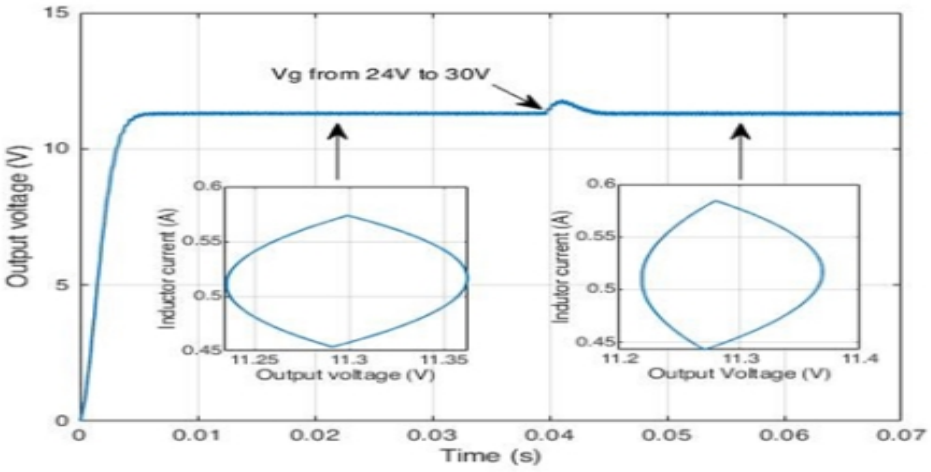

(a)

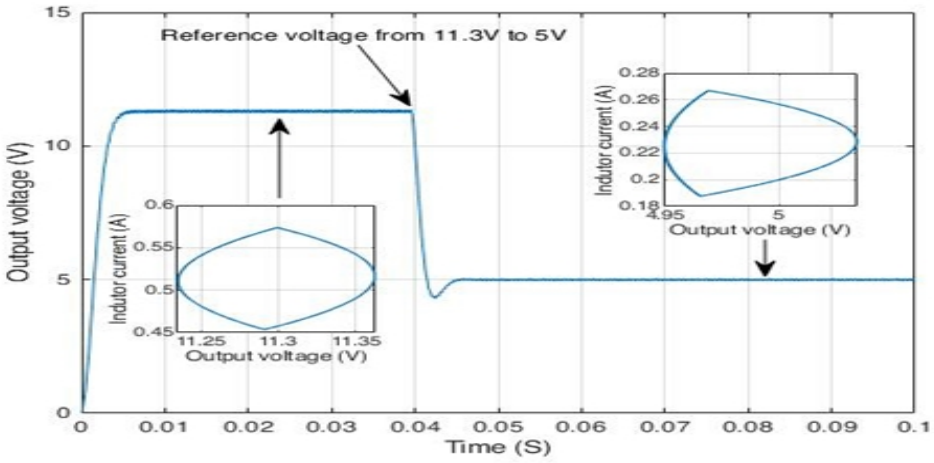

(b)

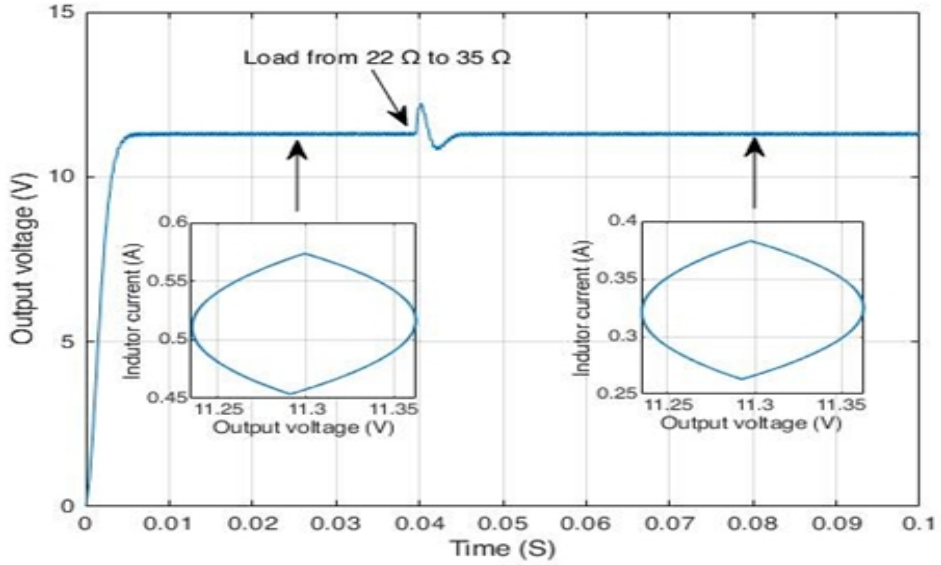

(c)

Figure IV. 14. Response of the system to changes in (a). Input Voltage (b). Reference voltage (c). Load

7. Conclusion

In this chapter, and in order to validate the proposed approach, we employed a simulation and experimental study using the DSPACE 1104R&D board and MATLAB. Through simulation, we created a mathematical model that closely resembled the real-world system. This allowed us to thoroughly test the performance of the optimized controller under various operating conditions by varying different parameters and observing the behavior of the system. The simulations revealed promising results, indicating that the optimized controller effectively addressed the issue of undesirable and nonlinear behaviors that were present in the original system. It consistently maintained the stability of the system across a wide range of parameters, providing a robust and reliable control mechanism.

Furthermore, to ensure the reliability of the proposed approach, we conducted an experimental setup using the DSPACE 1104R&D board. This allowed us to assess the real-time performance of the optimized controller in a practical setting. By connecting the system to the physical hardware and subjecting it to real-world conditions, we were able to observe the behavior of the optimized controller in a more accurate and realistic manner. The experimental results corroborated the findings from the simulations, demonstrating that the optimized controller was indeed successful in eliminating undesirable and nonlinear behaviors. It consistently maintained the stability of the system, regardless of the variations in parameters encountered during the experiments. Overall, the combined evidence from both simulations and experiments provided strong validation for the effectiveness of the optimized controller in improving system behavior and stability.

General conclusion

General conclusion

In this thesis, a new control strategy based on metaheuristic optimization techniques to improve the performance of converters has been proposed, in order to address the control and elimination of nonlinear phenomena in power conversion systems.

Firstly, we presented the basics of static converters and an overview of the modeling of the statics converters, this part allowed us to build the model for the converters to explore the different nonlinear behaviors, then we presented the key definitions of the different behaviors of dynamic systems, including chaos and bifurcation, the most complex and unpredictable behaviors, followed by simulation results that illustrate the various nonlinear phenomena that emerge as the parameters of the buck converter are varied.

Furthermore, we presented the meta-heuristic optimization algorithms that will be used to design the optimal controller for a buck converter, and then we validated the optimization results in terms of improving the behavior of the buck converter using simulation of the optimized analogic controller. The obtained results demonstrate the efficiency of the proposed controller in enhancing the behavior of static converters without the need for any additional circuitry or complex algorithms.

To further validate the proposed controller, a digital control with the Dspace-1104R&D board to ensure real-time communication between the converter and the microcomputer containing the control logic. This has greatly facilitated the control task and resulted in time and cost savings. The results show the good performance of the proposed controller, which is in agreement with the previous results.

Finally, the research carried out in this work and recent research on the nonlinear phenomena in grid-connected PV systems have given us new ideas for future work regarding using the optimization algorithm to design a controller that guarantees the elimination of the undesired nonlinear behaviors and global stability for the photovoltaic grid-connected inverter, which is widely used and a strongly nonlinear system.

Bibliography

[1] R.W. Erickson, D. Maksimovic, Fundamentals of Power Electronics. Kluwer Academic Publishers, Boston, Dordrecht, London, 1999.

[2] D.C. Hamill, D.J. Jefferies, Subharmonics and chaos in a controlled switched mode power converter, IEEE Transactions on Circuits and Systems, 1988.

[3] D.C. Hamill, J.H.B. Deane, D.J. Jefferies, Modeling of chaotic DC/DC converters by iterative nonlinear mappings, IEEE Transactions on Power Electronics , 1992.

[4] J H.B. Deane,D.C. Hamill, Analysis, simulation and experimental study of chaos in the Buck converter, IEEE power electronics specialists conference, 1990.

[5] P. T. Krein, R. M. Bass, Type of instabilities encountered in simple power electronics circuits: Unboundedness, chattering and chaos, IEEE Applied Power Electronics, Conference and Exposition, 1990.

[6] C. K. Tse, Flip bifurcation and chaos in a three-state Boost switching regulator, IEEE Transactions on Circuits and Systems I: Fundamental Theory and Applications, 1994.

[7] C. K. Tse, Chaos from a Buck switching regulator operating in discontinuous mode, International Journal of Circuit Theory and Applications, 1994.

[8] Chan, W. C., & Tse, C. K. (1997). Study of bifurcations in current-programmed DC/DC boost converters: from quasiperiodicity to period-doubling. *IEEE Transactions on circuits and systems I: Fundamental theory and applications*, *44*(12), 1129-1142.

[9] K. Chakrabarty, G. Poddar, S. Banerjee, Bifurcation behavior of the Buck converter, IEEE Transactions on Power Electronics, 1995.

[10] W. C. So, C. K. Tse and Y. S. Lee, An experimental fuzzy controller for DC/DC converters, IEEE Conference of Power Electronics Specialists, 1995.

[11] C. K. Tse, S. C. Fung, K. W. Kwan, Experimental confirmation of chaos in a current programmed Cuk converter, IEEE Transactions on Circuits and Systems I: Fundamental Theory and Applications, 1996

[12] E. Fossas, G. Olivar, Study of chaos in the Buck converter**,** IEEE Transactions on Circuits and Systems-I Fundamental Theory And Application, 1996

[13] J. L. R. Marrero, J. M. Font, G. C. Verghese, Analysis of the Chaotic Regime for DC-DC converters under current-mode control, IEEE power electronics specialists conference, 1996

[14] J. H. B. Deane, D. C. Hamill, Chaotic behavior in current-mode DC-DC converter, Electronic Letters, 1991.

[15] J. H. B. Deane, Chaos in a current-mode controlled Boost DC-DC converter, IEEE Transaction on Circuits and Systems, 1992

[16] W. C. Y. Chan, C. K. Tse, Study of routes to chaos in current programmed DC/DC converters, IEEE Conference on Power Electronics Specialists, 1996.

[17] W. C. Y. Chan, C. K. Tse, Study of bifurcation in current programmed DC/DC converters: from quasi-periodicity to period-doubling, IEEE Transactions on Circuits and Systems I: Fundamental Theory and Applications, 1997.

[18] S. Banerjee, K. Chakrabarty, Nonlinear modeling and bifurcation in the Boost converter, IEEE Transaction on Power Electronics, 1998.

[19] S. Banerjee, E. Ott, J. A. Yorke, G. H. Yuan, Anomalous bifurcation in DC/DC converters: Borderline collisions in piecewise smooth maps, IEEE Power Electronics Specialists Conference, 1997.

[20] S. Banerjee, C. Greboji, Border collision bifurcations in two-dimensional piecewise smooth maps, Physical review E, 1999.

[21] J. L. R. Marrero, R. S. Bueno, G. C. Verghese, Analysis and control of chaotic dcdc switching power converters, IEEE International Symposium on Circuits and Systems, 1999.

[22] A. El Aroudi, L. Benadero, E. Toribio, G. Olivar, Hopf bifurcation and chaos from torus breakdown in a PWM voltage-controlled DC-DC Boost converter, IEEE Transaction on Circuits and Systems, 1999

[23] A. El Aroudi, L. Benadero, E. Toribio, S. Machiche, Quasiperiodicity and chaos in the DC-DC Buck-Boost converter, International Journal of Bifurcation and Chaos, 2000

[24] M. Di-Bernardo, F. Garofalo, L. Glielmo and F. Vasca, Switchings, bifurcations and chaos in dc-dc converters, IEEE Trans. on Circuits and Systems, pp. 133-141. 1998.

[25] M. Di-Bernardo and F. Vasca, Discrete-time maps for the analysis of bifurcations and chaos in dc/dc converters, IEEE Trans. on Circuits and Systems, pp. 130-143, 2000.

[26] C. K. Tse, Y. M. Lai, Controlling bifurcation in power electronics: a conventional practice re-visited, Latin American applied research, 2000.

[27] C. K. Tse, Y. M. Lai, H. H. C. Iu, Hopf bifurcation and chaos in free running current controlled Cuk switching regulator, IEEE Transactions on Circuits and Systems I: Fundamental Theory and Applications, 2000.

[28] C.K. Tse, Complex Behavior of Switching Power Converters, CRC Press, Boca Raton, USA, 2003.

[29] IU, Herbert Ho-Ching. Study of nonlinear phenomena in switching DC/DC converters. 2001. PhD Thesis. Hong Kong Polytechnic University (Hong Kong).

[30] A. Kavitha, G. Uma, Bifurcation analysis of DC-DC converters using discrete time model, IEEE Transactions on Power Electronics, 2008.

[31] A. Kavitha, G. Uma, Experimental verification of Hopf bifurcation in DC–DC Luo converter, IEEE Transactions on Power Electronics 2008

[32] L. Hong, L. Zhong, W. A. Halang, B. Zhang, and G. Chen, Analyzing chaotic spectra of DC–DC converters using the Prony Method, IEEE Transactions on Circuits and Systems—II: Express Briefs, 2007.

[33] F. El Guazer, Modélisation et Simulation des Systèmes Dynamiques Hybrides Affines par morceaux. Exemples en Électronique de Puissance, Thèse Institut National des Sciences Appliquées de Toulouse 2009.

[34] A. H. Nayfeh, B. Balachandran, Applied nonlinear dynamics : analytical, computational, and experimental methods, New York: Wiley, 1995.

[35] C.K. Tse, Complex Behavior of Switching Power Converters. Boca Raton, FL: CRC Press, 2004.

[36] R. G. Ghoachani. Comportement dynamique non-linéaire dans les convertisseurs statiques : régulateurs de courant et stabilité des réseaux DC. Energie électrique. Université de Lorraine, 2012. Français.

[37] S. Banerjee, G. C. Verghese, Nonlinear phenomena in power electronics: Attractors, bifurcations, chaos, and nonlinear control, New York: IEEE Press, 2001.

[38] D. Giaouris, S. Banerjee, B. Zahawi, V, Pickert. Stability analysis of the continuous-conduction-mode buck converter via Filippov's method. *IEEE Transactions on Circuits and Systems I: Regular Papers*, *55*(4), 1084-1096, 2008.

[39] Dhiman, G., & Kumar, V. Spotted hyena optimizer: a novel bio-inspired based metaheuristic technique for engineering applications. *Advances in Engineering Software*, *114*, 48-70, 2017.

[40] Eberhart, R., & Kennedy, J. A new optimizer using particle swarm theory. In *MHS'95. Proceedings of the sixth international symposium on micro machine and human science* (pp. 39-43). IEEE, 1995.

[41] KENNEDY, James; EBERHART, Russell. Particle swarm optimization. In: *Proceedings of ICNN'95-international conference on neural networks*. IEEE, 1995. p. 1942-1948.

[42] MIRJALILI, Seyedali; MIRJALILI, Seyed Mohammad; LEWIS, Andrew. Grey wolf optimizer. *Advances in engineering software*, 2014, 69: 46-61.

[43] Muro C, Escobedo R, Spector L, Coppinger R. Wolf-pack (Canis lupus) hunting strategies emerge from simple rules in computational simulations. Behav Process 2011;88:192–7.

[44] Ott, E., Grebogi, C., & Yorke, J. A. (1990). Controlling chaos. *Physical review letters*, *64*(11), 1196.

[45] Pyragas, K. (1992). Continuous control of chaos by self-controlling feedback. *Physics letters A*, *170*(6), 421-428.

[46] Pyragas, K. (2001). Control of chaos via an unstable delayed feedback controller. *Physical Review Letters*, *86*(11), 2265.

[47] Fradkov, A. L., & Evans, R. J. (2005). Control of chaos: Methods and applications in engineering. *Annual reviews in control*, *29*(1), 33-56.

[48] Al-Hindawi, M. M., Abusorrah, A., Al-Turki, Y., Giaouris, D., Mandal, K., & Banerjee, S. (2014). Nonlinear dynamics and bifurcation analysis of a boost converter for battery charging in photovoltaic applications. *International Journal of Bifurcation and Chaos*, *24*(11), 1450142.

[49] Singha, A. K., Kapat, S., Banerjee, S., & Pal, J. (2015). Nonlinear analysis of discretization effects in a digital current mode controlled boost converter. *IEEE Journal on Emerging and selected Topics in Circuits and Systems*, *5*(3), 336-344.

[50] Yfoulis, C., Giaouris, D., Stergiopoulos, F., Ziogou, C., Voutetakis, S., & Papadopoulou, S. (2015). Robust constrained stabilization of boost DC–DC converters through bifurcation analysis. *Control Engineering Practice*, *35*, 67-82.

[51] Angulo-Garcia, D., Angulo, F., Osorio, G., & Olivar, G. (2018). Control of a dc-dc buck converter through contraction techniques. *Energies*, *11*(11), 3086.

[52] Farooq, U., Gu, J., El-Hawary, M. E., Balas, V. E., & Asad, M. U. (2015, August). Experimental study of optimal Takagi Sugeno fuzzy controller for rotary inverted

pendulum. In *2015 IEEE International Conference on Fuzzy Systems (FUZZ-IEEE)* (pp. 1-7). IEEE.

[53] Hu, W., Zhang, B., & Yang, R. (2019). Bifurcation mechanism and stabilization of V 2 C controlled buck converter. *IEEE Access*, *7*, 77174-77182.

[54] Gozim, D., Guesmi, K., & Mahi, D. (2018). On the elimination of nonlinear phenomena in DC/DC converters using type-2 fuzzy logic controller. *Diagnostyka*, *19*.

[55] Duranay, Z. B., Guldemir, H., & Tuncer, S. (2018). Fuzzy sliding mode control of DC-DC boost converter. *Engineering, Technology & Applied Science Research*, *8*(3), 3054-3059.

[56] Behih, K., Benmahammed, K., Bouchama, Z., & Harmas, M. N. (2019). Real-time investigation of an adaptive fuzzy synergetic controller for a DC-DC buck converter. *Engineering, Technology & Applied Science Research*, *9*(6), 4984-4989.

[57] Ayati, M., Bakhtiyari, A., & Gohari, A. (2016, January). Chaos control in buck converter using fuzzy delayed-feedback controller. In *2016 4th International Conference on Control, Instrumentation, and Automation (ICCIA)* (pp. 362-365). IEEE.

[58] Yuan, Y., Chang, C., Zhou, Z., Huang, X., & Xu, Y. (2015, May). Design of a single-input fuzzy PID controller based on genetic optimization scheme for DC-DC buck converter. In *2015 International Symposium on Next-Generation Electronics (ISNE)* (pp. 1-4). IEEE.

[59] A.G. Perry, G. Feng, Y. L. Liu, and P.C. Sen, "A design method for PI-like fuzzy logic controller for DC-DC converter," IEEE Transactions on Industrial Electronics, Vol. 54, No. 5. pp. 2688-2695, Oct. 2007.

[60] Abderrezek, H., Ameur, A., & Harmas, M. N. (2017). Robust DC/DC converter controllers using PSO. *Electrotehnica, Electronica, Automatica*, *65*(1), 31.

[61] Fu, C. B., Tian, A. H., Yu, K. N., Lin, Y. H., & Yau, H. T. (2018). Analyses and control of chaotic behavior in DC-DC converters. *Mathematical Problems in Engineering*, *2018*, 1-13.

[62] Abdelgawad, H., & Sood, V. (2016). Boost Converter Controller Design Based On Particle Swarm Optimization. *International Journal on Power Engineering and Energy (IJPEE)*, *7*, 647-659.

Appendix A

A.1. Buck components selection

Many parameters controls the selection of any component of the converter, those parameters are:

- Maximum current and voltage
- Power dissipation
- Switching frequency
- The cost

A.1.1 Inductor selection

The inductance value for the boost and buck converters are calculated as follow respectively:

$$L = \frac{V_g(V_o - V_g)}{\Delta I_L \times f_s \times V_o} \quad \text{(A.1)}$$

$$L = \frac{V_o(V_g - V_o)}{\Delta I_L \times f_s \times V_g} \quad \text{(A.2)}$$

V_g = Typical input voltage

V_o= Desired output voltage

f_s = Minimum switching frequency of the converter

ΔI_L = Estimated inductor ripple current.

A.1.2. Diode Selection

Schottky diodes are ideal for this type of converter due to their low forward voltage, which leads to reduced conduction losses, as well as their fast transition from the on state to the off state, resulting in a very low reverse recovery time.

For a buck converter the reverse voltage and the average current of the diode can be calculated as follow:

$$V_R = \mathrm{V}_g \tag{A.3}$$

$$\mathrm{I_F} = \mathrm{i_{o(max)}} \times (1 - \mathrm{d}) \tag{A.4}$$

Meanwhile for a boost converter V_R and $\mathrm{I_F}$ are calculated as follow:

$$V_R = V_o \tag{A.5}$$

$$I_F = i_{o(\max)} \tag{A.6}$$

$\mathrm{I_F}$ = Average forward current of the diode

$\mathrm{i_{o(max)}}$ = Maximum output current necessary in the application

V_R= Reverse voltage of the diode

d = Duty cycle

A.1.3. Capacitor Selection

For a buck converter, the value of the capacitor is given as in

$$\mathrm{C_{o(min)}} = \frac{\Delta \mathrm{I_L}}{8 \times \mathrm{f_s} \times \Delta \mathrm{V_o}} \tag{A.7}$$

The ESR of the output capacitor adds some more ripple, given with the equation:

$$\Delta \mathrm{V_{out(ESR)}} = \mathrm{ESR} \times \Delta \mathrm{I_L} \tag{A.8}$$

$\mathrm{C_{o(min)}}$ = minimum output capacitance

$\Delta \mathrm{I_L}$ = estimated inductor ripple current

$\mathrm{f_s}$ = minimum switching frequency of the converter

$\Delta \mathrm{V_o}$ = desired output voltage ripple

$\Delta \mathrm{V_{out(ESR)}}$ = additional output voltage ripple due to capacitors ESR

ESR = equivalent series resistance of the used output capacitor

For a boost converter

$$\mathrm{C_{o(min)}} = \frac{\mathrm{i_{o(max)}} \times \mathrm{d}}{\mathrm{f_s} \times \Delta \mathrm{V_o}} \tag{A.9}$$

The ESR of the output capacitor adds some more ripple, given with the equation:

$$\Delta V_{o(ESR)} = ESR \times \left(\frac{i_{o(max)}}{1-d} + \frac{\Delta i_L}{2} \right) \quad (A.10)$$

A.1.4. Power Switch

The MOSFET transistor has become the go-to transistor of choice since the early 1980s due to its high switching speed and the relative simplicity of its control circuit. This control circuit is typically a "push-pull" configuration, allowing for the charging of the transistor's source gate capacitor.

The maximum current and voltage of the MOSFET can be estimated as follow:

For buck converter

$$i_{sw(max)} = \frac{\Delta I_L}{2} + i_{o(max)} \quad (A.11)$$

$$V_{sw(max)} = V_g \quad (A.12)$$

For boost converter

$$i_{sw(max)} = \frac{\Delta I_L}{2} + \frac{i_{o(max)}}{1-d} \quad (A.13)$$

$$V_{sw(max)} = V_{out} \quad (II.15)$$

Appendix B

B.1. dSPACE DS1104 board description

The DS1104 R&D Controller Board is a cost-effective and convenient way to upgrade a PC into a development tool for rapid control prototyping. It features I/O interfaces and a real-time processor on a single board, which can be plugged directly into a PC with a free PCI or PCIe slot. It is ideal for smaller control applications and for educational purposes, as it comes with Real-Time Interface (RTI) blocks for graphical I/O configuration in Simulink.

B.1.1. PowerPC (PPC)

- MPC8240 processor with PPC 603e.
- CPU clock: 250 MHz.

B.1.2. The Digital Signal Processing (DSP)

- Texas Instruments TMS320F240 DSP.
- 10 PWM outputs

B.1.3. A/D converter

- 4 multiplexed channels (1x16-bit), with conversion time 2μs.
- 4 parallel channels (4x12-bit), with conversion time 0.8 μs.

B.1.4. D/A converter

- 8 channels (16-bit).

B.1.5. Digital I/O

- 20-bit parallel I/O.
- TTL input/output levels.

Abstract:

In this thesis, we proposed a method to eliminate the nonlinear phenomena and expand the stability range of the converters without the need of the complicated analyses methods or additional circuits. Using the powerful tools of MATLAB and the state-space model of the buck converter as an example, we designed a PID regulator that guarantees both the global stability of the system and parameters disturbance rejection (load, input voltage, reference voltage); this design is based on metaheuristic algorithms to determine the optimum gains of the controller using an appropriate adaptation coefficients. The experimental results using DSPACE 1104 and the simulation on MATLAB demonstrate the efficiency of the proposed controller in enhancing the behavior of static converters without the need for any additional circuitry or complex algorithms.

Key words: *Energy converter, bifurcation, chaos, metaheuristic optimization methods, PID controller.*

Résumé:

Dans cette thèse, nous avons proposé une méthode pour éliminer les phénomènes non linéaires et étendre la plage de stabilité des convertisseurs sans avoir besoin d'analyses complexes ou de circuits supplémentaires. En utilisant les puissants outils de MATLAB et le modèle d'espace d'état du convertisseur Buck en tant qu'exemple, nous avons conçu un régulateur PID qui garantit à la fois la stabilité globale du système et le rejet des perturbations des paramètres (charge, tension d'entrée, tension de référence) ; ce conception est basé sur des algorithmes méta-heuristiques qui déterminent les gains optimaux du contrôleur en utilisant des coefficients d'adaptation appropriés. Les résultats expérimentaux obtenus à l'aide du DSPACE 1104 et les simulations sur MATLAB démontrent l'efficacité du contrôleur proposé pour améliorer le comportement des convertisseurs statiques sans avoir besoin de circuits supplémentaires ou d'algorithmes complexes.

Mot clé **:** *Convertisseur d'énergie, bifurcation, chaos, méthodes d'optimisations méta-heuristique, contrôleur PID.*

ملخص:

في هذه الأطروحة، اقترحنا طريقة لإزالة الظواهر غير الخطية وتوسيع نطاق الاستقرار للمحولات دون الحاجة إلى التحليلات الصعبة أو الدوائر الإضافية. باستخدام أدوات قوية من MATLAB ونموذج فضاء الحالة للمحول الخافض كمثال، تم تصميم محكم PID الذي يضمن كلا من استقرار العام للنظام و رفض التشويشات في المعلمات (الحمولة والجهد الإدخال والجهد المرجعي) ؛ وهذا التصميم يستند إلى الخوارزميات المتاهيوريستية لتحديد الجزئيات الأمثل للمحكم باستخدام معاملات التكيف المناسبة .نتائج التجربة التي تم إجراؤها باستخدام DSPACE 1104 والمحاكاة في MATLAB تظهر كفاءة محكم المقترح في تحسين سلوك المحولات الثابتة.

كلمات مفتاحية: *محول طاقة, تفرعات, فوضى, طرق التحسين المتاهيوريستية, محكم PID.*